Dynamics of vascular normalization during anti-angiogenic therapy: Implications for combination therapy

by

Ricky T. Tong

B.S. Chemical Engineering
California Institute of Technology, 2000

SUBMITTED TO THE HARVARD-MIT DIVISION OF HEALTH SCIENCES AND TECHNOLOGY IN PARTIAL FULFILLMENT OF THE REQUIREMENTS FOR THE DEGREE OF

DOCTOR OF PHILOSOPHY IN MEDICAL ENGINEERING
AT THE
MASSACHUSETTS INSTITUTE OF TECHNOLOGY

May 2005 [June 2005]

Signature of Author: _____
Harvard-MIT Division of Health Sciences and Technology
May 5, 2005

Certified by: _____
Rakesh K. Jain, Ph.D.
Andrew Werk Cook Professor of Tumor Biology
Harvard Medical School/Massachusetts General Hospital
Harvard-MIT Division of Health Sciences and Technology
Thesis Supervisor

Accepted by: _____
Martha L. Gray, Ph.D.
Edward Hood Taplin Professor of Medical and Electrical Engineering
Co-Director Harvard-MIT Division of Health Sciences and Technology

Abstract

Dynamics of vascular normalization during anti-angiogenic therapy: implications for combination therapy

Ricky T. Tong

Submitted to the Harvard/MIT Division of Health Sciences and Technology on May 5, 2005 in Partial Fulfillment of the Requirements for the degree of Doctor of Philosophy in Medical Engineering

Solid tumors require blood vessels for growth, and the goal of anti-angiogenic therapy is to destroy the tumor vasculature. Recent findings suggest that anti-angiogenic therapy enhances radiation and chemotherapy responses. These findings seem paradoxical, since anti-angiogenic therapy prunes tumor vasculature while chemotherapy and radiation therapy rely on the vasculature to transport cancer drugs and oxygen, respectively, to cancer cells. To resolve this paradox, we propose that anti-angiogenic therapy can "normalize" the tumor vasculature transiently, resulting in a more efficient delivery of drugs and oxygen to cancer cells. We first show that DC101, a monoclonal antibody targeting Vascular Endothelial Growth Factor Receptor 2 (VEGFR2), prunes immature blood vessels, reduces vascular diameter and improves pericyte and basement membrane coverages. Functionally, the vascular permeability to macromolecules and interstitial fluid pressure are reduced. By lowering interstitial fluid pressure while maintaining microvascular pressure, DC101 induces a hydrostatic pressure gradient across the vascular wall, which leads to enhanced penetration of macromolecules in tumors. Tumor hypoxia is also reduced, and it is associated with the increased red blood cell velocity after DC101 treatment. Using gene array, real time PCR and Western blot analyses, changes in angiopoietin-2 level during DC101 treatment are identified. To test if similar effects happen in clinical setting, we obtained tumor biopsy samples from rectal adenocarcinoma patients treated with bevacizumab, an anti-VEGF monoclonal antibody. Our analysis shows that after bevacizumab treatment, microvascular density of the tumors decreases while pericyte coverage increases. The level of angiopoietin-2 also decreases, similar to the pre-clinical data. Thus our work shows a potential mechanism that explains the synergism between anti-angiogenic therapy and conventional therapies. These findings should facilitate the design of optimal dose and schedule of anti-angiogenic therapy.

Thesis Supervisor: Rakesh K. Jain
Title: Andrew Werk Cook Professor of Tumor Biology
Harvard Medical School/Department of Radiation Oncology, Massachusetts General Hospital

Biographical Sketch

EDUCATION

2000	California Institute of Technology, Chemical Engineering, B.S.

PROFESSIONAL EXPERIENCE

6/96-9/96	Engineering Assistant, Project Technical Liaison Associates, Inc., TX
1/97-6/97	Research Assistant, California Institute of Technology, Department of Chemistry and Chemical Engineering. Advisor: Professor John D. Roberts
1/97-6/98	Research Assistant, California Institute of Technology, Department of Chemistry and Chemical Engineering. Advisor: Professor Jacqueline K. Barton
6/98-9/98	Research Assistant, Chinese University of Hong Kong, Department of Chemistry. Advisor: Professor Lee Hung Kay
6/99-9/99	Summer Intern, Genentech, Protein Engineering Department. Advisor: Dr. Andrea Cochran
9/98-6/00	Research Assistant, California Institute of Technology, Department of Chemistry and Chemical Engineering. Advisor: Professor Mark E. Davis
9/00-Present	Doctoral Candidate, Medical Engineering, Harvard-MIT Division of Health Sciences and Technology
2/01-Present	Research Fellow, Massachusetts General Hospital and Harvard Medical School. Advisor: Professor Rakesh K. Jain

HONORS AND AWARDS

Howard Hughes Medical Institute SURF Fellow (1997), Donald S. Clark Award (1998), Caltech Merit Scholar Award (1998 and 1999), Vice President of CCSA Caltech Chinese Student Association (1997-99), Officer of the Entrepreneur Club (1998-00), Treasurer of the Caltech Student Chapter of Tau Beta Pi (1999-00), President of the Caltech Student Chapter of the American Institute of Chemical Engineers (1999-00), President and Founder of the Student Chapter of the Biomedical Engineering Society (1999-00), NSF Graduate Fellowship (2000-03), Angiogenesis Foundation Honorable Mention (2003), Susan Komen Foundation Fellowship (2003-05)

PROFESSIONAL ACTIVITIES

Teaching assistant in Transport Phenomena (2000)
Teaching assistant in Tumor Pathophysiology (2003)
Harvard-MIT Division of Health Sciences and Technology Social Chair (2001)
Harvard-MIT Division of Health Sciences and Technology Ph.D. Admissions Committee (2004-2005)

PUBLICATIONS

Holmlin, R. E., **Tong, R. T.**, and Barton, J. K. (1998). Long-range triplet energy transfer between metallointercalators tethered to DNA: Importance of intercalation, stacking, and distance. Journal of the American Chemical Society *120*, 9724-9725.

Cochran, A. G., **Tong, R. T.**, Starovasnik, M. A., Park, E. J., McDowell, R. S., Theaker, J. E., and Skelton, N. J. (2001). A minimal peptide scaffold for beta-turn display: Optimizing a strand position in disulfide-cyclized beta-hairpins. Journal of the American Chemical Society *123*, 625-632.

Alexandrakis, G., Brown, E. B.*, **Tong, R. T.***, McKee, T. D., Campbell, R. B., Boucher, Y., and Jain, R. K. (2004). Two-photon fluorescence correlation microscopy reveals the two-phase nature of transport in tumors. Nature Medicine *10*, 203-207. * These authors contributed equally.

Willett, C. G., Boucher, Y.*, Di Tomaso, E.*, Duda, D. G.*, Munn, L. L.*, **Tong, R. T.***, Chung, D. C., Sahani, D. V., Kalva, S. P., Kozin, S. V., Mino, M., Cohen, K. S., Scadden, D. T., Hartford, A.C., Fischman, A. J., Clark, J. W., Ryan, D. P., Zhu, A. X., Blaszkowsky, L. S., Chen, H. X., Shellito, P. C.,

Lauwers, G. Y., and Jain, R. K. (2004). Direct evidence that the VEGF-specific antibody bevacizumab has antivascular effects in human rectal cancer. Nature Medicine *10*, 145-147. * These authors contributed equally.

Tong, R. T., Boucher, Y., Kozin, S. V., Winkler, F., Hicklin, D. J., and Jain, R. K. (2004). Vascular normalization by vascular endothelial growth factor receptor 2 blockade induces a pressure gradient across the vasculature and improves drug penetration in tumors. Cancer Res *64*, 3731-3736.

Winkler, F.*, Kozin, S. V.*, **Tong, R. T.**, Chae, S. S., Booth, M. F., Garkavtsev, I., Xu, L., Hicklin, D. J., Fukumura, D., di Tomaso, E., Munn, L. L., and Jain, R. K. (2004). Kinetics of vascular normalization by VEGFR2 blockade governs brain tumor response to radiation; Role of oxygenation, angiopoietin-1, and matrix metalloproteinases. Cancer Cell *6*, 553-563. * These authors contributed equally.

Xu, L., **Tong, R. T.**, Cochran, D. M., and Jain, R. K. (2005). Blocking PDGF-D/PDGFRβ signaling inhibits human renal cell carcinoma progression in an orthotopic mouse model. Cancer Res (In press)

INVITED TALKS

Tong, R.T., "Dynamics of vessel normalization following VEGF blockade." *2004 Keystone Symposia: Angiogenesis*, Jan 1, 2004.

Tong, R.T., "Vascular normalization by VEGFR2 blockade improves molecules penetration and radiation response in two tumor models." *2005 American Association for Cancer Research Annual Meeting*, April 20, 2005.

ABSTRACTS

Tong, R.T., Jain, R.K., "The effects of anti-angiogenic therapy on the anatomical and functional properties of solid tumors," *HST Forum*, (2002).

Tong, R.T., Boucher, Y., Kozin, S.V., Jain, R.K., "Anti-VEGFR2 blocking antibody normalizes the tumor vasculature and microenvironment." *MGH Clinical Research Day* (2003).

Tong, R.T., Jain, R.K., "The effects of anti-angiogenic therapy on the anatomical and functional properties of solid tumors," *HST Forum*, (2003).

Tong, R.T., Boucher, Y., Jain, R.K., "Dynamics of vessel normalization following VEGF Blockade," *SAC MGH Research Symposium*, (2004).

Tong, R.T., Boucher, Y., Hicklin, D.J., Jain, R.K., "Dynamics of vessel normalization following VEGF Blockade," *Proceedings of the American Association for Cancer Research*, 2556 (2004).

Tong, R.T., Boucher, Y., Kozin, S.V., Hicklin, D.J., Jain, R.K., "Dynamics of vessel normalization following VEGF Blockade," *Breast Cancer Research at Harvard*, (2004).

Tong, R.T., Jain, R.K., "Dynamics of vessel normalization following VEGF Blockade," *HST Forum*, (2004).

Tong, R.T., Boucher, Y., Kozin, S.V., Hicklin, D.J., Jain, R.K., "Vascular normalization by VEGFR2 blockade induces a pressure gradient across the vasculature and improves drug penetration in tumors." *MGH Clinical Research Day* (2004).

Tong, R.T., Jain, R.K., "Vascular normalization in tumors by anti-angiogenic therapy: from animal models to clinical trial." *HST Forum* (2005).

Acknowledgements

"If you think in terms of a year, plant a seed; if in terms of ten years, plant trees; if in terms of 100 years, teach the people."

Confucius, BC 551-479

I would like to start by thanking my thesis advisor, Professor Rakesh Jain for his guidance and advice. He is always inspirational and constantly pushes me to reach my full potential. I am very grateful for all of his help as I learn to become an independent researcher. He has also provided me with numerous opportunities to work with other lab members and outside collaborators and to attend conferences. His attitude towards work and colleagues has created a very friendly and supportive working environment.

I would like to thank the members of my thesis committee, Professors Robert Langer (MIT), Professor William Deen (MIT), and Professor Bruce Zetter (HMS). Their advice, input, and support have been invaluable. I would also like to thank the Harvard-MIT Division of Health Sciences and Technology and the MIT Chemical Engineering Department for opening many educational avenues and building solid and rigorous foundation for my career.

My colleagues and friends in the Steele Lab have always been there for me when I need them the most. I am deeply grateful for their help and time. They have always been very patient with me, as I often have many questions and need lot of assistance. In particular, I would like to thank Frank Winkler and Sergey Kozin as they are part of the "normalization team". I truly enjoy working with them to discover the wonders of DC101 together. I would like to thank Yves Boucher, Dan Duda, Emmanuelle di

Tomaso, Lance Munn, Edward Brown, Mike Booth, and Dai Fukumura for their help, which I immensely appreciate. I have also benefited tremendously through working with George Alexandrakis, Lei Xu, Igor Garkavtsev, and Jeroen Hagendoorn. I would also like to thank Patrick Au, Wilson Mok, and Satoshi Kashiwagi for many of our wonderful discussions. I can always expect them to be in lab with me late at night. I would like to thank Sylvie Roberge, Julia Khan, and Peigen Huang for their help with the animal work. I would like to thank Chelsea Swandal, Melanie Berg, Russell Delgiacco, Lucine Petit, and Carolyn Smith for their outstanding technical support and dedication to the projects. I am deeply grateful for the help from Phyllis McNally, Tara Belezos, and Doug Stay throughout the years. I would like to thank David Cochran, Ryan Lanning, Pooja Pathak, Dennis Dolman, Naoto Koike, Tim Padera, Brian Stoll, Josh Tam, Rosemary Jones, and Hide Isaka for their valuable input into my work. A special thank to Marek Ancukiewicz for all the last minute help on statistics. I am very thankful for all of the interesting discussion with James Baish, and for his help on fractal analysis on tumor vasculature. I would also like to thank my UROP students Jennifer Lobo, Jenny Ruan, Margaret Kim, and Sam Kwei. I would not have had the luxury to work on as many projects without their assistance.

I would like to thank Christopher Willett and Tracy Batchelor for providing me the wonderful opportunities to work on clinical trials. They have opened my eyes to the exciting world of clinical research. I would also like to thank my outside collaborators, Peter Carmeliet (University of Leuven), Annelii Ny (University of Leuven), Raju Kucherlapati (HMS), Qingcong Lin (HMS), Badri Roysam (Rensselaer Polytechnic Institute), and Alex Tyrrell (Rensselaer Polytechnic Institute). Working with them led

me to appreciate the broad spectrum of cancer research. I would like to thank Dan Hicklin (ImClone) for DC101, Eugene Renkin (University of California Davis) for nylon wicks, David Jackson (Oxford University) for LYVE-1 antibodies. I am grateful to the NSF and Susan G. Komen Foundation for funding my research.

Mostly I would like to thank my family and friends. My parents, YuShan and Winnie Tong, and my brother, James Tong, provide me the support and encouragement that a child dreams of. Their sacrifice allowed me to pursuit my dream, and has made my PhD study seems completely painless. Finally, I can never thank enough my friends who have been endlessly editing my papers, thesis, and application essays. Chirag, Sophia, Paul, Janice, Jackie, Karen, Clay, Richard, Kevin, Lisa, Sindy thank you so much for all of your help and support.

Thank you to all of the people who have been so patient and helpful in molding my career and future.

Table of contents

List of Figures

List of Tables

Chapter 1: Original Contribution

Recent pre-clinical and clinical trials suggest that anti-angiogenic therapy should be combined with cytotoxic/radiation therapy for successful treatment of solid tumors. However, there are no generally accepted guidelines for optimal scheduling of these therapies. The synergistic results seen in combined therapy also present a paradox. One would expect that anti-angiogenic therapy, which aims to destroy tumor vasculature, would severely compromise, instead of enhance, the delivery of oxygen and therapeutics to the solid tumors, and thus lead to a less effective chemotherapeutic/radiation response. The primary goal of this thesis is to resolve this paradox by understanding the dynamic changes during anti-angiogenic therapy. We propose that anti-angiogenic therapy will transiently "normalize" the tumor vasculature by passively pruning immature tumor blood vessels and actively remodeling the remaining vasculature. We further hypothesize that the changes in vascular function during this normalization time window will enhance the delivery of molecules in tumors. This work will drive our understanding of general tumor pathophysiology and may improve treatment of solid tumors using anti-angiogenic therapy.

To get a better picture of the effects of anti-angiogenic therapy on tumors, multiple approaches were used to characterize the changes. By implanting tumors in a chronic window model such as the dorsal skinfold chamber window or cranial window in mice, daily three dimensional images of tumor vasculature were captured using two photon laser scanning microscopy (Chapter 6). A few days after DC101 treatment, an anti-murine VEGFR2 antibody, vascular density and diameter significantly decreased. Surprisingly, many of the vessels became less tortuous during the treatment.

The cellular structure around the tumor vasculature was analyzed using immunostaining techniques to determine if some tumor blood vessels were more vulnerable to anti-angiogenic therapy than others. The results demonstrated for the first time that anti-angiogenic therapy improves pericyte coverage and basement membrane coverage around tumor blood vessels. Interestingly, by monitoring pericyte coverage throughout the treatment, it became apparent that anti-angiogenic therapy both preferentially pruned tumor blood vessels with no pericyte coverage, and at the same time, indirectly increased the pericyte coverage of the remaining vessels.

Next, the effects of these structural changes in the tumor vasculature on vascular function, tumor microenvironment, and more importantly, the delivery of molecules in tumors were studied. Using intravital microscopy, tumor blood vessels were demonstrated to be less leaky during the treatment (Chapter 7). Of interest, interstitial fluid pressure (IFP) was significantly lowered after the treatment. Using the micropipette technique, microvascular pressure (MVP) and interstitial fluid pressure were measured in one preparation. While interstitial fluid pressure was reduced after DC101 treatment, no changes were observed in microvascular pressure. Thus, anti-angiogenic therapy induced a hydrostatic pressure gradient across the vascular wall.

Fluid movement across the vascular wall is governed by the Starling's equation:

$J_v = L_p [(MVP - IFP) - \sigma(\pi_p - \pi_i)]$

which states that the rate of fluid movement across a unit area of vascular wall, or fluid flux (J_v), is proportional to both hydrostatic (MVP, IFP) and oncotic pressure (π_p, π_i) difference across the vascular wall. Interestingly, we found that the modification in hydrostatic pressure was accompanied by a change in interstitial oncotic pressure.

Moreover, by using experimentally measured values and the mathematical model developed by Baxter and Jain (Baxter and Jain 1989), it also showed that DC101 lowered interstitial fluid pressure throughout the entire tumor, and the model further predicted an increase in interstitial fluid velocity. Using two photon line scan method, we showed that red blood cell velocity increased after DC101 treatment, and the increase was associated with a reduced tumor hypoxia.

Next, to determine the molecular changes in tumors during anti-angiogenic therapy, tumor samples were obtained, and mRNA and protein were examined (Chapter 8). Gene array and real time PCR data showed that angiopoietins were modified during the treatment. The change was further confirmed by Western blot analysis.

But are these experiments in mice relevant to cancer patients? Our clinical collaborators began a phase I clinical trial using bevacizumab, an anti-VEGF monoclonal antibody, to characterize its effects on rectal cancer (Chapter 9). Patients with primary and locally advanced adenocarcinoma of the rectum were enrolled in a preoperative treatment protocol of bevacizumab administration alone, followed 2 weeks later by concurrent administration of bevacizumab with 5-fluorouracil and external beam radiation therapy to the pelvis. Surgery was performed to resect remaining disease 7 weeks after treatment completion. Tumor biopsies were obtained before and 12 days after initial bevacizumab administration, and immunohistochemistry was performed on these samples. Confirming the results from the animal studies, the human tumors showed decreased microvascular density with increased pericyte coverage after bevacizumab treatment. Furthermore, angiopoietin-2 level was also lowered after the treatment. These results further

confirmed that anti-angiogenic therapy normalized tumor vasculature, and provided a potential mechanism for the synergistic effects seen in combined treatment.

In summary, this dissertation provides a thorough examination of the effects of VEGFR2 blockade on tumors at structural, cellular, functional, and molecular levels. Biopsies from rectal carcinomas taken from patients treated with bevacizumab show similar cellular modification as in animal models. The continued progress in this field will provide clues on multiple avenues, such as designing an optimal schedule for combined therapies and discovering surrogate markers for anti-angiogenic therapy. It will also help establish guidelines for future anti-angiogenic clinical trials.

Table 1.1: Original contribution

Specific Aim	Experiment	Novelty	Contribution*
1a	Vascular density and diameter		RT
1b	Pericyte coverage	Y	RT
1b	Basement membrane coverage	Y	RT
2a	Vascular permeability		RT
2b	Red blood cell velocity	Y	RT
2c	Interstitial fluid pressure measurement in spontaneous tumors	Y	RT
2c	Microvascular and interstitial fluid pressure measurements	Y	RT
2c	Plasma and interstitial oncotic pressures	Y	RT
2d	Macromolecule distribution/penetration	Y	RT
2d	Hypoxia	Y	RT, FW, SK
3a	Gene array		RT
3b	Real-time PCR		RT
3c	Western blot		RT
4a	Microvascular density		RT, EdT
4a	Pericyte coverage	Y	RT, YB
4b	Angiopoietin 2 staining	Y	RT

* RT: Ricky Tong; FW: Frank Winkler; SK: Sergey Kozin; EdT: Emmanuelle di Tomaso; YB: Yves Boucher

Chapter 2: Introduction

Cancer is a major health problem in the world. Since 1990, the United States has seen nearly 15 million new cancer cases diagnosed (Fig. 1). 1.3 million new cases of cancer were diagnosed in 2004, excluding an estimated 59,000 new cases of breast carcinoma *in situ*, and 41,000 new cases of *in situ* melanoma (Jemal et al. 2004). Over half a million Americans will die of cancer this year alone, a daily average of more than 1,500 people. Men have approximately 45% lifetime risk of developing cancer, whereas for women, the risk is about 38%. Cancer is clearly an important public health concern in the US and around the world, and has been for centuries.

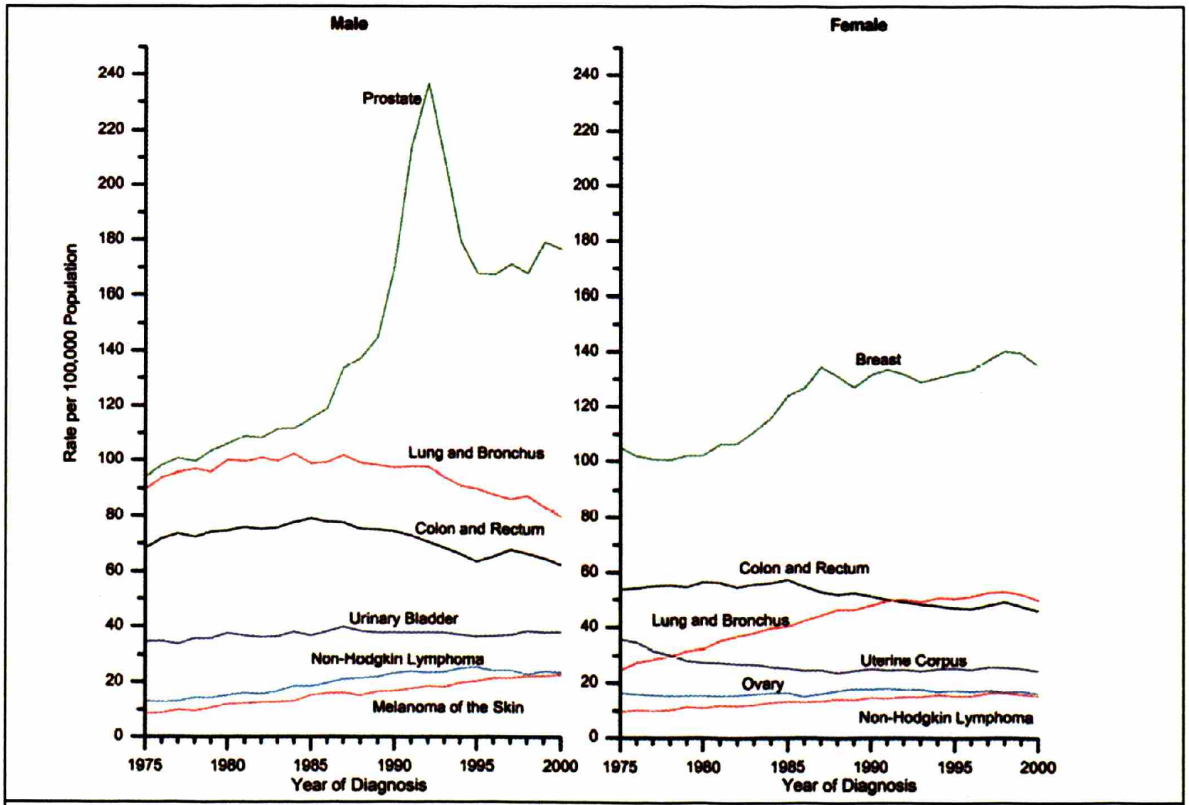

Figure 2.1: Cancer incidence rates among males and females for selected cancer types in the US from 1975 to 2000.

The rates are age adjusted to the 2000 US standard population (Jemal et al. 2004)

As a result, the prevention, detection, and treatment of cancer constitute a significant portion of the current national health budget. Despite this effort, the number of people

living with cancer has been predicted to double between the years 2000 and 2050 (Simmonds 2003). Furthermore, the annual percent change for the number of cancer deaths has not decreased significantly (Figure 2). Thus, a tremendous amount of effort has been put forth in the search for new and innovative treatments for cancers.

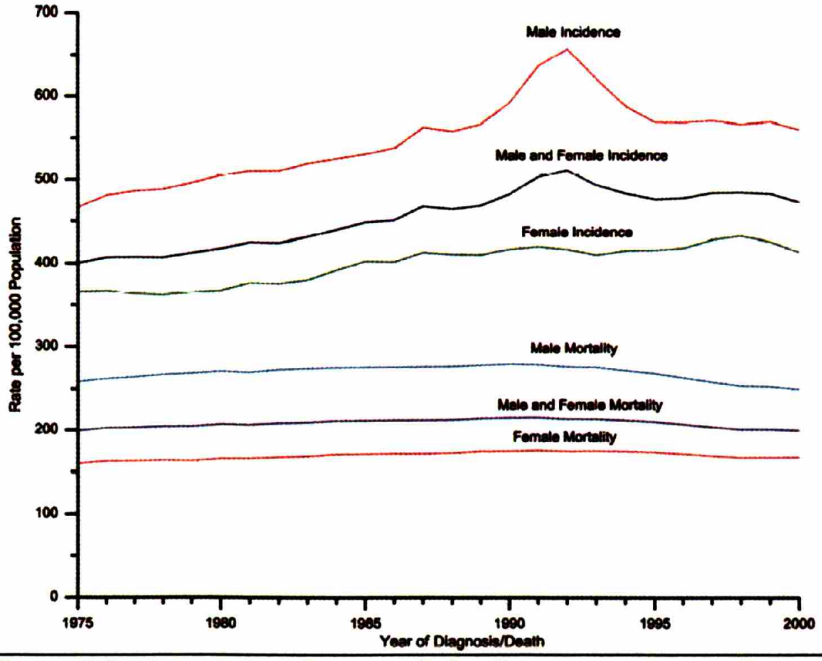

Figure 2.2: Cancer incidence and death rates among males and females in the US from 1975 to 2000.

The rates are age adjusted to the 2000 US standard population (Jemal et al. 2004).

Surgery has been the most effective way to eradiate primary tumors; however, studies have shown that approximately 30% of patients newly diagnosed with solid tumors have already developed metastases (Cotran et al. 1999). The presence of metastases is a strong indication of poor prognosis, and that is what makes cancer so lethal (Ruoslahti 1996). Once cancer cells have metastasized to many locations in the body, it is almost

impossible to remedy with surgery. Thus, systemic therapies such as chemotherapy are often employed to treat metastasized tumors or as post-surgery preventive care.

However, in order for chemotherapy to be effective, therapeutic agents must reach all cancer cells in sufficient quantity to promote anti-cancer activity without causing major systemic toxic effects. A number of cytotoxic drugs have shown potent anti-cancer properties in a laboratory setting; however, existing therapeutic agents have not dramatically reduced the number of deaths caused by solid tumors (Jemal et al. 2003). Due to both drug delivery barriers and the development of drug resistance in cancer cells, many chemotherapy trials have not lived up to expectations (Jain 1989; Jain 1994; Jain 1998). Anti-angiogenic therapy, which targets the genetically stable endothelial cells, may overcome some of the obstacles offered by conventional therapy and has become a promising anti-cancer modality (Folkman 1971; Kerbel and Folkman 2002).

Interestingly, recent clinical studies have shown that anti-angiogenic therapy is more effective when combined with chemotherapy/radiation therapy (Kabbinavar et al. 2003; Hurwitz et al. 2004). However, these results present an apparent paradox: while anti-angiogenic therapy aims to eradicate tumor blood vessels, chemotherapy and radiation therapy rely on tumor vasculature to deliver cancer drugs and oxygen, respectively, to cancer cells. The lack of mechanistic understanding of the effects of anti-angiogenic therapy has been a major challenge to the evaluation of treatment efficacy and the design of optimal treatment schedules. This thesis focused on the effects of anti-angiogenic therapies, DC101 and Avastin, both blocking Vascular Endothelial Growth Factor (VEGF) pathway, on the tumor vasculature and microenvironment. It also rigorously tested the "normalization" hypothesis put forward in 2001 by Dr. Rakesh Jain (Jain 2001)

(Fig. 2.3). According to this hypothesis, VEGF blockade can normalize tumor vasculature and enhance drug and oxygen delivery. We identified the structural, functional, and molecular changes in tumor blood vessels as well as determined the mechanism responsible for the synergistic effects of anti-angiogenic therapy combined with radiation therapy.

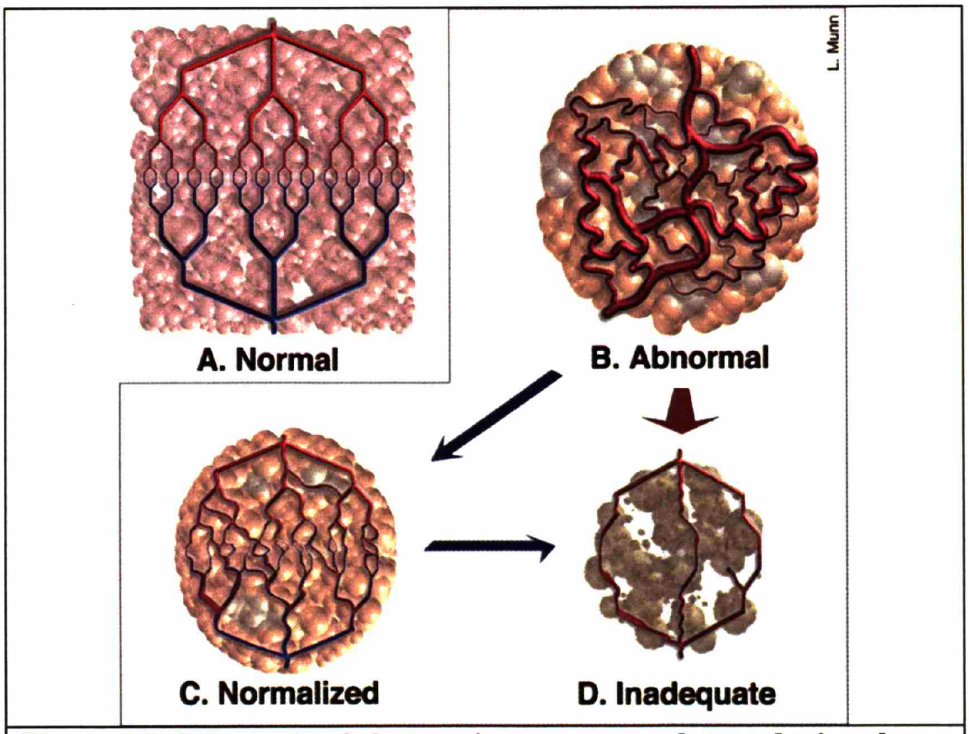

Figure 2.3: Schematic of changes in tumor vasculature during the course of anti-angiogenic therapy.

A. Normal microcirculation with mature vessels. B. Chaotic, irregular tumor blood vessels composed mostly of immature vessels. C. Judiciously applied anti-angiogenic therapy might prune immature vessels, leading to a more normalized tumor vascular network. D. Excessive pruning leads to inadequate oxygenation and drug delivery for combination therapy (Jain 2001).

Chapter 3: Specific Aims

Anti-angiogenic therapy has been shown to enhance the efficacy of cytotoxic and radiation therapies; however, the mechanism responsible for this synergism and the optimal dose or schedule have not been determined. Each of the following specific aims addresses a critical aspect to understand and resolve this issue.

Hypothesis: VEGF blockade by DC101, an anti-VEGFR2 antibody, prunes immature tumor vessels and normalizes the remaining vasculature by modulating genes that stabilize and fortify the vascular wall. The improved vascular function enhances the delivery of therapeutic agents during the normalization time window.

Specific Aim 1: Determine the structural changes of tumor vasculature during DC101 treatment. Hypothesis: DC101 prunes immature blood vessels and normalizes the remaining vasculature.

Specific Aim 1a: Examine the effects of DC101 on tumor vessel architecture.

Mice with tumors implanted in either the dorsal skinfold chamber or cranial window were treated with DC101. Dynamic changes in vascular density and diameter were measured *in vivo* by both conventional fluorescence and two photon microscopy. A computer algorithm was used to extract the changes in tumor blood vessel morphology.

Specific Aim 1b: Determine the effects of DC101 on pericyte and basement membrane coverage.

Tumor blood vessels have abnormal and heterogeneous pericyte and basement membrane coverage. Endothelial cell survival is dependent on pericyte coverage and VEGF levels, thus DC101 could target immature blood vessels with limited pericyte coverage.

Immunohistochemistry was used to detect and quantify the changes in pericyte and basement membrane coverage.

Specific Aim 2: Determine the functional changes in the tumor vasculature and the resulting changes in tumor microenvironment during DC101 treatment. Hypothesis: DC101 improves vascular function by decreasing vascular permeability to macromolecules, re-establishing a hydrostatic pressure gradient across the vascular wall, and increasing red blood cell (RBC) velocity.

Specific Aim 2a: Characterize the vascular permeability of the normalized tumor vasculature.

The tumor vasculature has an abnormally high vascular permeability and a slow blood flow rate. The effects of DC101 on macromolecule permeability were measured before and after DC101 treatment by either conventional fluorescence or two photon microscopy.

Specific Aim 2b: Examine the changes in red blood cell velocity after anti-angiogenic treatment

Lowering vascular permeability by VEGF blockade may prevent flow stasis in vessels and should improve RBC velocity in tumor vessels. The effect of DC101 on RBC velocity was measured before and after DC101 treatment by two photon microscopy.

Specific Aim 2c: Determine the hydrostatic and oncotic pressure profiles across the vascular wall.

Convective flow across tumor vessels is determined by differences in oncotic (osmotic pressure of proteins) and hydrostatic pressures across the tumor vasculature (Starling's equation). Oncotic and hydrostatic pressures were measured both inside and outside

tumor blood vessels in tumors treated with DC101 or control IgG antibody. The changes in oncotic and hydrostatic pressures were related to vascular permeability measurements and lymphatic drainage.

Specific Aim 2d: Measure the distribution/penetration of molecules during the normalization time window.

Modifications in the tumor vasculature and pressure profiles induced by DC101 could affect the distribution of molecules in tumors. Fluorescently labeled macromolecules were injected into the circulation and the distribution/penetration of macromolecules was determined. Hypoxia was also measured during DC101 treatment by immunohistochemistry.

Specific Aim 3: Determine the molecular changes during DC101 treatment. Hypothesis: DC101 modulates genes that stabilize the vascular wall.

Specific Aim 3a: Determine the modification of gene expression by DC101 treatment.

Total RNA was obtained from both the control and DC101 treated groups. Gene array analysis was performed with angiogenic gene array chips.

Specific Aim 3b: Confirm the changes in gene expression level by real time (RT)-PCR.

Several genes identified in specific aim 3a were studied and quantified by RT-PCR. Gene expression was compared between the control and DC101 treated groups.

Specific Aim 3c: Confirm the changes in protein level by Western blot analysis.

In order to further confirm the RT-PCR findings in specific aim 3b and to determine cell types associated with the changes in gene expression, Western blot and immunostaining were performed for both the control and DC101 treated groups.

Specific Aim 4: Examine the effects of bevacizumab in rectal adenocarcinomas in patients. Hypothesis: Similar to DC101 treatment in mice, bevacizumab decreases vascular density, increases perivascular cell coverage and decreases angiopoitein-2 levels in tumors.

Specific Aim 4a: Determine the effects of bevacizumab on pericyte coverage in rectal adenocarcinoma in patients.

Human biopsy samples of rectal adenocarcinomas were obtained before and 12 days after treatment with bevacizumab, an anti-VEGF monoclonal antibody. Perivascular cells and blood vessels were stained with antibodies against αSMA and CD31, respectively, and the percentage of vessels covered by perivascular cells was measured.

Specific Aim 4b: Determine the changes in Angiopoietin-2 level in rectal adenocarcinomas in patients treated with bevacizumab.

Angiopoietin-2 expression was identified by immunohistochemistry in biopsy samples of rectal adenocarcinomas obtained before and 12 days after treatment with bevacizumab. A computer algorithm was used to quantify the staining.

Chapter 4: Background

Barriers to drug delivery: A need for finding a new therapy

For any anti-cancer therapy to be successful, it must meet at least two criteria: first, the agent must be potent and effective at inhibiting the growth of tumors or destroying tumor cells. Second, it must reach tumor cells in sufficient quantity (Jain 1998). Most cancer research has been focused on the first criteria, and many potent cytotoxic agents are now available to physicians. However, cancer cells rapidly develop drug resistance to anti-cancer drugs due to their inherent genetic instability (Lehne et al. 1998). Chemoresistance is a major clinical problem and ultimately leads to treatment failure in many cancer patients.

Furthermore, physiological barriers impede the delivery of chemotherapeutic drugs to tumor cells (Jain 1998). Tumor vessels are structurally and functionally abnormal, and the chaotic blood supply in tumors limits the delivery of blood-borne agents (Jain 1988; Jain 1989). These abnormalities lead to a heterogeneous tumor blood flow, with some regions having inadequate perfusion. The second barrier is the vascular wall (Jain 1987). The variability in vessel permeability results in variable drug delivery to different parts of the tumor. In addition, the elevated interstitial fluid pressure (IFP) reduces intratumoral transvascular convection, thus limiting extravasation (Baxter and Jain 1989; Boucher et al. 1991; Netti et al. 1999). The third barrier is the tumor interstitium. The interstitial space consists of a matrix of collagens, proteoglycans, and other molecules that hinder the delivery of molecules (Jain 1987; Netti et al. 2000; Brown et al. 2003). Thus, for any therapeutic agent to be effective, it must pass through all these barriers and successfully reach target cells in optimal quantity.

Tumor Pathophysiology

The tumor vasculature differs from normal vessels in both structure and function. The imbalance in the production of pro-angiogenic factors and anti-angiogenic factors leads to the formation of angiogenic vessels. As a result of the excess angiogenic factors, tumor blood vessels are leaky, dilated, chaotic, and poorly organized (Baish and Jain 2000; Jain 2003). The chaotic and heterogeneous vascular network further prevents blood-borne molecules to be delivered uniformly in sufficient quantities (Baish and Jain 2000). Tumor blood flow is also highly heterogeneous, and this is partly due to the increased leakiness of tumor blood vessels (Chaplin and Hill 1995; Netti et al. 1996; Baish et al. 1997).

In addition, pericytes around tumor vessels are loosely associated with endothelial cells, and some vessels are even completely devoid of perivascular cells (Morikawa et al. 2002). The lack of pericytes leads to endothelial hyperplasia and signs of increased transendothelial permeability (Hellstrom et al. 2001). Proper pericyte coverage has been shown to be essential for vessel maturation (Darland and D'Amore 1999; Jain 2003). Thus, the tumor vasculature is considered immature due to the abnormality in or absence of pericyte coverage along blood vessels. Basement membrane of some tumor blood vessels is often thick and becomes multi-layered, while many of the vessels lack a complete basement coverage (Baluk et al. 2003; Kalluri 2003).

Tumor Interstitial Fluid Pressure

Since 1950, several investigators have demonstrated that interstitial hypertension is a characteristic of solid tumors (Young et al. 1950; Jain 1987; Boucher et al. 1991; Netti et al. 1999). In normal tissues, the excess fluid filtered from blood vessels is drained by

lymphatic vessels to maintain the IFP close to zero (mmHg). In tumors, IFP homeostasis is perturbed due to impaired lymphatic drainage (Leu et al. 2000; Padera et al. 2002) as well as abnormalities in vascular structure and function (Jain 2003). The lack of functional lymphatics in tumors prevents the removal of interstitial fluid from the extracellular space, thereby increasing the IFP. Furthermore, tumor blood vessels generally have a higher permeability than normal vessels (Jain 1987; Jain 1994). As a result, an abnormally high concentration of plasma proteins leaks out of the vessels, which leads to a negligible oncotic pressure difference across the vessel wall (Stohrer et al. 2000). Thus, both the oncotic and hydrostatic transvascular pressure gradients are reduced, which reduces the fluid filtration within solid tumors (Boucher et al. 1990; Boucher and Jain 1992). In addition, elevated IFP coupled with high vascular permeability can also reduce blood perfusion in solid tumors and further limit the delivery of drugs (Netti et al. 1996). Thus, the combination of inefficient blood vessels and tumor microenvironment hinders the adequate delivery of blood-borne molecules such as oxygen and cytotoxic drugs throughout the tumor tissues during anti-cancer therapy.

Angiogenesis

Researchers have long recognized that tumor growth and metastasis are dependent upon the formation of a vascular network (Folkman 1971). Angiogenesis is the growth of new blood vessels from pre-existing ones, and it is involved in developmental processes, wound healing, tissue regeneration, chronic inflammation, and other pathological states (Folkman 1995; Carmeliet and Jain 2000; Jain and Carmeliet 2001; Kerbel and Folkman 2002; Carmeliet 2003). Without angiogenesis, a solid tumor cannot grow beyond 1-2

mm in diameter (about 106 cells) due to limitation in the diffusion of oxygen and other nutrients (Carmeliet and Jain 2000; Hlatky et al. 2002). When cancer cells turn on the "angiogenic switch", they recruit vessels from the surrounding normal blood vessels, which permit tumors to continue growth and proliferation.

Because of their crucial role in tumor growth, many angiogenic and anti-angiogenic factors have been studied extensively in the quest for novel anti-cancer treatments. Some angiogenic factors stimulate endothelial cells to proliferate and migrate while others degrade the basement membrane (Cross and Claesson-Welsh 2001). Vascular Endothelial Growth Factors (VEGFs) are the most studied angiogenic factor family (Ferrara 2002). VEGF, also known as Vascular Permeability Factor (VPF), has been shown to induce angiogenesis in solid tumors. VEGF was originally discovered in the context of its ability to increase permeability of microvessels *in vivo*, and termed vascular permeability factor (Senger et al. 1983). To date, six members of the VEGF family have been identified: VEGF-A (VEGF), VEGF-B, VEGF-C, VEGF-D, VEGF-E (also called Orf virus VEGF), and PlGF (Veikkola et al. 2000). The physiological importance of VEGFs and VEGF receptors (VEGFRs) in blood vessel formation has been demonstrated with knockout mice (Ferrara et al. 2003). Targeted deletions of the VEGF (Carmeliet et al. 1996; Ferrara et al. 1996), VEGFR1 (Fong et al. 1995), and VEGFR2 genes (Shalaby et al. 1995) in mice resulted in embryonic lethal phenotypes due to their inability to form normal vasculature. In humans, VEGF and VEGFRs are abundantly expressed and play significant role in the neovascularization of glioma (Plate et al. 1992), neuroblastoma (Rossler et al. 1999), breast (Yoshiji et al. 1996), bladder (O'Brien et al. 1995), renal (Takahashi et al. 1994), and gastro-intestinal (Brown et al. 1993; Takahashi et al. 1995)

cancers. VEGF can be induced by hypoxia (Shweiki et al. 1992) and inhibit endothelial cell apoptosis through the PI3-kinase/Akt signaling pathway (Gerber et al. 1998). Due to the importance of VEGF in tumor angiogenesis, we selected the inhibition of the VEGF signaling pathway to test the normalization hypothesis.

Anti-angiogenic treatment

Anti-angiogenic therapy can potentially overcome the two main problems experienced by conventional chemotherapy – drug resistance and barriers to drug delivery. Anti-angiogenic therapy targets tumor endothelial cells, which are presumably derived from normal blood vessels or from circulating endothelial cells. Compared to cancer cells, endothelial cells are considered to have a lower turnover rate and are genetically more stable (Boehm et al. 1997; Kerbel 1997). Thus, patients treated with anti-angiogenic therapy are less likely to develop drug resistance. Furthermore, the target of many anti-angiogenic agents is the vascular lining, and these agents do not face the same transport barriers as conventional chemotherapeutic agents that target cancer cells. Since a large number of tumor cells depend on a small number of endothelial cells to supply nutrients and oxygen, anti-angiogenic treatment might also amplify the therapeutic effect. Finally, compared to chemotherapy or radiation therapy, anti-angiogenic therapies are less toxic (Folkman 1995).

VEGF is an attractive target for anti-angiogenic therapy because its receptors are expressed mostly on endothelial cells, and are upregulated on tumor endothelium compared to normal endothelial cells (McCarty et al. 2003). Several anti-angiogenic therapies that target VEGF/VEGFR activities, such as VEGF antisense (Cheng et al. 1996; Saleh et al. 1996), VEGF-toxin conjugate (Ramakrishnan et al. 1996; Arora et al.

1999), soluble VEGFR (Kendall and Thomas 1993), anti-VEGF mAb (Kim et al. 1993), anti-VEGFR2 mAb (Prewett et al. 1999), anti-VEGFR2 single-chain antibody (Zhu et al. 1998), VEGFR2 tyrosine kinase inhibitor (Fong et al. 1999), dominant negative anti-VEGFR2 mutant (Millauer et al. 1994), and a DNA vaccine against VEGFR2 (Niethammer et al. 2002) have been shown to inhibit tumor growth. DC101, a neutralizing monoclonal antibody, binds to the murine VEGFR2 receptor with high affinity and blocks ligand-induced receptor activation. It has been demonstrated that DC101 can inhibit or delay tumor growth in several human cancer xenografts (Prewett et al. 1999; Bruns et al. 2000; Kunkel et al. 2001), and spontaneous sarcomas and adenocarcinomas (Izumi et al. 2003). In this study, the effects of DC101 were investigated extensively as an anti-angiogenic agent. As for the translation part of the thesis, bevacizumab (Avastin) was used to treat patients with rectal adenocarcinoma. Bevacizumab is a monoclonal antibody targeting human VEGF. Various immunostaining studies were performed to test the validity of pre-clinical findings.

Vascular Normalization

While anti-angiogenic treatment alone seems promising, numerous studies also suggest that anti-angiogenic agents can potentiate the effects of radiation therapy and chemotherapy (Appendix 1 and 2). Encouraging results have demonstrated that combining anti-angiogenic therapy with either conventional chemotherapy or radiation therapy has additive or synergistic effects (Teicher 1996; Mauceri et al. 1998; Klement et al. 2000; Kozin et al. 2001). Interestingly, anti-VEGF treatment can enhance tumor oxygenation (Lee et al. 2000) and increase intratumoral uptake of therapeutic agent CPT-11 (Wildiers et al. 2003). In a recent clinical study, patients with colorectal cancers

showed improved response when treated with anti-VEGF antibody combined with cytotoxic agents (Hurwitz et al. 2004).

However, the results appear to be counter-intuitive initially. Anti-angiogenic therapy aims to starve off cancer cells by eliminating the tumor blood vessels. On the other hand, chemotherapy and radiation therapy rely on tumor blood vessels to transport cancer drugs and oxygen, respectively, to cancer cells. Therefore, anti-angiogenic therapy should further impede the delivery of therapeutic agents and reduce the effectiveness of conventional therapies. In 2001, the "normalization" hypothesis was put forward to explain this apparent paradox (Jain 2001). Anti-angiogenic therapy prunes the immature vessels in solid tumors and actively remodels the rest, leaving a more "normal" vasculature (Figure 2.3). It improves the integrity and function of the remaining network, which enhances the delivery of therapeutic agents. Thus, we hypothesize that the normalization of tumor blood vessels by anti-angiogenic agents can enhance drug delivery and the efficacy of cytotoxic agents.

Chapter 5: Material and Methods

The material and methods section is divided into five parts: i) animal models and therapeutic agents, ii) microscopy and iii) quantitative measurements and procedures, iv) histology, and v) molecular techniques.

5.1 Animal models and therapeutic agents

All animal models were developed using procedures carried out following the Public Health Service Policy on Humane Care of Laboratory Animals and approved by the Massachusetts General Hospital Institutional Review Board Subcommittee on Research Animal Care (MGH SRAC protocol 2004N000050, 2002N000138 and 2004N000002). The experiments were continuously monitored by the MGH veterinary staff. The mice were 8-10 weeks old. Unless otherwise specified, they were bred and maintained in our defined flora- and specific-pathogen-free animal colony.

5.1.1 Harvesting tumor cells

Tumor cells were harvested from either nude, C3H, or severe combined immunodeficient (SCID) mice with either human or murine tumors growing in the subcutaneous space. The mice were euthanized with an intraperitoneal injection of sodium pentobarbital (Fatal-Plus, 200 mg/kg). The incision was made, and the connective tissue surrounding the tumor was severed and the excised tumor was placed on a sterile plate. Tumors were then cut into small pieces (0.01 to 0.03 mm^3) and were ready for implantation. If tumor slurry was required for the particular experiment, the tumor was then minced with 0.05 ml of Hanks solution until the tissue had a paste-like texture. For this thesis work, multiple cell lines were used: MCaIV murine mammary carcinoma, U87 human glioblastoma, and LS174T human colon adenocarcinoma.

5.1.2 Dorsal skinfold chamber

The dorsal skinfold chambers were prepared as previously described (Leunig et al. 1992). The entire preparation was done under anesthesia (100 mg of ketamine hydrochloride/10 mg of xylazine per kg body weight intramuscularly) in aseptic conditions inside the animal colony. Briefly, the back of the mouse was shaved and hair was removed using hair removal cream. Two symmetrical titanium frames were stitched on to fix the extended double layer of dorsal skin between the frames. Roughly 15 mm diameter of skin was removed from one side, leaving the opposite side of the skin, striated muscle and subcutaneous tissue intact. The fascia was carefully removed, and a cover glass was mounted into the frame. The animals were allowed for at least one day of recovery before using them in experiments.

5.1.3 Cranial window

The procedure of cranial window preparation was described in previous studies (Yuan et al. 1994). The entire preparation was done under anesthesia (100 mg of ketamine hydrochloride/10 mg of xylazine per kg body weight intramuscularly) in aseptic conditions inside the animal colony. A stereotactic apparatus was used to fix the head of the mouse. The skin of the frontal and parietal regions of the skull was cleaned and removed in a circular manner on top of the skull. Using a small high speed air-turbine drill, a 6 mm diameter circle was drilled on the skull. Cold saline was applied to the skull during the drilling process to avoid thermal damage to the brain. When the bone flap became loose, a blunt blade was used to remove the bone flap. The dura membrane was cut completely from the surface of both brain hemispheres. Finally, a cover glass was glued on the bone to cover up the brain. A few days after the surgery, the cover glass was removed. With a 23G needle, a path was made under the surface of the brain

adjacent to the sagittal sinus. A piece of tumor tissue was inserted inside the brain through the path. A new cover glass was glued on.

5.1.4 Spontaneous tumor model

C3H mice were maintained in the animal colony and allowed to live their normal life span. Aged C3H mice were screened weekly for tumor development. The experiments were started when tumors became visible and palpable.

5.1.5 Anti-VEGFR2 monoclonal antibody, DC101

Rat anti-mouse VEGFR2 monoclonal antibody DC101 was developed and provided by ImClone Inc., and negative control polyclonal rat IgG was purchased from Jackson ImmunoResearch Laboratories. DC101 or control IgG was given at 40 mg/kg every 3 days i.p., unless otherwise noticed.

5.2 Microscopy

5.2.1 Intravital microscopy

Light from a mercury lamp was directed into the objective lens and then into the sample through a dichroic mirror. Fluorescence emission was collected by the same objective lens. After passing through the appropriate band pass filter, the signal was collected by a CCD camera. The CCD camera was connected to a signal amplifier and a computer. The image was capture using NIH Image (NIH, Bethesda, MD).

5.2.2 Confocal laser scanning microscopy

The confocal laser scanning microscopy allows three-dimensionally resolved imaging using a confocal aperture to reject fluorescence light that originates from outside of the focal plane. Briefly, the confocal microscopy (Olympus) was equipped with three

different laser sources. The laser beams were focused into the samples through objective lens. A z-stepper motor allowed 3D imaging by taking a stack of 2D optical sections.

5.2.3 Two photon laser scanning microscopy

Two photon microscopy enables one to acquire 3D sub-micron resolution images (Brown et al. 2001). Briefly, a tunable MilleniaX-pumped Tsunami Ti:Sapphire laser (Spectra-Physics, Mountain View, CA) was directed into a Zeiss microscope (Zeiss, Jena, Germany) through a galvanometer-driven x-y scanner (MRC600, Bio-Rad, Hemel Hempstead, England). The laser light entered through the side and was deflected into the objective lens by a dichroic mirror. A piezo-driven stepper motor was used to adjust axial position during data acquisition. Fluorescence emission was collected through the same objective lens using photomultiplier tubes (HC125-02 PMTs, Hamamatsu Photonics, Bridgewater, NJ).

5.3 Quantitative measurement and procedures

5.3.1 Angiography

FITC-dextran 2M MW (Sigma) or Rhodamine-dextran 2M MW was used to trace blood vessels *in vivo*. Prior to imaging, the mouse was anesthesized using ketamine/xylazine solution, and was injected 0.1 ml of fluorescent dye by tail vein cannulation. Extra care was given to ensure no air bubbles were injected into the blood circulation. The animals with either dorsal skinfold chambers or cranial windows were then fixed and stabilized on specially designed plates for imaging.

5.3.2 Analysis of intravital microscopy images

Vascular density and diameter calculation were performed using NIH Image. Briefly, vessels were traced and diameter was determined for each individual vessel. Vascular volume density was calculated by assuming the vessels were cylindrical shape.

5.3.3 Permeability measurement

The effective vascular permeability was measured using cyanine-5-labeled BSA (Cy5 Bis NHS Ester, Amersham Biosciences Corp., Piscataway, NJ) or Tetramethylrhodamine (TRITC) BSA (Molecular Probes, A23016), according to published methods (Yuan et al. 1993; Yuan et al. 1994). The extravasated fluorescent BSA signal at a given region in the tumor was measured and quantified every two minutes for 23 minutes immediately after the injection. Measurements were done both before and three days after the injection of DC101 in the same tumor region. A macro computer program was used to quantify the rate of extravasation of BSA normalized by the density of blood vessels in the same region.

5.3.4 Red blood cell velocity measurement

Red blood cell (RBC) velocity was measured using the line-scan method (Brown et al. 2001). Under fluorescent microscopy and two photon microscopy, RBCs appear as dark spots in the vessel because the cells absorb the fluorescent signal. By scanning the same location (same line) repeatedly at a known speed, the rates of RBCs passing through the vessels were calculated.

5.3.5 Interstitial fluid pressure measurement using wick-in-needle technique

Tumors were implanted subcutaneously into the hind legs of mice. Interstitial fluid pressure (IFP) was measured when the tumors reach a mean diameter of 6 mm. IFP was measured using the wick-in-needle technique (Fadnes et al. 1977; Boucher et al. 1991)

before and during DC101 treatment. In brief, 23-gauge needles with a 2-3 mm side-hole at 4-5mm from the tip were filled with surgical sutures (6-0 Ethilon) to increase the contact area and improve fluid communication. The needle was connected to a pressure transducer (Model P23XL; Spectramed Inc., Oxnard, CA) through polyethylene tubing filled with sterile, heparinized (70 units/ml) saline. The pressure transducer was connected to a preamplifier (Model 11-G4113-01; Gould, Inc., Cleveland, OH), and the signal was sent to an analogue-to-digital converter (Powerlab 4/20; ADInstruments, Colorado Springs, CO). A measurement was acceptable when the pressure measurements following compression and decompression did not differ by more than 15%, as this ensured that the fluid communication was satisfactory. The pressure was determined from the stable values after compression and decompression. For each time point, IFP was measured in two different tumor regions.

5.3.6 Micropipette preparation

Capillary tubing was used (0.86 mm o.d.; 0.38 mm i.d.) to make micropipettes with a horizontal pipette puller (Narishige PN-3; Narishige International USA, Inc., Long Island, NY). The inner tip diameter was grinded to around 2.5 micron. The micropipettes were filled with 1M NaCl solution.

5.3.7 Microvascular and interstitial fluid pressure measurements using micropipette technique

MCaIV tumors were implanted in the dorsal skinfold chambers of SCID mice. The dorsal skinfold chamber provides a stable and easy access environment for IFP and MVP measurements using the micropipette technique (Boucher and Jain 1992). Since the success rate was quite low for this type of measurement, and the measurement was a

rather invasive one, only one time point (3 days after the injection of DC101/control IgG) was measured. For each mouse, several measurements were made for both MVP and IFP. Briefly, after anesthetizing the animals, tumors in the dorsal skinfold chambers were continuously flushed with warm saline to keep the tumors at body temperature and wet throughout the measurements. The pressure measurements were performed using micropipettes and a servo-null device (Model 5; Instrumentation for Physiology and Medicine, Inc., San Diego, CA).

A graded micromanipulator (Model 385, Spectra Physics, Mountain View, CA) was used to maneuver the micropipette and to measure the depth of insertion. Micropipettes were inserted inside and outside the tumor blood vessels to measure MVP and IFP, respectively. For IFP measurement, the micropipette was inserted at 0.5 to 1 mm from the surface of the tumor. The micropipette was positioned to penetrate the tumor perpendicularly. The insertion process was aided by the use of a stereomicroscope (Nikon SMZ-1; Charles Seifert Associates, Carnegie, PA). Each day before the measurement, the system was calibrated using a water column that can generate known pressures. The pressure was adjusted to zero in the saline film covering the tumor surface. The IFP measurement was accepted when (a) no visible distortion of the tumor or skin surface was observed, (b) fluid communication between the micropipette and the interstitial fluid was demonstrated electrically, (c) zero pressure in the saline film on the tumor surface was recorded both before the insertion and after the withdrawal of the micropipette from the tumor.

For the MVP measurement, 1M NaCl solution with Evans blue dye was introduced in the micropipettes by capillary action. Micropipettes were introduced perpendicularly to the

vascular wall (Boucher and Jain 1992). The pressure measurement was acceptable when the criteria (a) through (c) were satisfied. Furthermore, there was no significant modification of RBC velocity during the insertion of the micropipettes. The injection of Evans blue dye was used to confirm that the micropipettes were inserted inside the vessels, and there was blood flow within the vessels.

5.3.8 Plasma oncotic pressure measurement

For each animal, around 150 μL of blood was drawn using heparinized-coated capillary tubes (Fisher Scientific, Pittsburg, PA) through the venous sinus of the eyes without the use of anesthesia (Stohrer et al. 2000). The blood sample was immediately transferred to a 2-ml centrifuge tube. After centrifugation at a force of 1500g for 10 minutes, 8 μL of plasma fluid was collected for oncotic pressure measurements. To minimize any evaporation of the plasma fluid, the measurement was done immediately after the collection of fluid. A membrane colloid osmometer was used to measure oncotic pressure (Aukland and Johnsen 1974; Stohrer et al. 2000). Ultrafiltration membranes (Amicon PM10, Millipore Corp., Bedford, MA) with a molecular weight cutoff of 10,000 g/mole were used. Samples were applied on the membrane, and saline was loaded on the other side of the membrane. The osmometer was connected to a pressure transducer, a pre-amplifier, and then to a computer.

5.3.9 Interstitial fluid oncotic pressure measurement

Interstitial fluid was collected using the chronic wick technique (Kramer et al. 1986; Wiig et al. 1991). The wick was washed with acetone and ethanol, and was soaked in saline overnight. A long wick (~5 cm) was implanted together with the tumor in the flank region of SCID mice. After two weeks the wick was completely covered by the tumor

mass. The wick was collected post mortem to prevent bleeding or staining of the wick with blood. The entire process was done as quickly as possible to avoid any evaporation. Any portion of the wick that was stained with blood was cut off, and the remaining portion of the wick was quickly transferred to a centrifuge (Johnsen 1974). Around 8 μL of supernatant was used for the measurement. An osmometer was used to measure interstitial oncotic pressure.

5.3.10 Functional lymphatic assay

To identify functional lymphatic vessels in tumors, ferritin microlymphangiography and LYVE-1 immunostaining were performed according to published methods (Leu et al. 2000; Padera et al. 2002). Briefly, a total of 5 μL of ferritin (F4503, Sigma-Aldrich Corp., St. Louis, MO) was injected slowly into the subcutaneous MCaIV tumors in the hind legs of mice at three different locations over a period of five minutes. One hour after the injection, tumor tissues were fixed and embedded in paraffin sections. Any LYVE-1 positive lymphatic vessels containing ferritin were considered as functional lymphatic vessels.

5.4 Histology

5.4.1 Tissue preparation and sectioning

Mice were perfused and fixed with 4% paraformaldehyde to maintain vessel morphology. Briefly, mice were anesthesized with ketamine/xylazine solution. Other preparations were performed at that time depended on the experiments. For example, functional vasculature was labeled by injecting 0.1 ml of biotinylated lectin (Vector Laboratories). To perfuse the fixative, animals were pinned to a dissection block, and a small incision was made to open up the skin and ribs and to expose the beating heart and lungs. The

heart was held using forceps, and a small incision was made at the apex of the heart. A cannula was inserted through the incision, and 4% paraformaldehyde was pumped at 80 – 120 mmHg for 5 minutes. The tissues of interest were then prepared in one of the following procedures: i) to prepare for frozen blocks, the tissues were put in 4% paraformaldehyde for 3 hours, and then 30% sucrose overnight at 4°C. The tissues were then embedded in OCT solution (Sakura Finetek, California) at -20°C ; ii) to prepare for paraffin blocks, the tissues were transferred to formalin, and were embedded in paraffin using standard procedures at the MGH Pathology Department.

5.4.2 IHC protocol for αSMA and lectin double staining on thick frozen section

80 microns thick sections were cut using a cryostat. To remove OCT, the tissues were rinsed in PBS for 3x30 minutes. The tissues were then blocked with 3% BSA + 0.1% Triton-X for 1.5 hour at room temperature. The tissues were stained with streptavidin-conjugated fluorochrome (Alexa 488 or Alex 647, Molecular Probes) to label biotinylated-lectin perfused blood vessels for 90 minutes. The tissues were then rinsed in PBS for 3x30 minutes. The tissues were incubated at 4°C overnight with Cy-3 conjugated αSMA antibodies (Sigma). The sections were then put on coverslip with VectaShield.

5.4.3 IHC protocol for Collagen IV and lectin double staining on thick frozen section

80 microns thick sections were cut using a cryostat. To remove OCT, the tissues were rinsed in PBS for 3x30 minutes. Then the tissues were blocked with 3% BSA + 0.1% Triton-X for 1.5 hour at room temperature. The tissues were stained with streptavidin-conjugated fluorochrome (Alexa 488 or Alex 647, Molecular Probes) to label biotinylated-lectin perfused blood vessels for 90 minutes. The tissues were then rinsed in

PBS for 3x30 minutes. The tissues were incubated at 4°C overnight with rabbit anti-collagen IV (1:2000; Chemicon). Subsequently, the tissues were stained with Cy3-conjugated secondary antibodies (1:200, Jackson ImmunoResearch). The sections were then put on a coverslip with VectaShield.

5.4.4 IHC protocol for αSMA and CD31 double staining on paraffin section

1. Deparaffinize and rehydrate sections through graded ethanol baths to water.
    a. 2x3 minutes in xylene
    b. 2x3 minutes in 100% ethanol
    c. 2x3 minutes in 96% ethanol
    d. 2x3 minutes in 70% ethanol
    e. 2x3 minutes in H_2O
2. Antigen retrieval: dilute 10x DAKO Target Retrieval Solution 1:10 with dH_2O.
    a. microwave at full power for 4 min;
    b. microwave at 10% (level 1) power for 6 min.
    c. cool for 20 min, then rinse in PBS 3x3 min.
3. Block endogenous peroxidase activity: Incubate slides in 3% H_2O_2 for 5 min.
4. Rinse in PBS for 3x3 minutes.
5. Block tissue with 3% BSA for 30 minutes.
6. Blot and apply CD31 antibody. Incubate for 30 min at room temperature.
7. Rinse in PBS for 3x3 minutes.
8. Apply HRP-labeled polymer (bottle 2 from EnVision kit). Incubate at room temperature for 30 min.
9. Rinse in PBS for 3x3 minutes.

10. Develop stain with DAB (1 drop substrate in 1 ml buffer). Monitor intensity under microscope then place slides in water to terminate reaction.
11. Rinse in PBS for 3x3 minutes.
12. Apply Doublestain Block (double staining Envision kit) for 5 min.
13. Apply mouse anti-human αSMA (DAKO, 1:5000). Incubate at 4°C overnight
14. Rinse in PBS for 3x3 minutes.
15. Apply AP-labeled polymer (double staining Envision kit).
16. Develop color with Alkaline Phosphatase Substrate Kit 1 (Vector Lab., SK5100)
    a. Add 2 drops of Reagent 1 to 5 ml of 100 mM Tris-HCl, pH 8.2-8.5 buffer (stock: Sigma T3038), mix well.
    b. Add 2 drops of Reagent 2 and mix well.
    c. Add 2 drops of Reagent 3 and mix well.
    d. Monitor reaction under microscopy (20 min). Terminate reaction in dH2O
17. Counterstain with hematoxlyin
18. Coverslip using Faramount (DAKO)

5.4.5 IHC protocol for LYVE-1 and ferritin staining

1. Deparafinize and rehydrate sections. Same procedure as described earlier.
2. Antigen retrieval. Same procedure as described earlier.
3. Rinse in TBS-T for 3x3 minutes.
4. TBST recipe:
    a. 0.05 M Tris
    b. 0.3 M NaCl

c. 0.1% Tween-20

5. Block endogenous peroxidase activity. Same procedure as described earlier.
6. Rinse in TBS-T 3x3 minutes.
7. Block tissue with 3% BSA solution in TBS-T at room temperature for 1 hour.
8. Incubate for 2 hours with Rabbit anti-mouse-LYVE-1 (from E. Rousalhti) (1:500) dilution in TBS-T/1% BSA at room temperature.
9. Rinse in TBS-T 3x3 minutes.
10. Incubate for 30 minutes in anti-rabbit labeled polymer (DAKO Envision Plus) @ RT.
11. Rinse in TBS-T 3x3 minutes.
12. Develop for 5'-10' with liquid DAB from DAKO Envision Plus kit. Stop with H2O.
13. Rinse in H2O 3x3 minutes.
14. Incubate with 50:50 solution of 20% HCl and 10% Potassium Ferrocynate for 40 minutes in humidified chamber @RT for Prussian Blue stain.
15. Rinse in H2O 3x3 minutes.
16. Stain with Hematoxylin (Fisher Gill's #2) (4 dips)/Rinse H2O/Scott's Water (4 dips)/Rinse in H2O.
17. Mount sections in DAKO Faramount Aqueous.

5.4.6 IHC protocol for Ang-2 staining

1. Deparafinize and rehydrate sections. Same procedure as described earlier.
2. Antigen retrieval. Same procedure as described earlier.
3. Rinse in PBS for 3x3 minutes.

4. Block endogenous peroxidase activity. Same procedure as described earlier.
5. Block tissue with 3%BSA for 1 hour.
6. Blot and apply primary antibody, goat-anti-human-Ang2 (1:200, R&D). Incubate at 4°C overnight.
7. Rinse in PBS for 3x3 minutes.
8. Incubate for an hour with rabbit anti-goat IgG HRP (1:200, DAKO) for an hour
9. Rinse in PBS 3x3 minutes.
10. Develop the color with DAB.
11. Rinse in H_2O for 3x3 minutes.
12. Counterstain with hematoxylin as described earlier.
13. Mount sections in DAKO Faramount Aqueous.

5.4.7 Macromolecule penetration assay

0.1 ml of TRITC-BSA (Molecular Probes) was injected intravenously one hour before perfusion fixation in tumor bearing mice. Biotinylated lectin was also injected 5 minutes before fixation. Three 10 μm thick frozen sections, 50 μm apart, were prepared from each tumor block. Images were taken with the two photon microscope. Perfused biotinylated lectin was used to identify functional vessels, and extravasation pattern of TRITC-BSA was analyzed using a program written in ImageJ. Briefly, ten concentric rings of 3.25 μm thickness were drawn starting at the vessel wall. Average intensity was calculated within each ring, and the intensity profile was fitted to an exponential decay function ($I = Ae^{-Bx} + C$; I = pixel intensity; x = distance from vessels; B = decay constant). The decay constants were compared between the two treatment groups.

5.4.8 Pimonidazole staining for tumor hypoxia

To detect tumor hypoxia, 60 mg/kg pimonidazole was injected i.v. 1 hour before brains were rapidly frozen at -80°C. The Hypoxyprobe-1 Kit (Chemicon) was used to detect pimonidazole-protein adducts in 2 brain regions per animal spaced 200 micron apart (n = 3 or 4 animals per group).

5.5 Molecular techniques

5.5.1 RNA isolation

Tumor tissues were isolated from animals and frozen down immediately using liquid nitrogen. Tissues were homogenized in 0.75 ml of TRIZOL LS Reagent (Life Technologies, Cat No. 10296-010). The homogenized samples were incubated for 5 minutes at 15 to 30°C to permit the complete dissociation of nucleoprotein complex. 0.2 ml of chloroform was added, and after shaking vigorously by hand for 15 seconds, the samples were centrifuged and RNA was collected in the aqueous phase. RNA was precipitated from the aqueous phase by mixing with isopropyl alcohol. Upon centrifugation, a RNA pellet was obtained. After several steps of washing and drying, RNA was dissolved using RNase-free water and the purity of RNA was checked and confirmed by UV spectrophotometer and electrophoresis.

5.5.2 Protein isolation

Frozen tumors were dissolved in 1 ml of RIPA buffer (Sigma), with 1:50 protease inhibitor cocktail (Sigma) and 1:50 phosphatase inhibitor cocktail 2 (Sigma). The tissues were homogenized using a syringe. 200 µl of homogenized solution was then mixed with 800 µl of lysis buffer (RIPA with the inhibitors). The homogenized solution was

centrifuged, and the pellet was discarded. To measure protein concentration, BioRad Protein Assay was used:

1. 5 μL of sample per well (always do duplicate).
2. 1 mL of A + 20 μL of S → add 25 μL/well.
3. Add 200 μL of B in each well
4. Wait for 15 min (in the dark); do reading afterward.
5. Use BSA & BGG Protein Assay Standard Sets (Pierce 23208) as standard.

5.5.3 Gene array analysis

Angiogenic gene array was purchased from SuperArray, and the experiment was performed following the GEArray Q and Series Kits protocol. Briefly, cDNA was prepared by the reverse transcription reaction, following by the linear polymerase reaction. The DNA probe was blocked by sheared salmon sperm at 100°C for 5 min, and cDNA was applied to the gene array membrane for hybridization overnight. After a series of washing steps, the probe was detected by adding chemiluminescent molecules. Gene expression from each group was normalized by cytoplasmic β-actin expression.

5.5.4 Real-time PCR analysis

The RT-PCR was performed according to SuperScript III First-Strand Synthesis System protocol provided by Invitrogen and standard PCR protocol. The fluorescently labeled primers were designed using LUX primer designer and ordered from Invitrogen.

5.5.5 Western blot

Protein was first denatured at 100°C for 5 minutes. Then it was put on ice immediately. After centrifugation, only the supernatant was collected for loading on the gel. 4-12% NuPAGE Bis-Tris Gel (InVitrogen) was used for the Western blot. Samples were loaded

on the gel, and the gel was run at 120V for an hour. Next, the proteins were transferred to a transfer membrane using the gel box in NuPAGE transfer buffer (InVitrogen) at 30V for an hour. After the transfer reaction, the membrane was washed 3 times with TBST. The membrane was then block using 5% milk in TBST for 2 hours. Primary antibody was then added and incubated overnight at 4°C. On the next day, the membrane was washed and shaken vigorously for an hour. Secondary antibody (HRP IgG) was added and incubated for an hour. After another round of washing, the membrane was stained using ECL Western Blotting Analysis System (Amersham Bioscience) and film was developed in the dark room.

Chapter 6: Vascular Structure in Tumors

Portions of this chapter have been taken from:

Tong, R. T., Boucher, Y., Kozin, S. V., Winkler, F., Hicklin, D. J., and Jain, R. K. (2004). Vascular normalization by vascular endothelial growth factor receptor 2 blockade induces a pressure gradient across the vasculature and improves drug penetration in tumors. *Cancer Res* 64, 3731-3736.

Winkler, F.*, Kozin, S. V.*, **Tong, R. T.**, Chae, S. S., Booth, M. F., Garkavtsev, I., Xu, L., Hicklin, D. J., Fukumura, D., di Tomaso, E., Munn, L. L., and Jain, R. K. (2004). Kinetics of vascular normalization by VEGFR2 blockade governs brain tumor response to radiation; Role of oxygenation, angiopoietin-1, and matrix metalloproteinases. *Cancer Cell* 6, 553-563. * These authors contributed equally.

Introduction

The current treatment of solid tumors is plagued by two problems: physiological barriers impair the delivery of therapeutic agents in optimal quantities, and genetic and epigenetic mechanisms contribute to drug resistance. Anti-angiogenic therapy has the potential to overcome or circumvent these problems. The result from a recent Phase III clinical trial provided the first clinical proof of the efficacy of anti-angiogenic therapy in the treatment against cancer. The combination of Avastin — a monoclonal antibody against VEGF — with conventional chemotherapy increased disease-free survival by 5 months in colorectal cancer patients compared to conventional therapy alone (Hurwitz et al. 2004). Before this clinical study, Beverly Teicher first proposed that the combined administration of an anti-angiogenic agent with a cytotoxic agent would yield the maximum benefit in eradicating tumors (Teicher 1996). The rationale was that cytotoxic agents would kill the cancer cells directly, while anti-angiogenic therapy targets the tumor endothelial cells. Thus, these two therapies aim to destroy two separate compartments of tumors. However, this explanation presents an apparent paradox. While anti-angiogenic therapy aims to target tumor blood vessels, chemotherapy and radiation therapy rely on tumor blood vessels to transport cancer drugs and oxygen molecules, respectively, to cancer cells. Thus, one would expect anti-angiogenic therapy would comprise the delivery of cytotoxic agents. To resolve this paradox, Dr. Rakesh Jain hypothesizes that anti-VEGF antibody can improve the delivery of cytotoxic agents to tumors by normalizing tumor vasculature and thus increases the effectiveness of combination therapy (Jain 2001). Tumor blood vessels are leaky, tortuous, dilated, and have heterogeneous distribution. Perivascular cells, which provide support to endothelial

cells, are often loosely associated with endothelial cells in tumors. Similarly, the basement membrane is often abnormal in tumors. Some vessels lack basement membrane coverage, while others have abnormally thick basement membrane. To test this hypothesis, we first examined the structural changes of the vascular architecture as well as of the vascular wall during anti-angiogenic treatment. The first part of my thesis examined the structural modification of tumor vasculature by DC101, an anti-VEGFR2 monoclonal antibody. Using two photon microscopy, dynamics of tumor blood vessels were examined *in vivo*. This was followed by examination of vascular wall integrity by performing immunostaining for perivascular cell and basement membrane.

Results

DC101 normalizes the architecture of the tumor vasculature.

In order to study the dynamic changes during anti-angiogenic therapy, we implanted tumors in chronic window models such as dorsal skinfold chamber and cranial window, and imaged the vessels using two-photon microscopy. Chronic windows allow us to non-invasively observe the formation of blood vessels and the effects of anti-angiogenic agents on tumor vasculature. Two photon microscopy can capture high resolution three dimensional tumor blood vessels images. Functional blood vessels were visualized under two photon microscopy by injection of fluorescent molecules (FITC-Dextran 2M MW) i.v. systemically. Figure 6.1 showed blood vasculature in normal striated muscle and murine mammary carcinoma, MCaIV, implanted in the dorsal skinfold chamber of SCID mice.

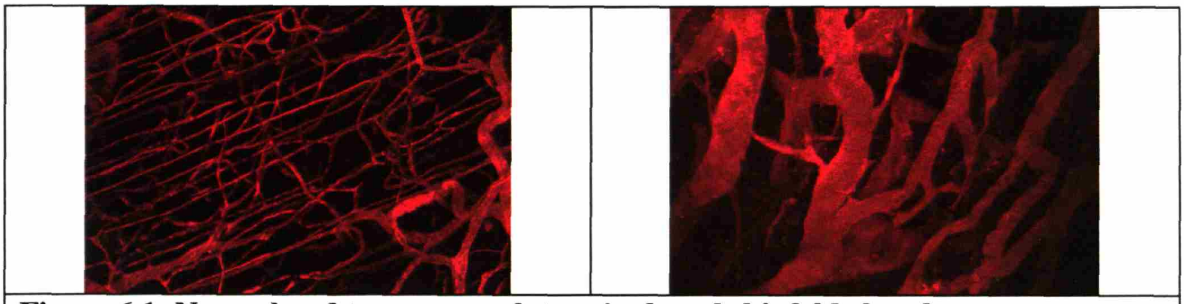

Figure 6.1: Normal and tumor vasculature in dorsal skinfold chamber.

Vasculature of (left) striated muscle and (right) MCaIV murine mammary carcinoma implanted in the dorsal skinfold chamber of mice. Tumor blood vessels were dilated, tortuous and heterogeneously distributed when compared to normal tissue. Image width: 500 microns.

Similarly, Figure 6.2 showed blood vessels of normal brain and human glioblastoma, U87, implanted in the cranial window of nude mice. As shown in right panel of Figure 6.2, tumor induced the growth of new blood vessels from the surrounding normal tissue. Tumor vessels were often dilated and tortuous when compared to normal blood vessels.

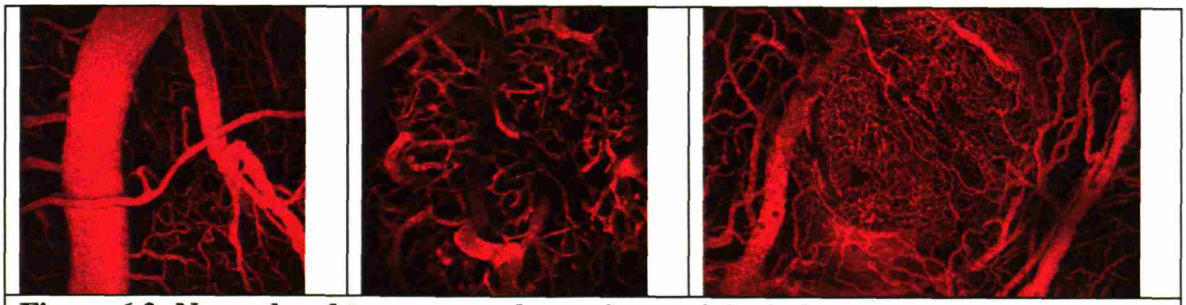

Figure 6.2: Normal and tumor vasculature in cranial window.

Vasculature of (left) normal brain and (center, right) U87 human glioblastoma implanted in the cranial window of mice. The right panel is a low resolution image in which the entire tumor vasculature can be observed. Image width: left and center: 700 microns; right: 2 mm.

To examine the effects of DC101 on the morphology of blood vessels, MCaIV murine mammary carcinoma was implanted in the dorsal skinfold chambers. We monitored the

same region of the tumor over 6 consecutive days using two-photon microscopy. This technique allows us to image up to 200 μm deep from the tumor surface with 1 μm resolution (Brown et al. 2001). In contrast to skeletal muscle, which had an organized vasculature with a relatively smooth vascular wall and uniform diameter (Figure 6.1), untreated MCaIV tumors had tortuous vessels with abrupt changes in vessel diameter. In MCaIV tumors treated with control IgG, the vessels became more dilated with time (Figure 6.3). While some vessels disappeared, most vessels either increased in size or remained the same size.

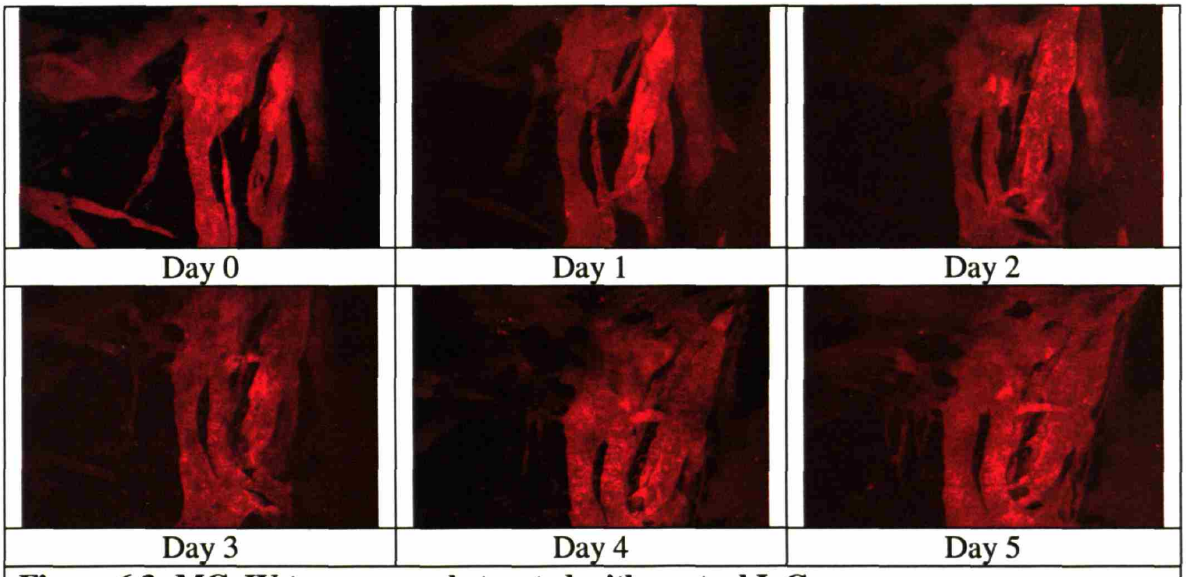

Figure 6.3: MCaIV tumor vessels treated with control IgG.

The images were taken over a period of 6 days. Image width = 500 microns.

On the other hand, after DC101 treatment, many vessels were either pruned or had a reduced diameter (Figure 6.4). Furthermore, many of these vessels also became less tortuous as they reduced in diameter. By day 5, some of these vessels regressed completely in some regions. Similarly, the vessels at the tumor-host interface also became less tortuous.

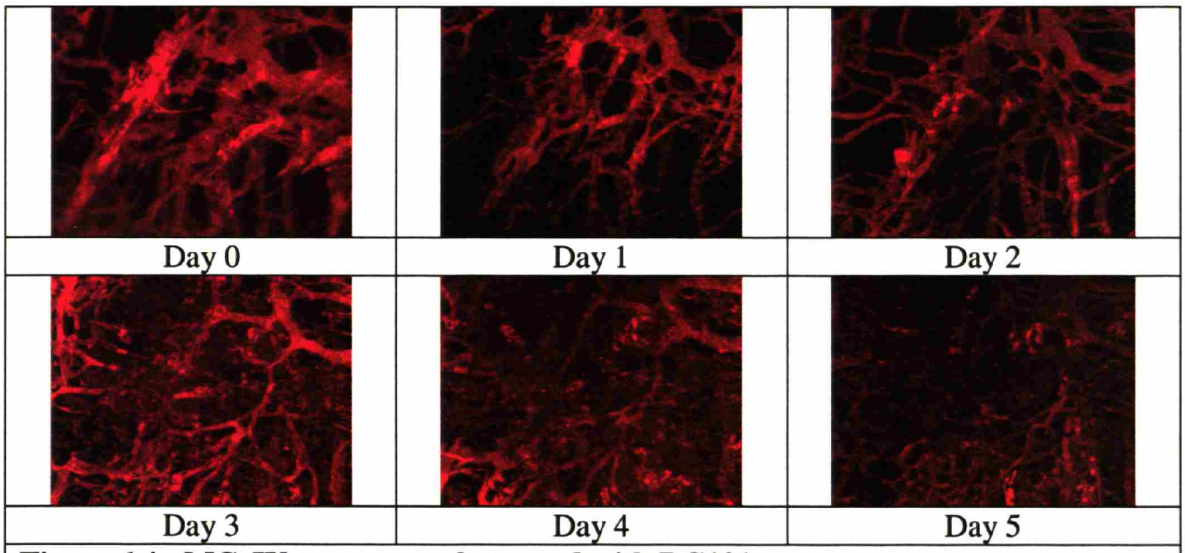

Figure 6.4: MCaIV tumor vessels treated with DC101.

The images were taken over a period of 6 days. Image width = 333 microns.

Similar striking vascular changes were also observed in the human colon adenocarcinoma LS174T (Figure 6.5). Thus, the two photon images showed that DC101 "normalizes" the architecture of the vascular network prior to complete regression.

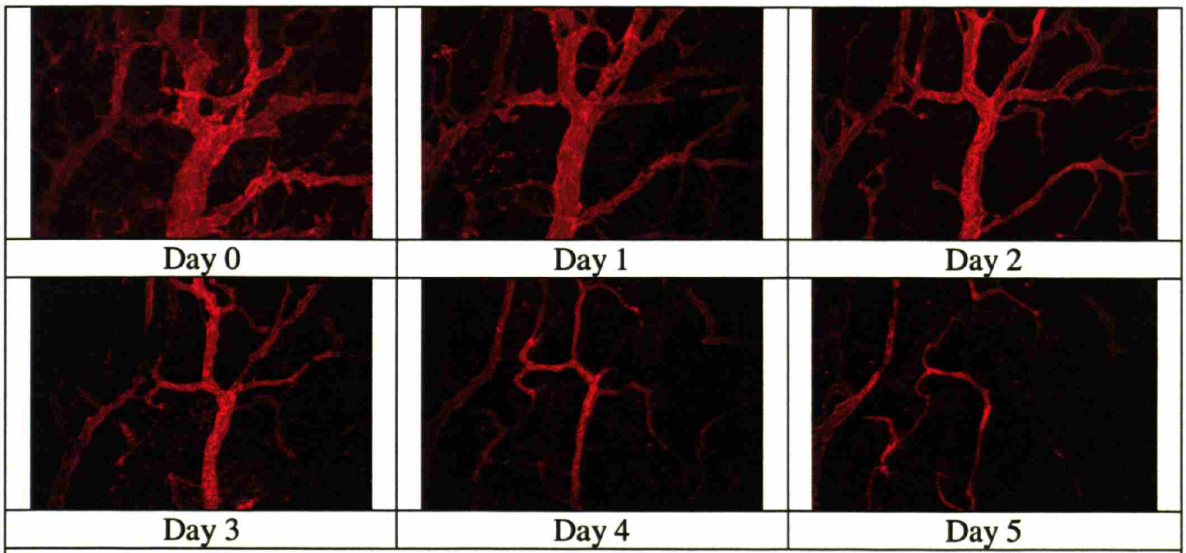

Figure 6.5: LS174T tumor vessels treated with DC101.

The images were taken over a period of 6 days. Image width = 333 microns.

Based on *in vivo* angiogram, we quantified the changes of vascular density and diameter after DC101 treatment (Figure 6.6). Three days after a single injection of DC101,

vascular length density decreased significantly from 58.8 ± 2.2 cm/cm^2 (vessel centerline length/image field; mean ± S.E.M.) to 41.9± 3.0 cm/cm^2. Similarly, DC101 lowered vascular diameter from 51.1 ± 3.7 μm to 32.2 ± 4.0 μm.

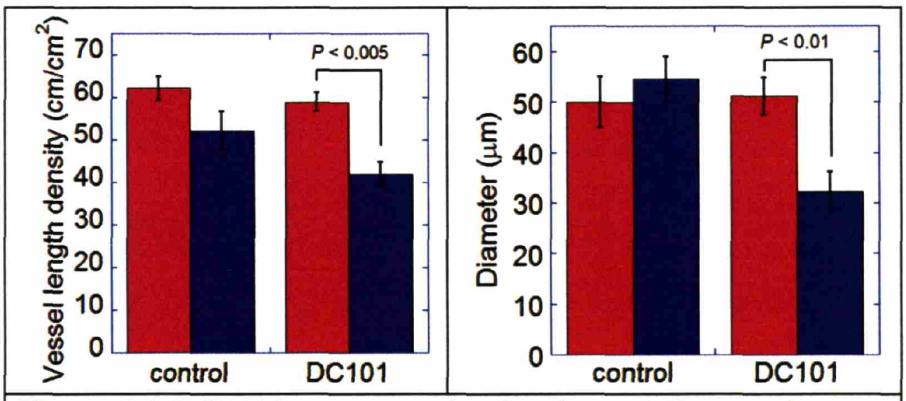

Figure 6.6: DC101 lowers vascular density and diameter in MCaIV tumors.

The quantification was done before (red) and three days after control IgG/DC101 treatment (blue).

By quantifying the number of vessels based on their diameters, the result showed that MCaIV had a significant number of extremely dilated vessels (Figure 6.7). However, after DC101 treatment, these vessels became smaller in diameter, and the overall distribution of vessel diameter shifted to one that was more similar to normal vasculature, in that the majority of the blood vessels (i.e. capillaries) had smaller diameters (F test. $P < 0.0001$).

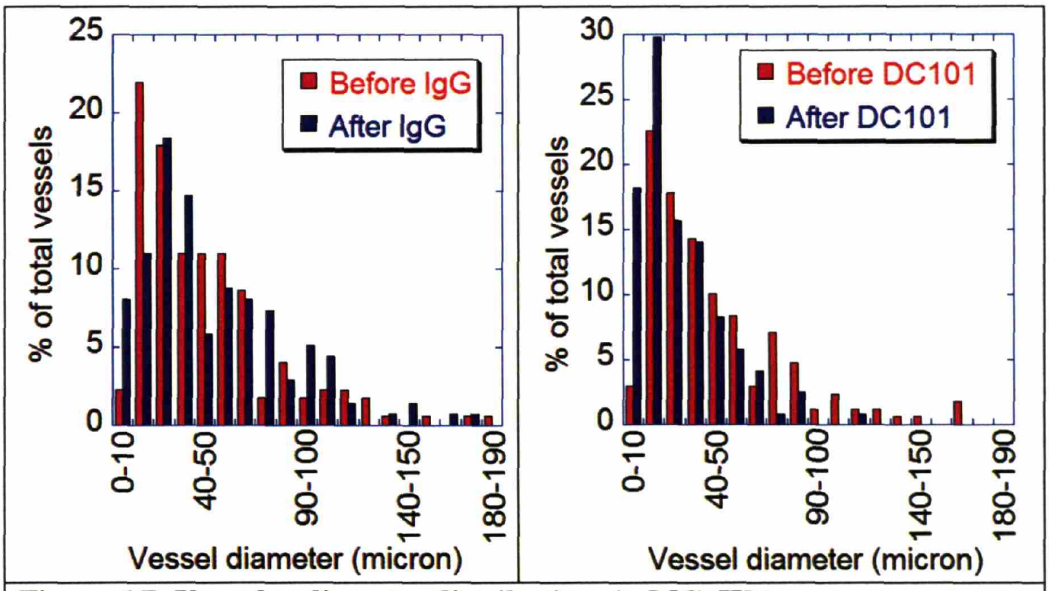

Figure 6.7: Vascular diameter distributions in MCaIV tumors.

Vessel diameters before and 3 days after control IgG (left) or DC101 (right) treatment. DC101 significantly altered the distribution of vessel diameter (F test. $P < 0.0001$)

To further verify the changes in tumor vasculature by DC101, another tumor model was used. In this model, U87 human glioblastoma tumor was implanted inside the brain of nude mice under cranial windows. The tumor was implanted about 100 μm beneath the surface of the brain. Treatment began when the tumors reached about 2 mm in diameter. Similar to the findings of MCaIV tumors, DC101 significantly reduced vascular density, volume density (assuming the vessels are cylindrical in shape), and vascular diameter in the U87 orthotopic tumor model (Figure 6.8).

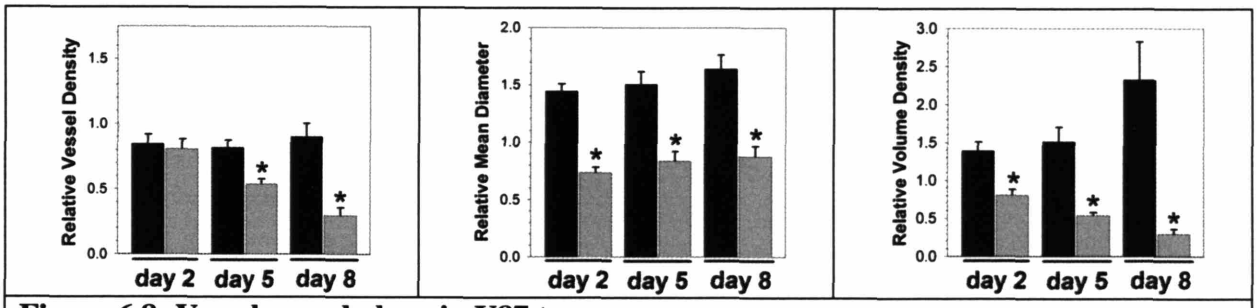

Figure 6.8: Vessel morphology in U87 tumors.

DC101 decreased vessel density, vascular diameter, and vessel volume density. * $P < 0.05$

DC101 improved perivascular cell coverage

In addition to vascular architectural abnormalities, the tumor vasculature was characterized by a paucity of, or abnormalities in, mural cells and basement membrane (Morikawa et al. 2002; Abramsson et al. 2003; Jain 2003). To test whether DC101 also normalizes the wall structure, we perfused the tumors with FITC-CD31 to label functional blood vessels and stained frozen sections for Cy3-αSMA, which labeled perivascular cells. In normal tissue, blood vessels were completely covered by αSMA-positive cells (Morikawa et al. 2002). In the left panel of Figure 6.9, αSMA-positive cells circumferentially covered endothelial cells in the arteriole. In MCaIV tumors, the organization of perivascular cells was completely different. Perivascular cells scattered along the blood vessels, and were loosely associated with endothelial cells. The cells also had extended cytoplasmic processes into the tumor tissue. While most of the vessels were covered by αSMA-positive cells, some vessels were completely devoid of perivascular cell coverage, as shown in the center panel of Figure 6.9.

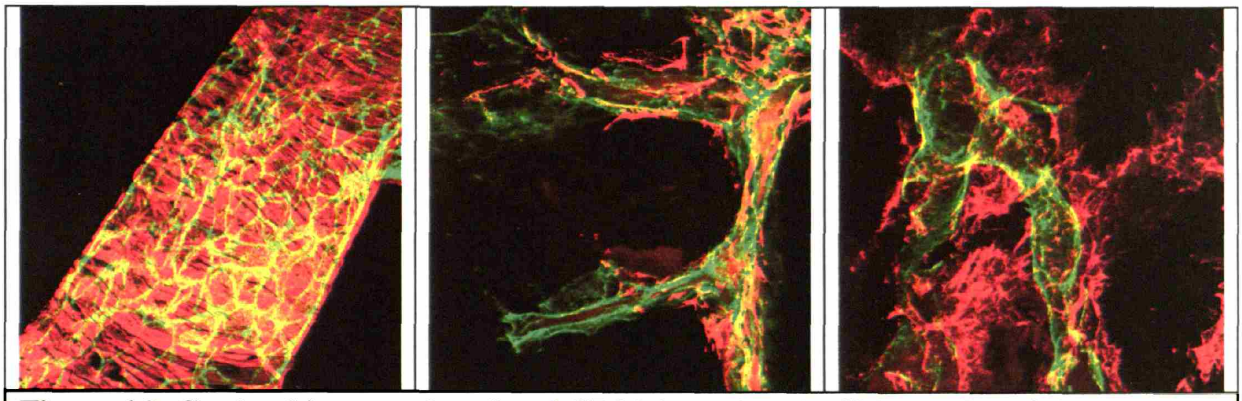

Figure 6.9: Confocal images of perfused CD31 (green) and αSMA (red) staining in MCaIV tumors.

αSMA is a common marker for perivascular cells. (left) Double staining CD31 and αSMA in normal arteriole. Double staining for CD31 and αSMA of MCaIV tumors treated with control IgG (middle) and DC101 (right). Image width = 230 microns.

Four mice per treatment group were used to quantify the αSMA-positive cell coverage. Vessel length and length of the vessel covered by αSMA-positive cells were traced in three different regions per tumor (each region was 921 μm by 921 μm) using 100 μm thick frozen sections. As shown in Figure 6.10, DC101 significantly increased the fractional coverage of tumor blood vessels by αSMA-positive cells. Approximately 25% of the vessels in untreated tumors had little or no perivascular cell coverage, but this fraction dropped to ~8% after DC101 treatment ($P < 0.005$). This suggested that DC101 pruned vessels that lack perivascular cell coverage, thus increasing the overall perivascular cell coverage during the normalization time window.

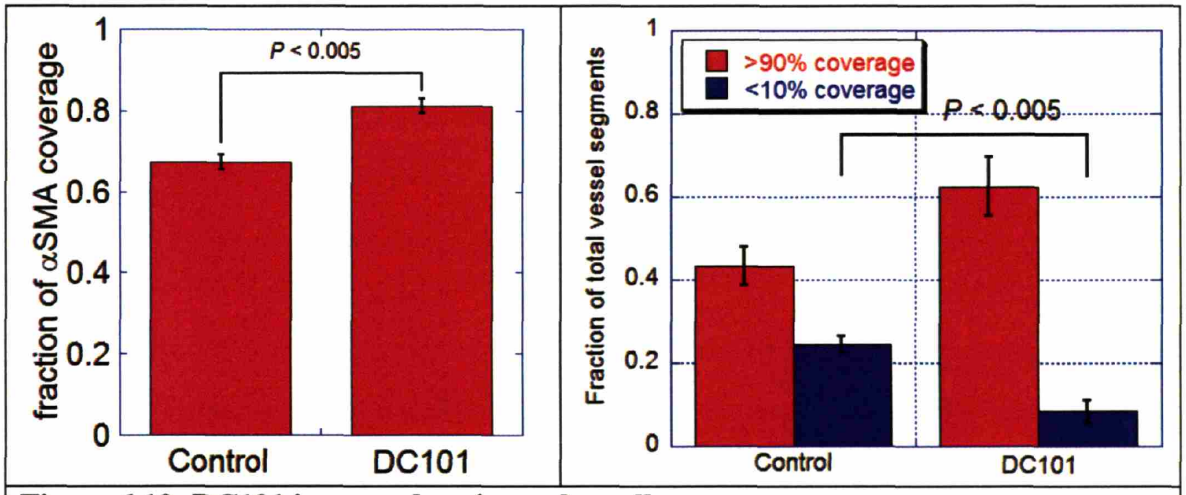

Figure 6.10: DC101 increased perivascular cell coverage.

(left) fraction of vessels with αSMA-positive cells coverage was significantly higher in DC101 treated group. (right) The fraction of vessel segments that were over 90% covered by αSMA-positive cells was the same between the DC101 and the control group (P = 0.65); but there was significant difference in the fraction of vessels segments that were less than 10% covered by αSMA-positive cells between DC101 and control-treated tumors.

Not only are endothelial cells and perivascular cells abnormal in tumors, many studies have shown that the basement membrane is also abnormal (Baluk et al. 2003). During tumor angiogenesis, factors such as matrix metalloproteinases (MMPs) are produced, and this leads to basement membrane degradation. The degradation of basement membrane can liberate endothelial cells to migrate and proliferate (Kalluri 2003). Unlike the vessels in normal muscle, the collagen IV staining around some vessels was below the detection limit in MCaIV tumors (center panel, Figure 6.11). While all vessels in normal muscle were covered by basement membrane, some tumor vessels lacked basement membrane coverage. Furthermore, the basement membrane in MCaIV tumors appeared to be thick

and multi-layered. Consistent with the normalization hypothesis, more vessels exhibited collagen IV staining after DC101 treatment (right panel, Figure 6.12).

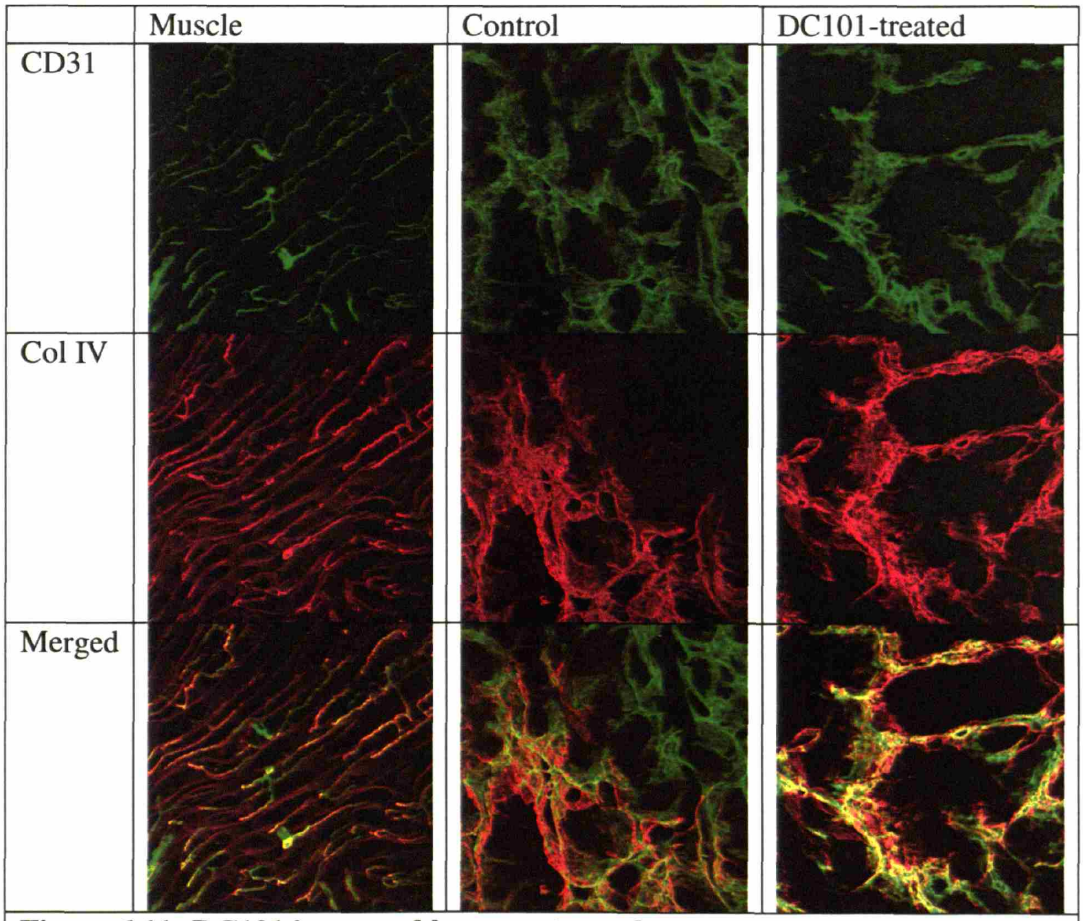

Figure 6.11: DC101 improved basement membrane coverage.

Vessels were perfused with FITC-CD31 (green) and basement membrane was stained with collagen IV antibody (red). (left) All vessels were covered by basement membrane. (center) In MCaIV control IgG-treated tumors, the basement membrane was abnormally thick in most regions, and appeared to be multi-layered. Some vessels lacked collagen IV staining. (right) After DC101 treatment, more vessels in MCaIV stained positive for collagen IV.

Quantification of basement membrane coverage showed that three days after DC101 treatment, the basement membrane coverage of MCaIV tumors significantly improved.

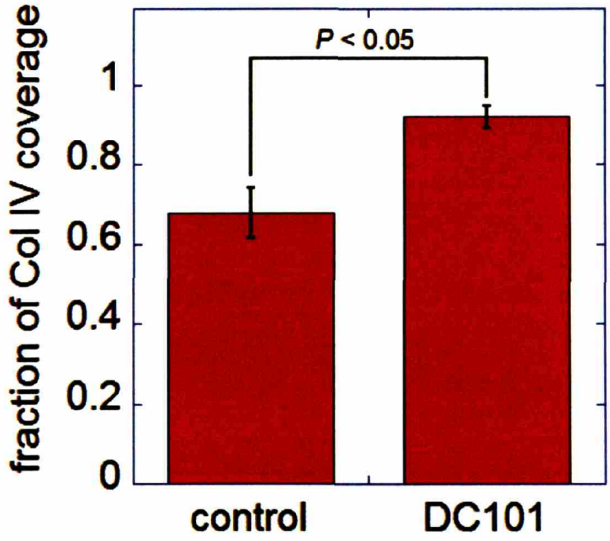

Figure 6.12: Quantification of collagen IV staining.

Fractional coverage of collagen IV vessels was significantly higher in the DC101 group (n = 6 in the control group, n = 5 in the DC101-treated group; $P < 0.05$).

Thus, DC101 induced structural normalization of the tumor vasculature by homogenizing the vessel size and reducing vessel tortuosity. It also increased the fractional coverage of perivascular cells and basement membrane. These structural modifications could affect the function of tumor blood vessels during the normalization time window (Chapter 7).

Conclusion

The normal microvasculature consists of arterioles that control the blood flow to smaller capillaries, post-capillary venules, and small veins that drain the blood to larger vessels (Figure 6.1). In tumors, this hierarchical organization of the vascular network was inexistent, and replaced by small and large vessels that were not uniformly distributed and were poorly organized (Figure 6.2). Three days after a single dose of DC101, the decrease in vessel length density was associated with an overall decrease in the diameter of MCaIV tumor vessels and a higher fraction of vessels with diameters of less than 20

μm. Similar effects were also seen in other tumor models such as LS174T and U87, as well as in published results (Yuan et al. 1996). Thus, by pruning the vasculature and reducing the caliber of blood vessels, DC101 induced a less abnormal vasculature in MCaIV tumors.

Another significant characteristic of the normal vasculature is the presence of perivascular cells that are tightly associated with the endothelium of arterioles, capillaries and post-capillary venules. In contrast, perivascular cells had a loose and poor association with the endothelium of tumor vessels (Morikawa et al. 2002). DC101 did not significantly modify the morphology of perivascular cells in the MCaIV model. Interestingly, in the LLC Lewis lung carcinoma tumor and RIP-Tag2 pancreatic islet tumor model, multiple changes occurred in perivascular cells after the treatment of VEGF-Trap, a potent small tyrosine kinase inhibitor against VEGFRs and PDGFRs (Inai et al. 2004). Using scanning electron microscopy, the authors showed that these perivascular cells became closely associated with surviving vessels after the VEGF-Trap treatment. The cells were oriented circumferentially, resembling smooth muscle in arterioles.

In our study, we showed that the normalized tumor vasculature was less tortuous and the vessels were more uniformly covered by perivascular cells and basement membrane. This result implied that vessels with less perivascular cell coverage were more vulnerable to DC101-induced regression. This interpretation was consistent with previous findings that demonstrated tumor vessels not associated with mural cells regress after VEGF withdrawal (Benjamin et al. 1999). Since we published our data, another group showed

that DC101 increased perivascular cell coverage in another tumor model (Vosseler et al. 2005).

The production of MMP9 and other proteases by cancer cells and stromal cells facilitates the degradation of ECM, resulting in tumor invasion and subsequent metastasis. *In vivo* and *in vitro* analyses of endothelial cell function showed a reduction in MMP9 production in endothelial cells after treatment with DC101 (Sweeney et al. 2002). Using double immunostaining with MMP9 and CD31 on orthotopic prostate cancer xenografts, the authors showed that there was a reduction in endothelial cell-associated murine MMP9 production. This reduction in MMP9 level might explain the observed increase in basement membrane coverage after DC101 treatment (see Chapter 8 for further discussion).

Chapter 7 examines how these changes in vascular structure affect its function.

Chapter 7: Vascular Function and Tumor Microenvironment

Portions of this chapter have been taken from:

Tong, R. T., Boucher, Y., Kozin, S. V., Winkler, F., Hicklin, D. J., and Jain, R. K. (2004). Vascular normalization by vascular endothelial growth factor receptor 2 blockade induces a pressure gradient across the vasculature and improves drug penetration in tumors. *Cancer Res* 64, 3731-3736.

Winkler, F.*, Kozin, S. V.*, **Tong, R. T.**, Chae, S. S., Booth, M. F., Garkavtsev, I., Xu, L., Hicklin, D. J., Fukumura, D., di Tomaso, E., Munn, L. L., and Jain, R. K. (2004). Kinetics of vascular normalization by VEGFR2 blockade governs brain tumor response to radiation; Role of oxygenation, angiopoietin-1, and matrix metalloproteinases. *Cancer Cell* 6, 553-563. * These authors contributed equally.

Introduction

Elevated interstitial fluid pressure (IFP) – a hallmark of solid tumors – can compromise the delivery of therapeutics to tumors (Jain 1989; Jain 1994; Jain 1998). In normal tissue, the excess fluid filtered from the blood vasculature is drained by lymphatic vessels to maintain interstitial fluid pressure close to zero. In tumors, however, lymphatic vessels are compressed by cancer cells, and Padera et. al shows that intratumoral lymphatics are non-functional (Padera et al. 2002; Padera et al. 2004). Defects in the vascular wall also contribute to abnormally high leakiness in tumor blood vessels. This leads to an increase in outflow of proteins and other molecules from blood vessels and thereby a rise in oncotic pressure in the tumor interstitium (Stohrer et al. 2000). Thus, the interstitial fluid homeostasis in tumors is perturbed by the abnormal tumor vasculature and impaired lymphatic function.

Similarly, tumor blood flow plays a crucial role in tumor growth, metastasis, and delivery of therapeutics. In normal tissue, the blood flow is primarily controlled by the pressure difference between arterial and venous sides, geometrical resistance, and the viscosity of blood. The abnormal tumor vasculature contributes to the temporal and spatial heterogeneity in tumor blood flow (Jain 1988; Baxter and Jain 1991; Chaplin and Hill 1995; Netti et al. 1996; Baish et al. 1997). The increased tumor vasculature leakage reduces the pressure gradient along the vessels, and thus reduces blood flow through the tumor vessels (Netti et al. 1996). The highly tortuous blood vessels and chaotic distribution of vessels can also lead to reduced blood flow (Gazit et al. 1997; Baish and Jain 2000). Importantly, the relatively stagnant flow in tumor vessels contributes to the poor delivery of oxygen and molecules.

In Chapter 6, I showed that DC101 normalized the vascular structure. In this chapter, I examine the effects of DC101 on vascular functions. First, I showed that DC101 lowered interstitial fluid pressure in multiple tumor models, and the changes were associated with lowering of vascular permeability. Furthermore, DC101 induced a hydrostatic pressure gradient, which led to improved macromolecule delivery. DC101 also alleviated tumor hypoxia, which could be partly explained by the increase in red blood cell velocity. Finally, all the measured parameters were fitted into a model developed by Baxter and Jain (Baxter and Jain 1989).

Result

DC101 lowered interstitial fluid pressure

We first confirmed that similar to a VEGF blocking antibody (Lee et al. 2000), DC101 decreased IFP in both human glioblastoma multiforme U87 (Figure 7.1) and human small cell lung carcinoma 54A xenografts (Figure 7.2). IFP decreased dramatically 3 days after the initial treatment, after which it stayed at a nearly constant level. As shown in Figure 7.1 and 7.2, it took approximately 3 days to reach the full effects of DC101 on the IFP of the two xenografts.

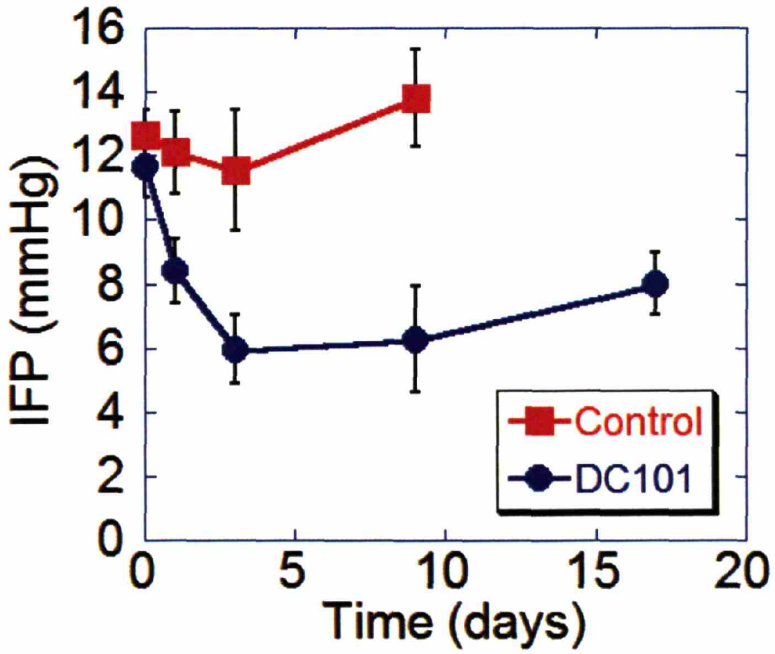

Figure 7.1: DC101 lowered interstitial fluid pressure in U87 tumors in nude mice.

IFP measurement was done by using wick-in-needle method. 40 mg/kg control IgG or DC101 was given i.p. every three days. Data are represented as mean ± S.E.M.

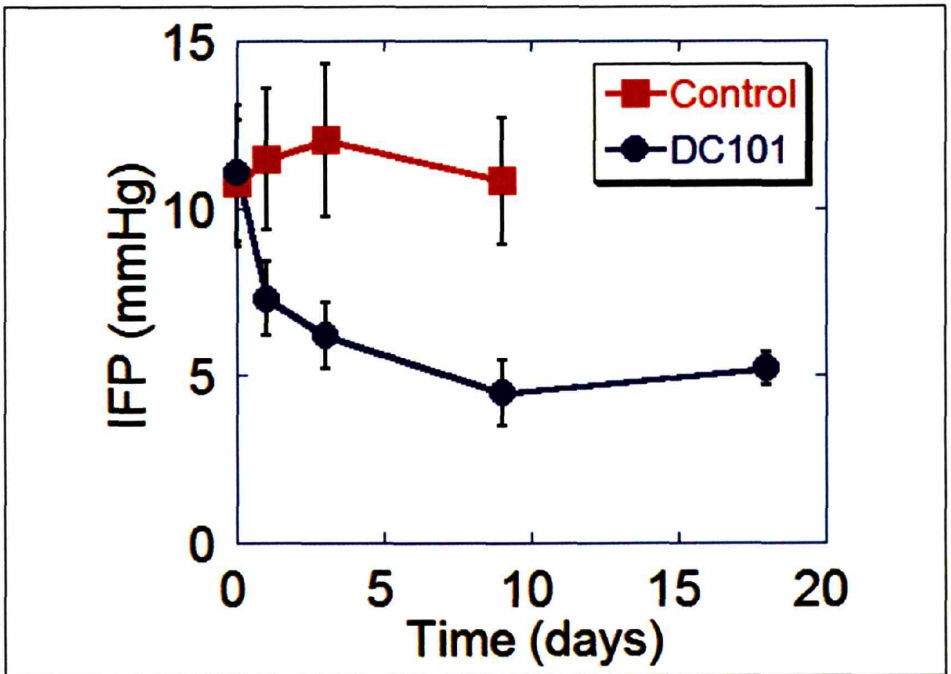

Figure 7.2: DC101 lowered interstitial fluid pressure in 54A tumors in nude mice.

IFP measurement was done by using wick-in-needle method. 40 mg/kg control IgG or DC101 was given i.p. every three days. Data are represented as mean ± S.E.M.

DC101 decreased IFP in spontaneous tumors developed in C3H mice

To further confirm the effects of DC101 on IFP in tumors, aged C3H mice that developed spontaneous tumors were used. Unlike other xenograft or transgenic tumor models, aged C3H mice developed spontaneous tumors naturally, similar to tumors in the human setting. Aged C3H mice were screened weekly for tumor development. The experiment was started when tumors became visible and palpable. As shown in Figure 7.3, DC101 also lowered the IFP in murine spontaneous tumors.

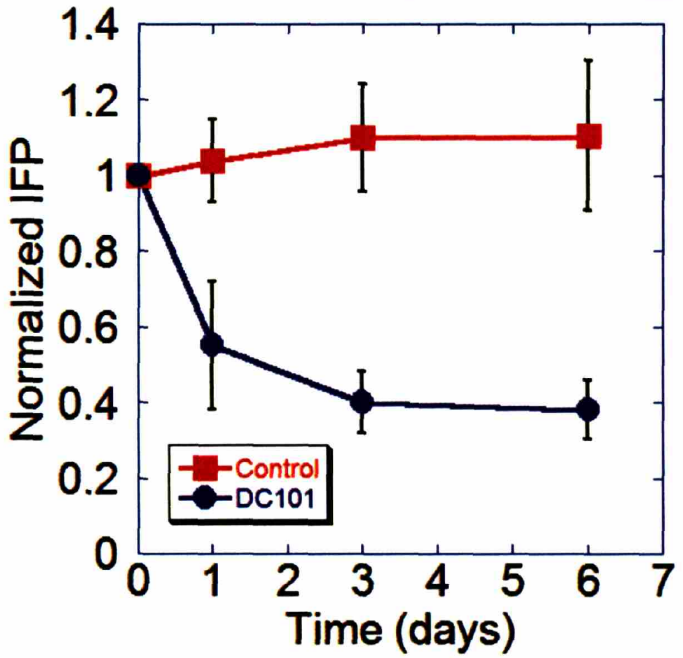

Figure 7.3: DC101 lowered interstitial fluid pressure in spontaneous tumors developed in aged C3H mice.

IFP measurement was done by using wick-in-needle method. 40 mg/kg control IgG or DC101 was given i.p. every three days. The IFP value was normalized by the value on Day 0. Data are represented as mean ± S.E.M.

DC101 does not enhance lymphatic function.

To test whether the reduction in IFP was associated with a change in lymphatic drainage, ferritin microlymphangiography and LYVE-1 immunostaining (which stains for lymphatic vessels) were performed on MCaIV tumors implanted in dorsal chambers and subcutaneously in the hind leg. Positive LYVE-1 staining structures were only observed in the normal tissue surrounding the tumor (Figure 7.4). Inside the tumor, ferritin was present only in the interstitium, with no intratumoral LYVE-1 positive structures surrounding it. Thus, we did not find any evidence of functional lymphatic vessels in the

tumors of both treated and control animals (Figure 7.4). Therefore the drop in IFP could not be attributed to modifications in lymphatic function.

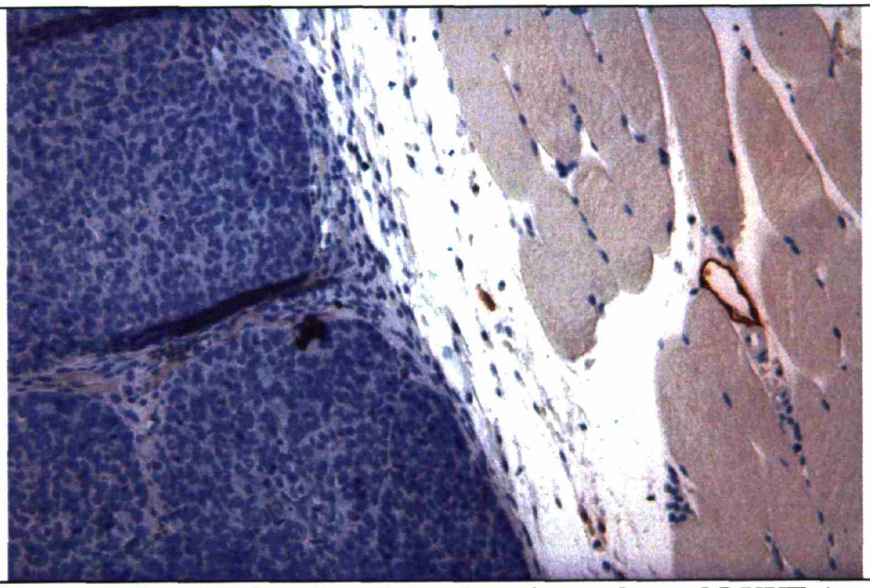

Figure 7.4: Ferritin functional lymphangiography and LYVE-1 staining in MCaIV tumors after DC101 treatment.

A LYVE-1 positive lymphatic vessel was seen in the muscular layer.

DC101 lowered vascular permeability

The other way to lower IFP was to alter the flow of fluid from the vasculature into the interstitial space. Thus, we looked at the effect of DC101 on the vascular permeability. Tumor vasculature had been shown to have high vascular permeability relative to normal vessels (Yuan et al. 1993; Yuan et al. 1994; Yuan et al. 1994; Yuan et al. 1995). It had also been shown that DC101 lowered vascular permeability in T241 murine fibrosarcoma (Kadambi et al. 2001). Thus, as expected, we found that DC101 lowered the vascular permeability in MCaIV tumors implanted in the dorsal skinfold chamber (Figure 7.5). Three days after the injection of DC101, the vascular permeability of albumin in MCaIV – a profoundly leaky tumor – was decreased by 51%.

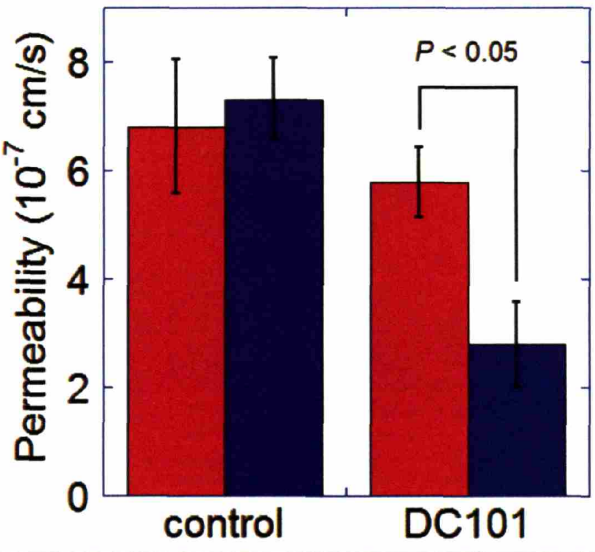

Figure 7.5: DC101 lowered vascular permeability of albumin in MCaIV tumors.

Red: before control IgG or DC101 treatment. Blue: 3 days after control IgG or DC101 treatment. Data are represented as mean ± S.E.M.

DC101 enhanced the oncotic pressure gradient across the tumor vasculature.

In general, leaky vessels in tumors led to an increase in the interstitial oncotic pressure (Stohrer et al. 2000), which became approximately equal to the plasma oncotic pressure. To determine whether changes in vascular permeability of tumor vessels translated into functional normalization, we measured both hydrostatic and oncotic pressure difference across the vascular wall. We found that 3 days after DC101 treatment, the interstitial oncotic pressure was significantly lower than in the control group (Figure 7.6), while the plasma oncotic pressure did not change. This decrease in interstitial oncotic pressure was consistent with the decrease in vascular permeability to macromolecules by DC101, and increased the oncotic pressure gradient across the vasculature.

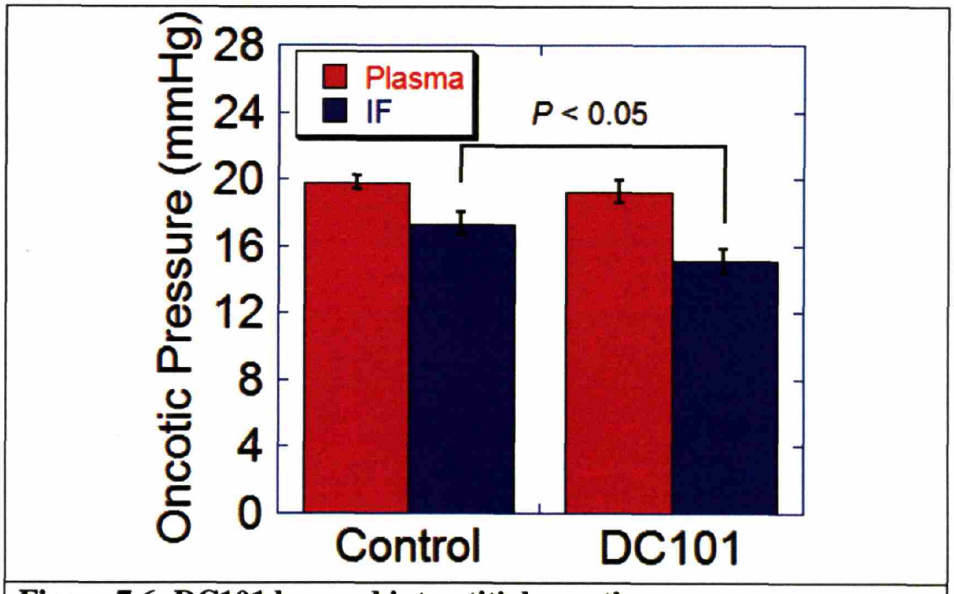

Figure 7.6: DC101 lowered interstitial oncotic pressure.

There was no change in plasma oncotic pressure in MCaIV tumors in the DC101 treated group when compared with the control group. However, the interstitial oncotic pressure dropped significantly in the DC101 group (n=5, P<0.05). Data are represented as mean ± S.E.M.

DC101 induced a hydrostatic pressure gradient across the tumor vasculature.

In solid tumors, MVP was approximately equal to IFP, leading to nearly zero pressure difference across the vessel wall (Boucher and Jain 1992). As a matter of fact, these two pressures were so closely coupled that changing the vascular pressure led to similar changes in the IFP within seconds, until they both became equal again (Netti et al. 1999). Thus the DC101-induced decrease in IFP might be accompanied by a similar decrease in MVP. To test this, we measured MVP in control and DC101-treated tumors by directly inserting micropipettes in MCaIV tumor vessels (Peters et al. 1980). We found that MVP was unaffected by DC101 treatment, while IFP decreased significantly by 2 mmHg (Figure 7.7). Thus, DC101 created a sustained hydrostatic pressure gradient across the vasculature.

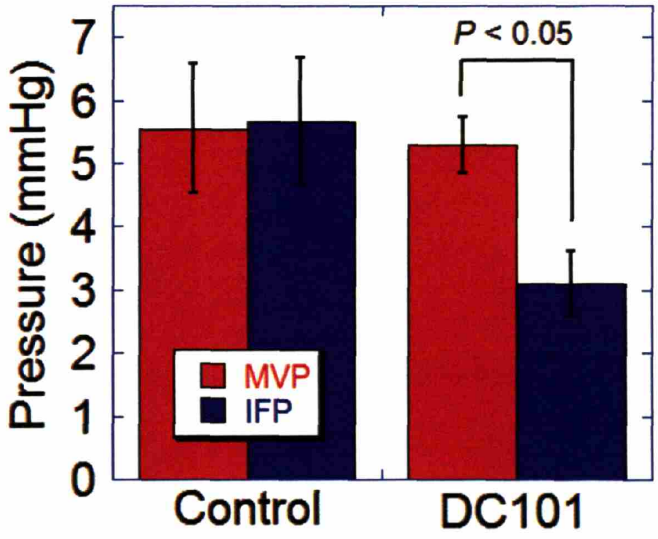

Figure 7.7: DC101 induced a hydrostatic pressure gradient across the vascular wall.

DC101 did not affect the microvascular pressure, whereas the interstitial fluid pressure was significantly reduced in MCaIV tumors. Data are represented as mean ± S.E.M.

DC101 increased BSA penetration in tumors.

Movement of molecules across vessel walls occurs by diffusion and convection. Diffusion is governed by the concentration gradient across the vessel wall, whereas convection is governed by the pressure gradient. To test if the DC101-induced pressure gradient across the vascular wall improved the penetration of large molecules, we injected fluorescently-labeled BSA intravenously into MCaIV tumor-bearing mice one hour before tumor fixation (Figure 7.8).

Using immunostaining, we observed the pattern of BSA extravasation. We identified functional blood vessels using biotinylated lectin. To quantify the results, 10 rings with increasing fixed distance from the vessels were drawn and the average intensity of extravasated BSA was calculated in Image J (http://rsb.info.nih.gov/ij/). The

extravasation of BSA was quantified by fitting the intensity profiles to an exponential function to yield a characteristic penetration length (n = 9 sections; 3 sections per tumor; 5 tumors per group; $P<0.05$). The characteristic penetration lengths were 7.26 ± 1.11 μm (mean ± S.E.M) and 11.23 ± 1.41 μm for the control and DC101 groups, respectively. Quantitative analysis showed that DC101 produced a significantly deeper penetration of BSA molecules into the tumor.

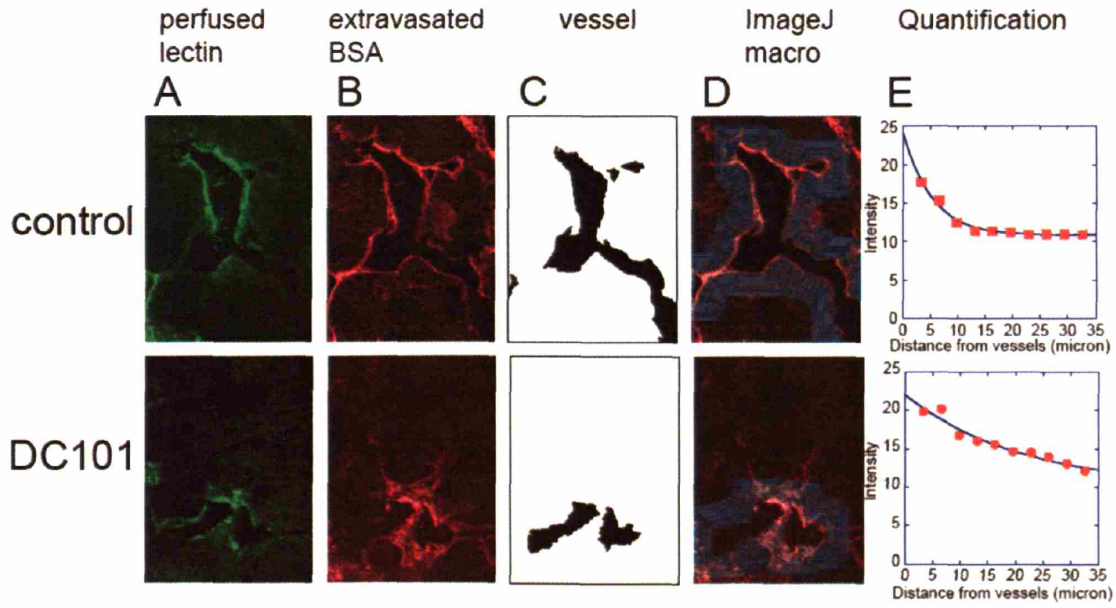

Figure 7.8: DC101 increased penetration of macromolecules from blood vessels.

Mice bearing s.c. MCaIV tumors were injected with tetramethylrhodamine isothiocyanate (TRITC)-BSA one hour before perfusion fixation. Examples of frozen sections of MCaIV tumors with perfused biotinylated lectin (A) and extravasated TRITC-BSA (B) were prepared. Vessels were identified (C); and using an automated routine in ImageJ, we quantified the average intensity of extravasated TRITC-BSA as a function of distance from the blood vessels wall (D and E).

DC101 reduced hypoxia in tumors

Inefficient delivery of oxygen in tumors lead to hypoxia and hypoxia significantly decreases the efficacy of radiotherapy. Thus, we hypothesized that DC101 also induced improvement in tumor oxygenation, which could explain the enhanced radiation response seen by our group and other researchers (See Discussion and Appendix 2). To measure tumor hypoxia, 60 mg/kg pimonidazole was injected i.v. 1 hour before the brain was rapidly frozen at -80°C. The hypoxyprobe-1 was used to detect pimonidazole-protein, which labels hypoxic regions in tumor sections. During DC101 treatment, tumor hypoxia dropped significantly on day 2, was almost abolished by day 5, and increased again by day 8 (Figure 7.9).

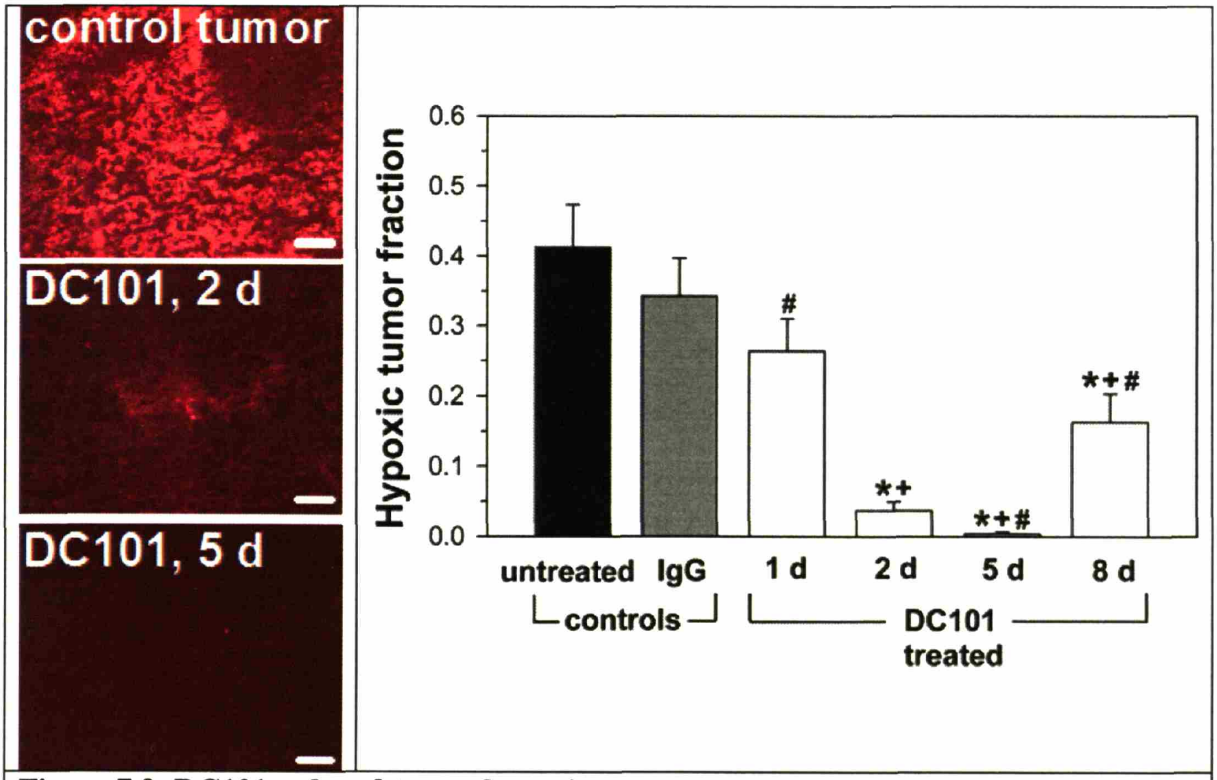

Figure 7.9: DC101 reduced tumor hypoxia.

Tumor hypoxia (pimonidazole staining, red) was severe in control tumors, but decreased for a limited time during monotherapy with DC101 at 40 mg/kg i.p. every three days. Hypoxia reached a minimum at day 5, and a partial relapse occurred at day 8. * $P < 0.05$, compared to untreated control; $^{+}$ $P < 0.05$, compared to control IgG treatment (day 2): # $P < 0.05$, compared to day 2 after initiation of DC101 treatment.

DC101 increased RBC velocity in tumors

Since DC101 affected both vascular architecture and vascular permeability, we suspected that it might also affect red blood cell (RBC) velocity in tumor blood vessels. In the past, our lab used either the four slit method or the fluorescent bead method to measure RBC velocity (Yuan et al. 1994). However, since these techniques were based on one photon fluorescent microscopy, the resulting images did not have high resolution or deep depth

penetration. Brown et al. introduced a line scan method, based on two photon microscopy, to measure RBC velocity in tumors (Brown et al. 2001). This technique was valid for the majority of blood vessels, with the exception of the vessels that have fast flow rates (>1000 μm/s). Using the normal scanning procedure, blood vasculature was imaged (Figure 7.10). Since red blood cells absorb fluorescent image, they appear as dark spots under fluorescent microscopy. By scanning the same region (the white line in Figure 7.10) with a known scan rate, a line scan output was generated (right panel of Figure 7.10). Line scans generated high-resolution t versus x images of RBC streaks. Unlike the single photon technique, blood flow was readily visible at depths over 300 μm in the brain and glioblastoma. By measuring the slope of the RBC streaks in t versus x images, the RBC velocities were calculated.

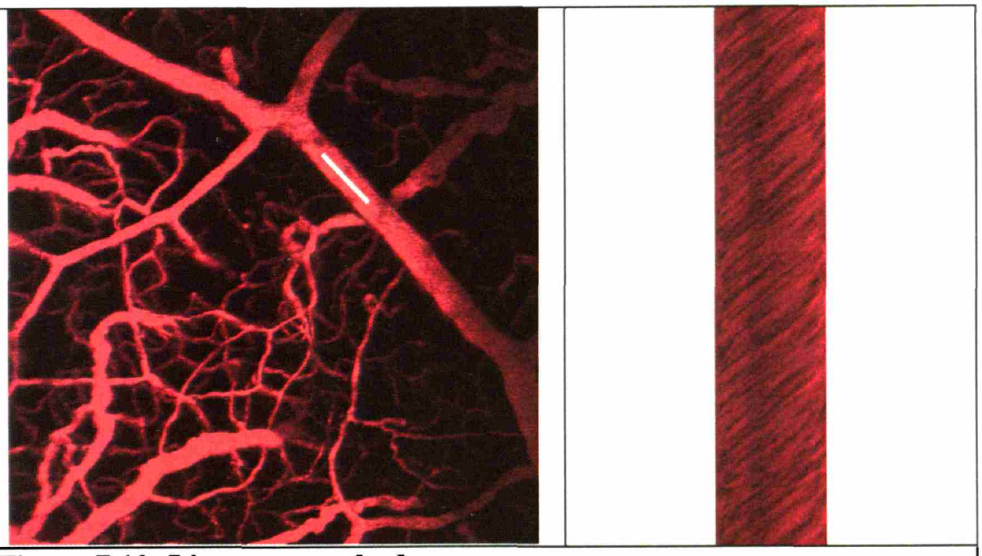

Figure 7.10: Line scan method.

(left) A two photon image of normal brain vasculature. White line showed the region where line scan method was applied. The two photon laser was continuously scanning the region with a known scan rate. (right) A line scan image with t versus x. By measuring the slope of the RBC streak, one could calculate RBC velocity of that particular vessel. Image width (left) = 700 μm.

First, we examined the RBC velocity in normal brain using the cranial window model. Maximum intensity projection images of normal brain vasculature were captured using two-photon microscopy (Figure 7.11). Ten vessels were picked randomly, and these vessels were monitored on Day 0 and 3 and 5 days after control IgG or DC101 treatment. Both vascular diameter and RBC velocity were measured for each of these vessels at each time point. Two line scan files were created per vessels, so that the measurement time could cover the bio-variability of red blood cell velocity due to normal heart beat. Five red blood cell velocity measurements were done per each line scan, thus ten measurements were done for each vessels.

Day 0	Day 3	Day 5

Figure 7.11: Normal brain vessels after control IgG treatment.

Maximum intensity projection of brain vasculature in nude mice. Normal brain vessels did not change after control IgG treatment. Image width = 700 μm.

Regardless of whether the mice were treated with control IgG or DC101, overall there were no changes in vessel diameter. Interestingly, while there were fluctuations in RBC velocity for some vessels, on average there was no difference during the 5 days period in both treatment groups.

By plotting RBC velocity versus vessel diameter, one could easily see that in general, as vessels became bigger, the RBC velocities were faster (Figure 7.12). As expected, arteries had much higher RBC velocities than veins and capillaries. As mentioned earlier, the line scan method was not accurate for vessels with fast flow rate, and this was reflected in the huge error bars for arteries with fast RBC velocities. The error bars for vessel diameter represented the measurement error. The measurement error for this experiment was roughly 3 microns.

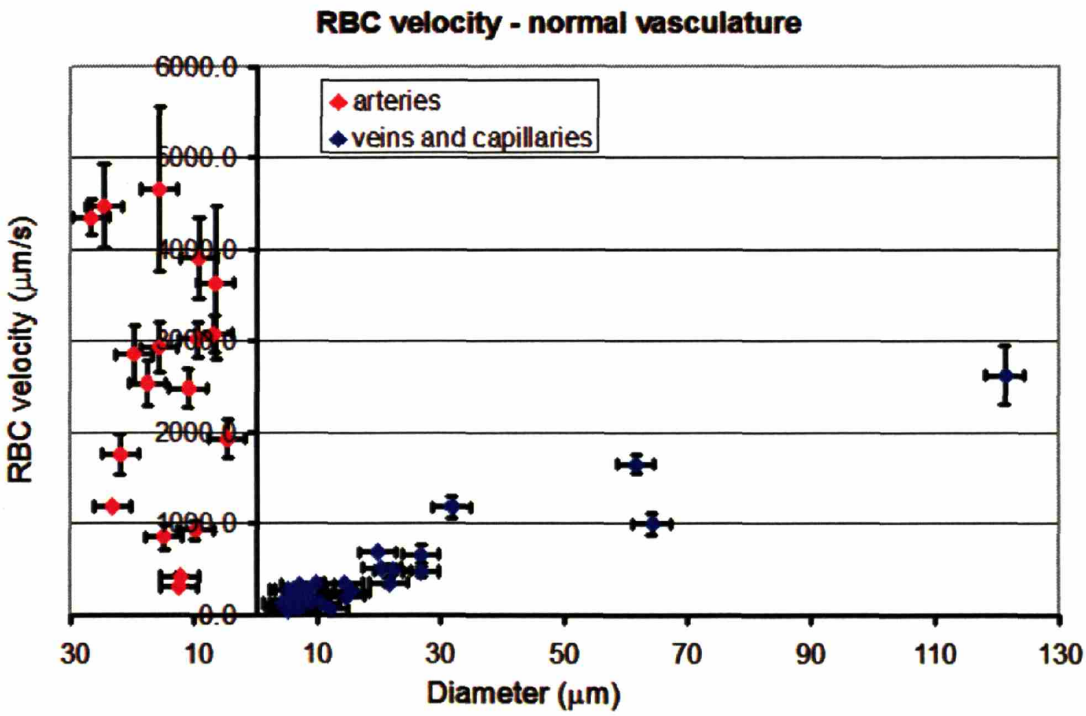

Figure 7.12: RBC velocities of normal brain vessels.

Arteries had a much higher RBC velocities than veins or capillaries. In general, RBC velocity was correlated with vessel diameter in the normal vascular network.

Before measuring tumor vessel RBC velocity, the variability in RBC velocity of a single vessel was assessed by making measurements in the same vessels over a period of 60 minutes. As shown in Figure 7.13, there were some small fluctuations in the RBC velocity for some vessels over that period. The fluctuations occurred for a variety of reasons. First of all, there could be changes in RBC velocity within minutes time scale, and this could be due to the effects of anesthesia, body temperature, changes in heart rate, etc. Furthermore, tumor vessels were known to have fluctuating blood flow (Jain 1988). Finally, the location of the scanning region could be slightly different from measurement to measurement. One would expect that the centerline of the blood vessels had the fastest RBC velocity. While great care was made to ensure all measurements were done

at the centerline, such measurements might be slightly off from time to time. Nevertheless, as shown in the figure, these fluctuations in general were no greater than the fluctuations that occurred during the two line scans and measurement error. Thus, measurements of RBC velocity using two separate line scans (ten measurements) were valid.

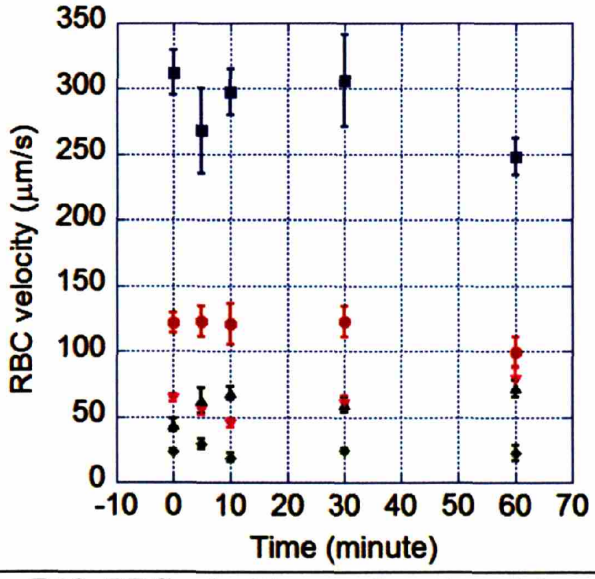

Figure 7.13: RBC velocities as a function of time.

The same vessels were measured at different time points. While there were some fluctuations within the 60 minute period, these fluctuations were within the errors of individual measurement.

To measure the effect of DC101 on RBC velocity, mice implanted with U87 glioblastoma tumor in the cranial window were divided into either control IgG or DC101 treatment group. Once the tumor reached 2 mm in diameter, control IgG or DC101 was injected i.p. on Day 0 and Day 3. RBC velocity was measured on Day 0, Day 3, and Day 5. As shown in Figure 7.14, the tumor vasculature became less tortuous and the diameter became smaller shortly after DC101 treatment. Ten vessels were followed throughout

the treatment. On Day 3 and Day 5, not all vessels were traced since some of the vessels either were pruned away or could be located.

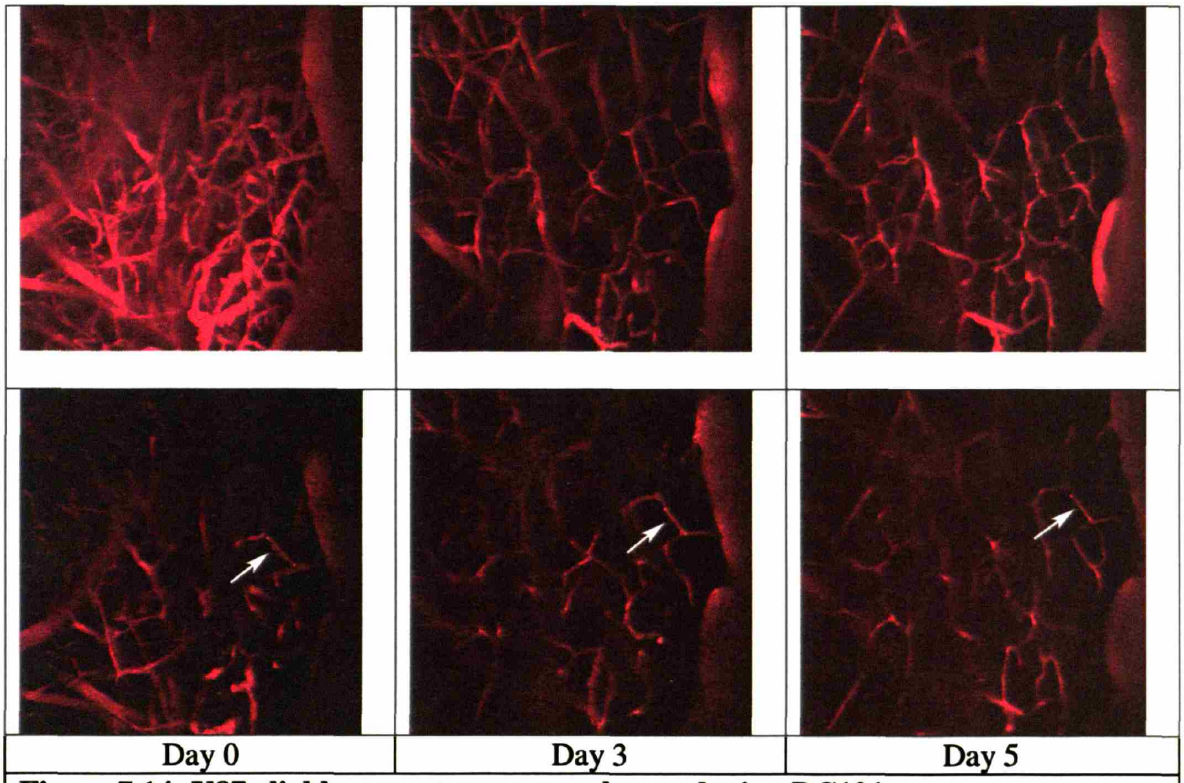

Figure 7.14: U87 glioblastoma tumor vasculature during DC101 treatment.

(top) Maximum intensity projection of the tumor vascular network. (bottom) A single optical slice out of the 3D image stack. White arrow points to a sample vessel that was traced during the DC101 treatment. Image width = 700 μm.

Figure 7.15 and 7.16 showed the RBC velocity and diameter for all traced vessels in the control IgG and DC101 groups, respectively. Unlike normal vasculature, the RBC velocity of most vessels was much slower in general. There was also a lack of correlation between RBC velocity and vessel diameter.

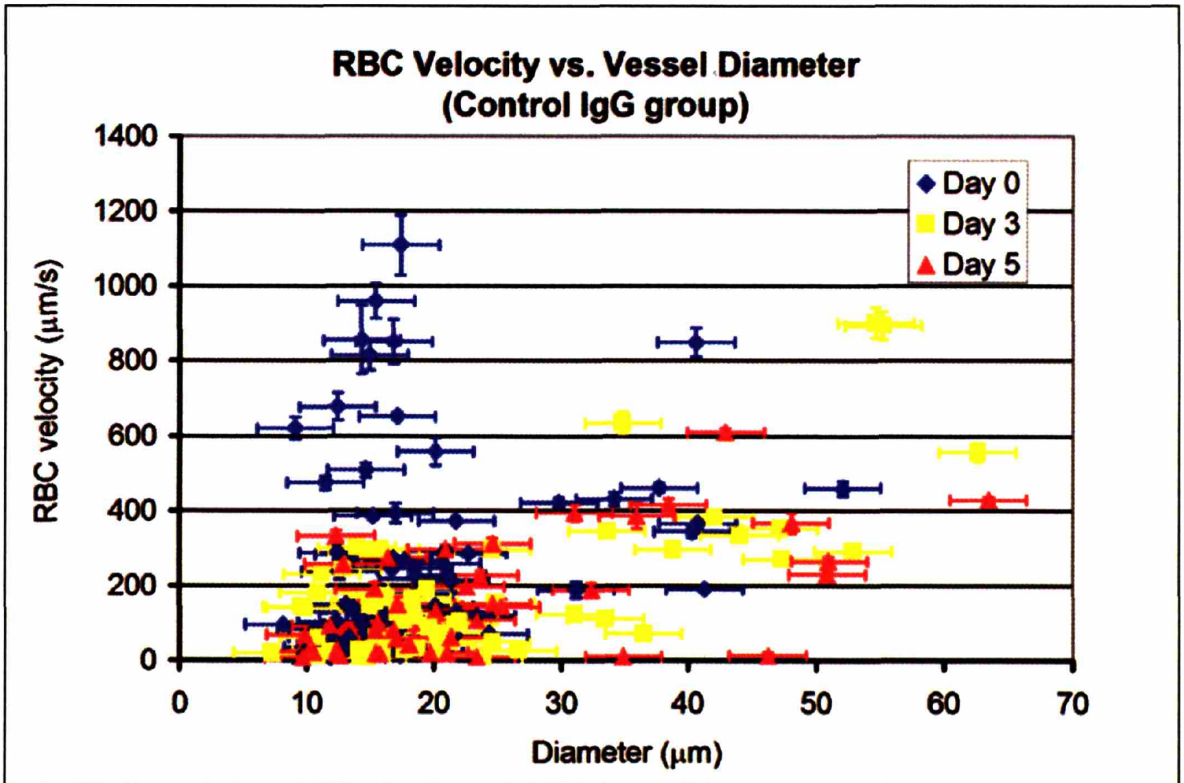

Figure 7.15: RBC velocity and vessel diameter of U87 tumors in the control IgG-treated group.

There was lack of correlation between RBC velocity and vascular diameter.

After DC101 treatment, there was still a lack of correlation between RBC velocity and vascular diameter. Thus, DC101 did not restore the correlation between RBC velocity and vessel diameter, as in the normal brain vasculature.

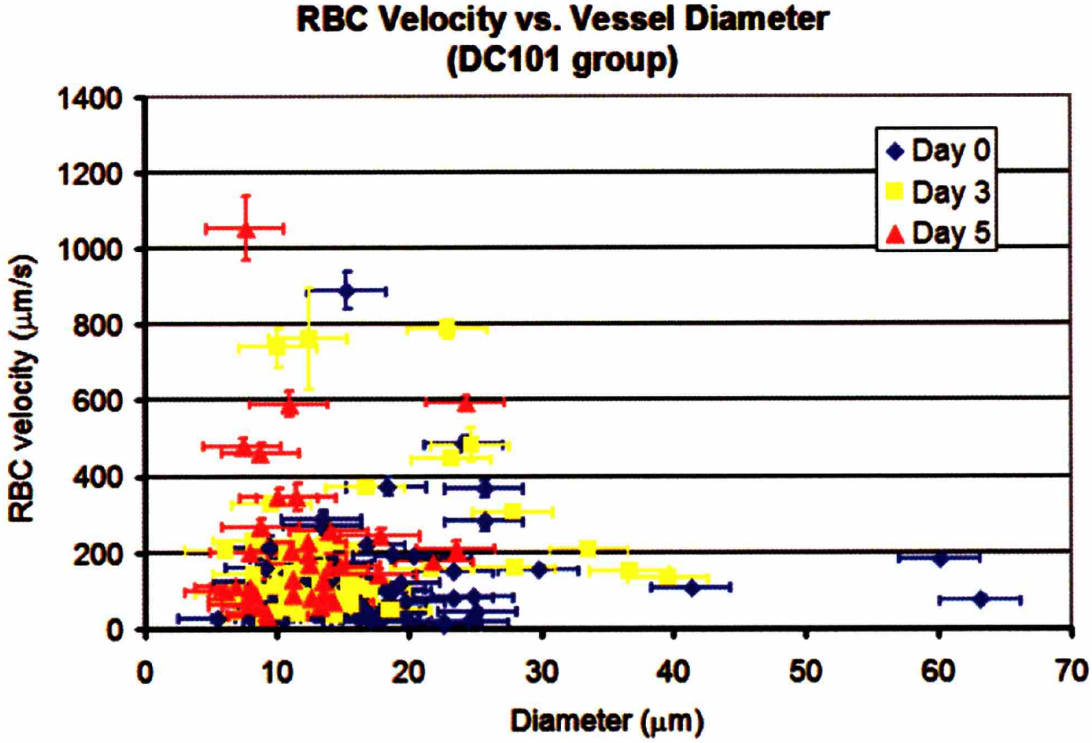

Figure 7.16: RBC velocity and vessel diameter of U87 tumors in the DC101-treated group.

There was lack of correlation between RBC velocity and vascular diameter.

To better understand the effects of DC101 on vessel diameter, vessel diameters of all measured vessels were grouped together depending on the treatment groups and time points. As shown in Figure 7.17, DC101 significantly lowered vessel diameter. This result confirmed the previous finding in MCaIV tumors implanted in the dorsal skinfold chamber. Since the same vessels were traced throughout the treatment, a normalized diameter could be calculated for each individual vessel by dividing the diameter at Day 3 or Day 5 by the diameter at Day 0. Similarly, this showed that DC101 reduces vascular diameter.

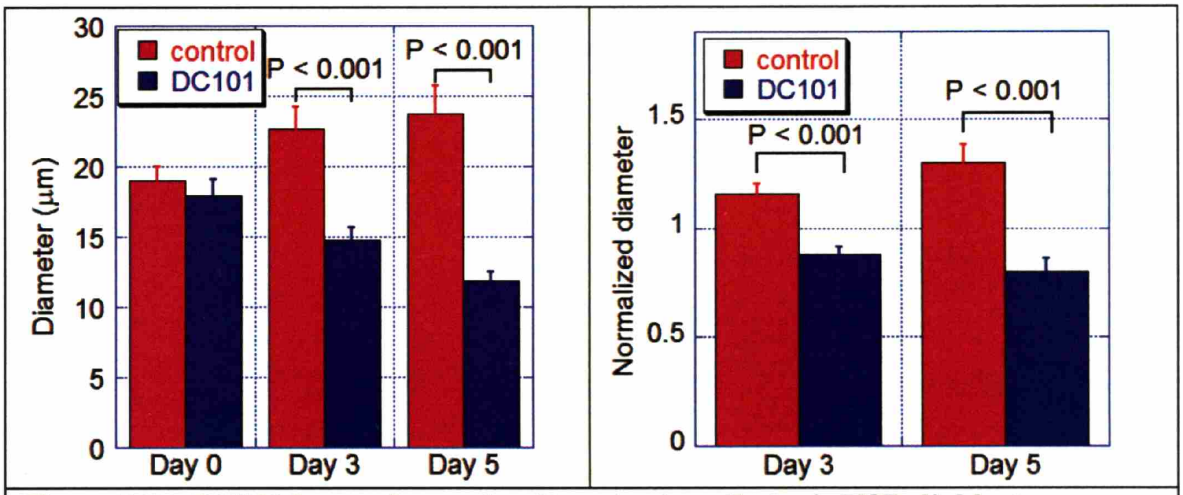

Figure 7.17: DC101 lowered vascular diameter in orthotopic U87 glioblastoma model.

(left) Using Wilcoxon test, DC101 was shown to reduce vascular diameter compared to the control group. (right) Vascular diameter on Day 3 and Day 5 was normalized by the value on Day 0.

Similarly, RBC velocities of all vessels were analyzed based on the treatment group and time. While the RBC velocity did not seem to be different between the two treatment groups, the normalized RBC velocity was significantly higher in the DC101 treated group on both Day 3 and Day 5 (See Appendix 3 for the analysis).

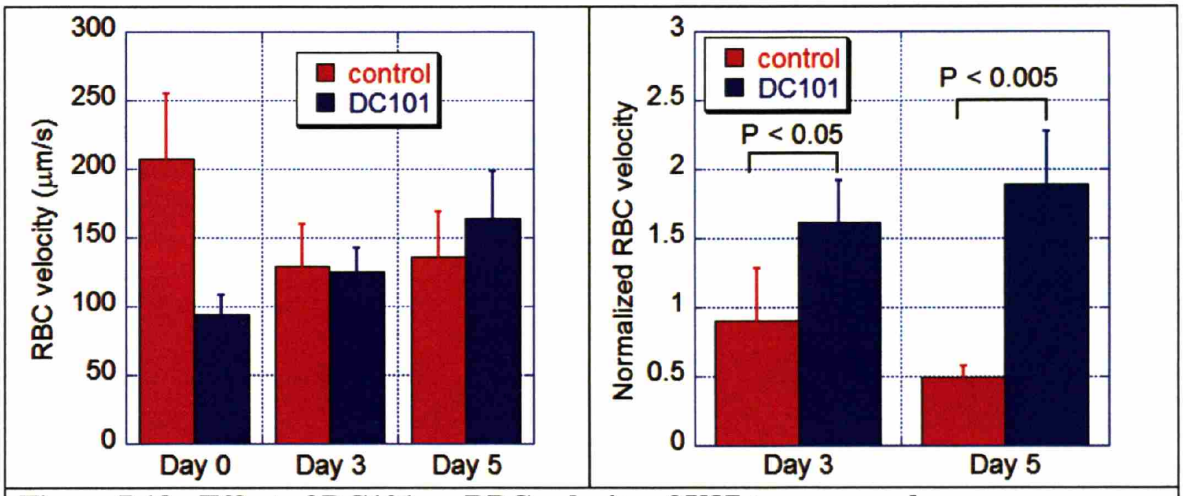

Figure 7.18: Effect of DC101 on RBC velocity of U87 tumor vessels.

(left) RBC velocity on Day 0, 3 and 5 of mice treated with either control IgG and DC101. The Wilcoxon test indicated no significant difference between control IgG group and DC101 group on all three days. (right) RBC velocity on Day 3 and Day 5 was normalized by the RBC velocity of the same vessel on Day 0.

Discussion

Young et al. were the first to show that IFP in tumors was higher than IFP in normal tissue (Young et al. 1950). Since then, many studies demonstrated an increase in IFP in both animal and human tumors. Elevated IFP constituted a major barrier for drug delivery in tumors (Jain 1989). Here we showed that blocking VEGF signaling by DC101, a VEGFR2 antibody, decreased IFP – not by restoring lymphatic function – but by producing a morphologically and functionally "normalized" vascular network. We have recently shown that an anti-VEGF antibody can lower IFP in transplanted tumors in mice (Lee et al. 2000) and in rectal carcinomas in patients (Willett et al. 2004). However, the mechanisms of IFP reduction and how this reduction affects drug delivery are not known. In normal tissues, the excess fluid filtered from blood vessels is drained by

lymphatic vessels to maintain the IFP close to zero (mmHg). In tumors, IFP homeostasis is perturbed due to impaired lymphatic function (Leu et al. 2000; Padera et al. 2002) and abnormalities in vascular structure and function (Jain 2003). Because of the high vascular permeability and the impaired lymphatic drainage, the oncotic and hydrostatic pressures in the microvascular and interstitial spaces are at equilibrium in tumors (Boucher and Jain 1992; Stohrer et al. 2000). To unravel the mechanism of IFP reduction induced by blocking VEGF signaling, we examined the effect of DC101 on the determinants of interstitial hypertension: including changes in the vascular morphology, vessel wall structure, lymphatic vessels and function of tumor vasculature during the course of treatment.

I showed that DC101 reduced IFP in multiple tumor models. The reason that IFP in MCaIV was lower than in 54A and U87 was probably because MCaIV was implanted in the dorsal skinfold chamber, while 54A and U87 were implanted in the leg. The blood circulation and the environment of the dorsal chamber might cause tumors to have a lowered interstitial fluid pressure compared to those implanted in the leg. Nevertheless, the IFP value was similar to the published result of LS174T human colon adenocarcinoma implanted in the dorsal skinfold chamber (Leunig et al. 1992).

As shown in Figure 7.5, we demonstrated that the reduction in IFP was associated with a decrease in vascular permeability. Two possible mechanisms could explain this decrease in vascular permeability. First, DC101 could induce the regression of vessels with less pericytes that have a higher permeability. Recent *in vitro* and *in vivo* studies suggested that the interaction between endothelial cells and mural cells controls vascular permeability and integrity. Endothelial cells co-cultured with smooth-muscle-like cells

had tighter junctions and a lower permeability than cultures of endothelial cells only (Kurzen et al. 2002). In PDGF-ß and PDGF receptor-ß deficient mice the lack of pericytes in angiogenic blood vessels had been associated with edema and morphological signs of increased endothelial permeability (Hellstrom et al. 2001). Alternatively, because VEGF enhanced vascular permeability, blocking VEGF signaling with DC101 might reduce the effective vascular permeability of most tumor vessels (Yuan et al. 1996; Dvorak et al. 1999).

Even though DC101 reduced vascular permeability, the permeability of the normalized vasculature was still significantly higher than that of normal tissues (Jain 1987; Yuan et al. 1996). The small drop in oncotic pressure from 19 to 17 mmHg induced by DC101, was also indirect evidence that the vascular permeability of DC101-treated MCaIV tumors was still elevated. For example, in subcutaneous tissue, the oncotic pressure was approximately 8 mmHg (Stohrer et al. 2000). Thus, macromolecules were still able to freely pass through normalized tumor blood vessels.

The exchange of fluid and plasma proteins between blood vessels, interstitial space, and lymphatic vessels plays a crucial role in balancing fluid within the body. It also plays an important part in determining the effectiveness in the delivery of chemotherapeutic agent during anti-cancer therapy. Due to the complexity of the system and limited information, mathematical models have been developed to simplify and describe the movement of molecules in tumors. In this study, I focused on transvascular transport since DC101 mainly affected the endothelial cells and the integrity of the vascular wall (Chapter 5).

To gain more insights into the effect of DC101 on fluid and solute transport in tumors, I employed a mathematical model developed by Baxter and Jain to describe the

macroscopic fluid and solute transport in tumors (Baxter and Jain 1989). This model aims to examine the overall interstitial fluid pressure and interstitial fluid velocity profile throughout the entire tumor. It assumes the tumor is spherical. This is a macroscopic model, and the length scale of the pressure and concentration profiles is on the order of the tumor radius. Thus, microscopic features such as blood vessels, cells, and the interstitial matrix are not considered explicitly. The model assumes a continuous, spatially distributed source throughout the tumor.

First, the transport of fluid in the tumor interstitium is described by Darcy's law.

$$u_i = -K\nabla P_i$$

where K is the hydraulic conductivity of the interstitium (cm^2/mmHg/s) and u_i is the fluid velocity (cm/s).

This equation is then combined with the continuity equation for steady-state incompressible flow:

$$\nabla \cdot u_i = \phi_v(r)$$

where $\phi_v(r)$ is the fluid source term (s^{-1}) given by the Starling's Law.

$$\phi_v(r) = \frac{J_v S}{V} = L_p \frac{S}{V}(P_v - P_i - \sigma(\pi_v - \pi_i))$$

where J_v is the fluid flux across the vascular wall (cm/s), S/V is the surface area of vessel wall per unit volume of tissue (cm^{-1}), L_p is the hydraulic conductivity of the vessel wall (cm/mmHg/s). P_v is the microvascular pressure (MVP), and P_i is the interstitial fluid pressure (IFP) as displayed in the result section. The hydrostatic pressure gradient (P_v - P_i) is balanced by the oncotic pressure gradient (the difference between π_v, plasma oncotic pressure and π_i, interstitial oncotic pressure), and the reflection coefficient, σ,

determines the effectiveness of the oncotic pressure gradient across the vascular wall. L_p and σ depend on the properties of solute (i.e. size, charge, configuration) and physiological properties of the vascular wall (pore size, charge). P_v, P_i, and the two oncotic pressures also depend on the properties of the tissue, blood and lymphatic vasculature.

This equation implies that the fluid source term is uniformly distributed throughout the tumors. This model assumes that there is no functional lymphatic vasculature inside the tumor to drain interstitial fluid (Padera et al. 2002).

The equation for Darcy's Law is then combined with the continuity equation to give:

$$-\nabla \cdot K\nabla P_i = \phi_v(r)$$

Assuming all parameters except for P_i are constant, the equation can be simplified to:

$$\nabla^2 P_i = \frac{\alpha^2}{R^2}(P_i - P_e), \qquad \text{where } \alpha = R\sqrt{\frac{L_p S}{KV}}$$

The effective pressure, P_e, is the interstitial fluid pressure that would yield zero fluid flux. P_e is equal to $[P_v - \sigma(\pi_v - \pi_i)]$.

As for the boundary conditions, it satisfies the no flux boundary condition at the center of the tumor due to symmetry:

$$\nabla P_i\big|_{r=0} = 0$$

At the surface of the tumor, two boundary conditions were used for this analysis. For tumors implanted in the dorsal skinfold chamber (Case I), since the tumor surface was exposed to atmosphere, where we calibrated P = 0, the boundary condition became:

$$P_i\big|_{r=R} = 0$$

When the tumor was implanted in the subcutaneous space (Case II), i.e. surrounded by normal tissue, the pressure decayed over some distance in normal tissue. Thus, the continuity of pressure and interstitial velocity hold:

$$P_i\big|_{r=R^-} = P_i\big|_{r=R^+} \qquad \text{and} \qquad -K_T \frac{dP_i}{dr}\bigg|_{r=R^-} = -K_N \frac{dP_i}{dr}\bigg|_{r=R^+}$$

where R^- and R^+ represent the tumor-host boundary at the tumor and host side, respectively. K_T and K_N is the hydraulic conductivity of tumor and normal tissue, respectively. The remaining boundary condition of Case II was that P_i becomes 0 as R approaches infinite, assuming that blood vessels and lymphatic vessels in normal tissue will eventually drain all excess interstitial fluid.

Solving the differential equations using the appropriate boundary conditions, pressure and interstitial velocity profiles can be solved analytically.

Case I: Tumor implanted in the dorsal skinfold chamber

$$\hat{P} = \frac{P_i}{P_e} = 1 - \frac{1}{\hat{r}} \frac{\sinh(\alpha \hat{r})}{\sinh(\alpha)}$$

$$\hat{u} = \frac{u_i R}{K P_e} = \frac{1}{\hat{r}} \left(\frac{\sinh(\alpha \hat{r})}{\sinh(\alpha)}\right.$$

Case II: Tumor implanted in the subcutaneous space (i.e. surrounded by normal tissue)

$$\hat{P} = 1 - \frac{(1+\alpha_N)}{\hat{r}} \frac{\sinh(\alpha_T \hat{r})}{(1+\alpha_N)\cdot\sinh(\alpha_T) + \hat{K}\cdot[\alpha_T \cdot \cosh(\alpha_T) - \sinh(\alpha_T)]}; \qquad r < R$$

$$\hat{P} = \frac{1}{\hat{r}} \frac{\hat{K}\cdot[\alpha_T \cdot \cosh(\alpha_T) - \sinh(\alpha_T)]\cdot e^{-\alpha_N \cdot \hat{r}}}{[\hat{K}\cdot\alpha_T \cdot \cosh(\alpha_T) - \sinh(\alpha_T) + (1+\alpha_N)\cdot\sinh(\alpha_T)]\cdot e^{-\alpha_N}}; \qquad r > R$$

where $\hat{P}$, $\hat{u}$, and $\hat{r}$ are dimensionless interstitial pressure, dimensionless interstitial velocity and dimensionless radial position (r/R). Subscript T stands for tumor and N stands for normal tissue and $\hat{K}$ is equal to K_T/K_N.

While P_v, π_v, and π_i have been measured in both the control and DC101-treated groups, several parameters such as L_p, K, σ and S/V need to be estimated before calculating P_i using the mathematical model.

Estimation of σ

There are no published values of σ for tumors in the literature, however, σ for normal tissue has been measured (Jain 1987). The value of σ for albumin varies between 0 for the liver (with a high vascular permeability) and 1 for the impermeable brain vessels, and lung has a σ of 0.5 (Parker et al. 1984; Aukland and Reed 1993). For albumin in normal muscle, σ was measured to be 0.91 for subcutaneous tissue (Ballard and Perl 1978). This is the value (for normal tissue) we used for the model. To estimate σ for tumors, a solid solute/cylindrical pore model was employed. In this model, BSA was modeled as a solid sphere, and vascular wall was assumed to have cylindrical pores (Anderson and Malone 1974; Deen 1987). σ can be estimated as:

$$\sigma = [1 - (1 - \lambda)^2]^2$$

where $\lambda = r_s$ (solute radius)/r_o (pore radius). BSA is reported to have a hydrodynamic radius of around 3.5 nm (Pluen et al. 2001; Alexandrakis et al. 2004). The vascular pore cutoff size of MCaIV tumors implanted in the dorsal skinfold chamber has been shown be between 1.2 and 2 microns (Hobbs et al. 1998). Based on scanning electron microscopy images, intercellular openings have an average of 1.7 microns in diameter and transcellular holes have an average of 0.6 microns in diameter (Hashizume et al.

2000). Thus, for this analysis, it was estimated that the pore size of MCaIV vessels was around 500 nm. Based on the solute radius and pore radius, the calculated σ was 0.0001. This was a reasonable value because MCaIV tumor vessel was extremely leaky, thus one would expect a really low σ.

To date no one has measured vessel pore size after anti-angiogenic treatment. However, it has been shown that hormone withdrawal leads to a drop in pore cutoff (to about a fifty of its original value) in Shionogi tumors, a hormone dependent tumor (Hobbs et al. 1998). Hormone withdrawal leads to a decrease in VEGF level, similar to VEGF blockade by DC101 (Jain et al. 1998). Thus, the pore size of normalized blood vessels was estimated to be 100 nm (one fifth of the value before DC101 treatment), and the calculated σ was 0.005. Even if the pore size decreased to 50 nm (ten times reduction), the calculated σ was still extremely small (0.02). This implied that there was negligible effect of oncotic pressure gradient in determining fluid flux across the vascular wall.

Estimation of L_p and K

To date, there is no value of L_p reported for tumors. On the other hand, L_p has been measured in various normal tissues in a variety of animals (Jain 1987; Baxter and Jain 1991). For capillaries in skeletal muscle in rats, L_p was calculated as 0.36×10^{-7} cm/mmHg-s (Rippe and Haraldsson 1986). In this model, L_p in tumors was estimated to be 2.8×10^{-7} cm/mmHg-s, same as what was estimated in the Baxter and Jain model (Baxter and Jain 1989).

It has been shown that there is a 5-fold increase in L_p in monolayers of endothelial cells *in vitro* after the addition of VEGF (Chang et al. 2000). Therefore, we estimated that L_p would decrease at least 5 times compared to control treatment when tumors were treated

with DC101 (VEGF blockade) compared to control treatment. Thus, L_p of vessels in the normalization time window was estimated to be 0.56×10^{-7} cm/mmHg-s. As shown in Chapter 6, after DC101 treatment there was significant increase in both perivascular cell and basement membrane coverage. Thus, one would predict that Lp would decrease even more.

Since no additional information was available for K, and we did not expect DC101 affected the interstitial matrix, the value for hydraulic conductivity would be the same as in the Baxter and Jain model (Baxter and Jain 1989).

Estimation of S/V

S/V (surface area of blood vessels per volume of tissue) was calculated based on two photon microscopy images. Two photon images of normal brain vasculature and glioblastoma tumor vasculature treated with either control IgG or DC101 were obtained after injecting a fluorescent tracer i.v. In collaboration with Alex Tyrell and Dr. Badri Roysam at the Rensselaer Polytechnic Institute, a computer algorithm was written to trace the 3D vascular network. Briefly, by combining active contour and super-Gaussian fitting, entire vessel segments could be traced starting from multiple seed points. The cross section of each vessel segment was fitted by an ellipse, and thus, the perimeter of the vessel segment could be obtained. By applying the convex hull technique, the outermost detectable vessels provided the boundary of tissue that needed to be analyzed.

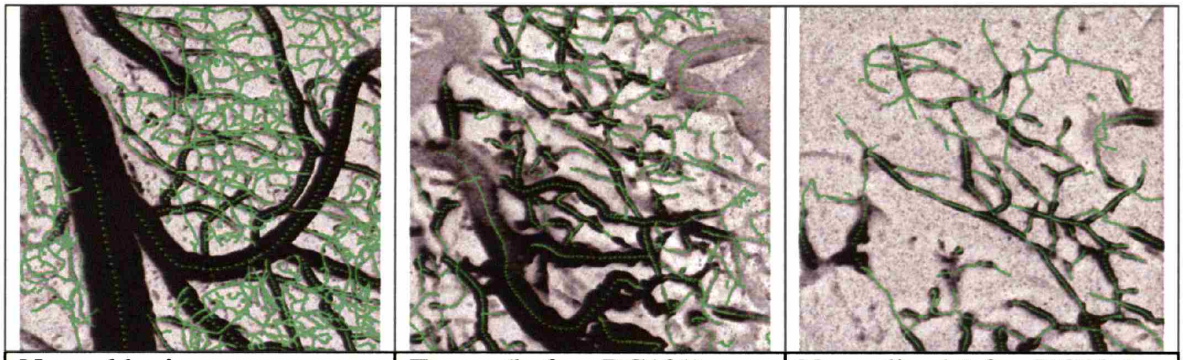

Normal brain	Tumor (before DC101)	Normalized (after DC101)

Figure 7.19: Computer traces of 3D vascular network.

Maximum intensity projection of 3D two photon images of blood vasculature: (left) normal brain, (center) U87 tumor before DC101 treatment, and (right) same region of U87 tumor after DC101 treatment. Green dots/lines were computer traces of the vascular network. Each dot contained information such as vascular diameter by fitting the cross sectional area with ellipse.

Based on these images, values of S/V for three different cases were calculated (~250 cm^{-1} for normal vasculature, ~250 cm^{-1} for tumor vasculature, and ~150 cm^{-1} for normalized tumor vasculature). These values were the same order of magnitude as the values used in Baxter and Jain model (200 cm^{-1} for normal tissue, 90 cm^{-1} for tumor), but slightly higher. The difference could be due to the increased sensitivity of two photon images. Interestingly, even though tumor vessels were dilated compared to the normal vessels, they had the same S/V, presumably due to the lower vascular density.

Parameter	Normal	Tumor	Normalized	Reference
L_p (cm/s/mmHg)	0.36×10^{-7}	2.8×10^{-7}	0.56×10^{-7}	See text, (Rippe and Haraldsson 1986; Baxter and Jain 1989)
K (cm^2/s/mmHg)	8.53×10^{-9}	4.13×10^{-8}	4.13×10^{-8}	(Swabb et al. 1974; Baxter and Jain 1989)
S/V (cm^{-1})	250	250	150	See text
P_v (mmHg)	15.6	5.9	5.3	See text, (Baxter and Jain 1989)
π_v (mmHg)	20	19.8	19.2	See text, (Baxter and Jain 1989)
π_i (mmHg)	10	17.3	15.1	See text, (Baxter and Jain 1989)
σ (BSA)	0.91	0.0001	0.005	(Ballard and Perl 1978; Baxter and Jain 1989)

Figure 7.20 and Figure 7.21 showed the calculated interstitial fluid pressure and interstitial fluid velocity profiles as a function of distance from the center of the tumor. The radius of the tumor was assumed to be 4 mm. Figure 7.20 represented the boundary condition used for Case I (dorsal skinfold chamber tumors) while Figure 7.21 represented the boundary condition used for Case II (subcutaneous tumors). Due to technical difficulties, MVP and IFP measurements were done in tumors implanted in dorsal skinfold chambers, while other experiments were done in subcutaneous tumors (see

Material and Methods section). For each case, pressure and velocity profiles were given for both the control group (red) and the DC101-treated group (blue).

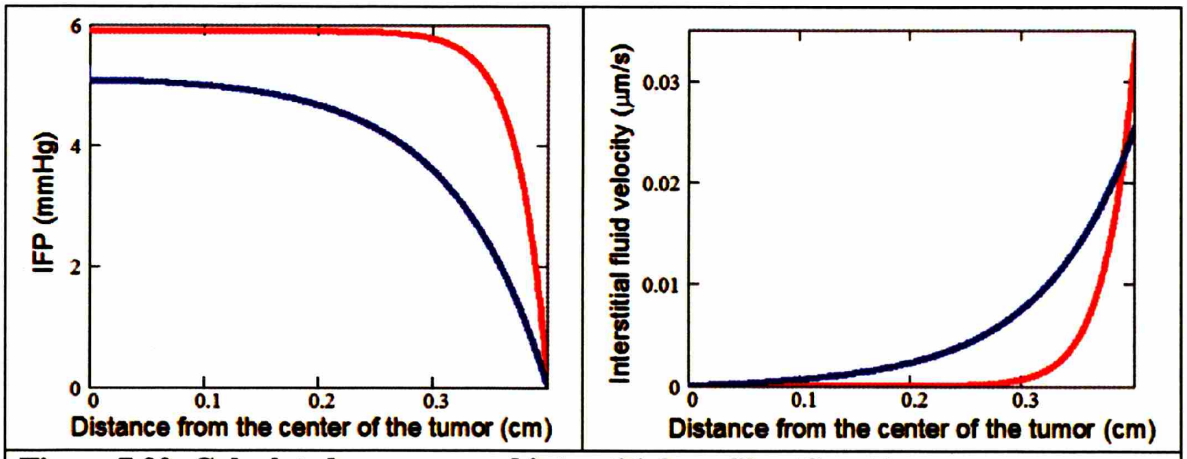

Figure 7.20: Calculated pressure and interstitial profiles (Case I).

The boundary conditions used in this model were valid for tumors implanted in the dorsal skinfold chamber (Case I). Red line was a tumor treated with control IgG, while blue line was a tumor treated with DC101.

Using the parameters and the mathematical model, pressure and interstitial fluid velocity profiles were calculated. The tumor in the control group had similar pressure profile as the previously published experimental results (Boucher et al. 1990). It predicted a reduction in IFP throughout the tumor (blue line). This result confirmed the IFP finding. Interestingly, this model also predicted higher interstitial fluid velocity in most regions of the tumor, possibly due to the induced hydrostatic pressure gradient.

For subcutaneously tumors, the profiles were similar (Figure 7.21), with the exception that both pressure and velocity did not abruptly terminate at the tumors' edge.

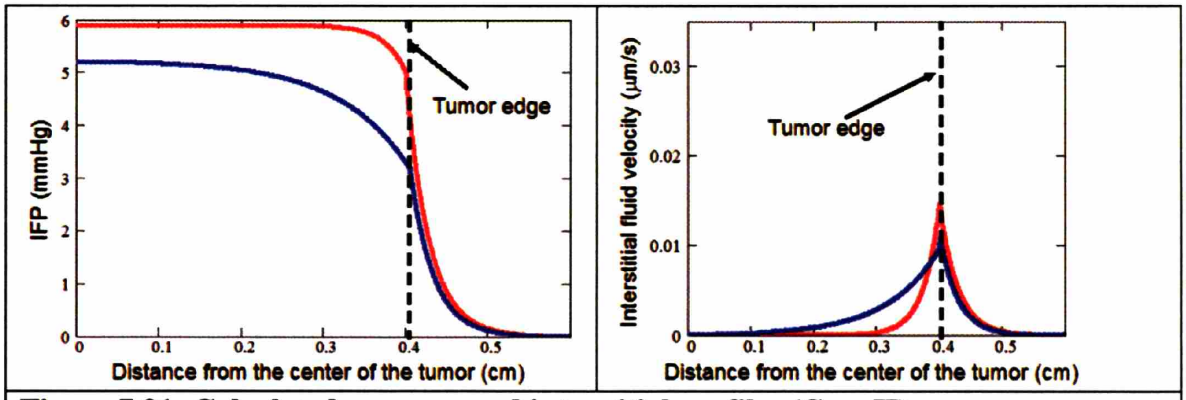

Figure 7.21: Calculated pressure and interstitial profiles (Case II).

The boundary conditions used in this model were valid for tumors implanted in subcutaneous space (Case II). The red line indicated a tumor treated with control IgG, while the blue line indicated a tumor treated with DC101.

The mathematical model, for both cases, predicted a reduction in IFP after DC101 treatment. It also predicted a higher interstitial fluid velocity in most region of the tumor. This implied that the interstitial fluid was not as stagnant as in the control group, and this would enhance the delivery of molecules in tumors.

We previously showed that angiotensin II could increase the systemic blood pressure in mice, and could create a pressure gradient across the vessel wall in tumors (Netti et al. 1999). Unfortunately, interstitial pressure caught up with vascular pressure, and the pressure gradient across the vessel wall dissipated in less than one minute. Nevertheless, even these short-lived gradients could increase the delivery of specific antibodies in tumors (Netti et al. 1999). Thus the sustained hydrostatic pressure gradient across the tumor vasculature, induced by DC101, could increase the transvascular convection of large molecules, despite a drop in vascular permeability to macromolecules, as shown by the predictions based on the mathematical model.

To test if reduced tumor hypoxia improved radiation response, we conducted a systematic evaluation of five treatment schedules using a combination of DC101 and γ radiation to treat U87 tumors growing orthotopically in the mouse brain (Figure 7.22). We found that, when used as a monotherapy, DC101 (given at 40 mg/kg on days 0, 3, and 6) produced a small, statistically insignificant tumor growth delay of ~2.5 days, while radiation (three daily fractionated doses of 7 Gy each) significantly delayed the growth by ~12.5 days. When DC101 was given in non-optimal combinations with radiation (RT1, RT2, RT3, RT5), the combined therapy had no more than an additive effect. However, giving radiation therapy on days 4 to 6 after DC101 treatment began (RT4) produced a synergistic effect in which the tumor growth delay significantly exceeded the expected additive effect. Collectively, these results demonstrated that DC101 led to improved vascular function (reduced tumor hypoxia) and enhanced response to radiation therapy.

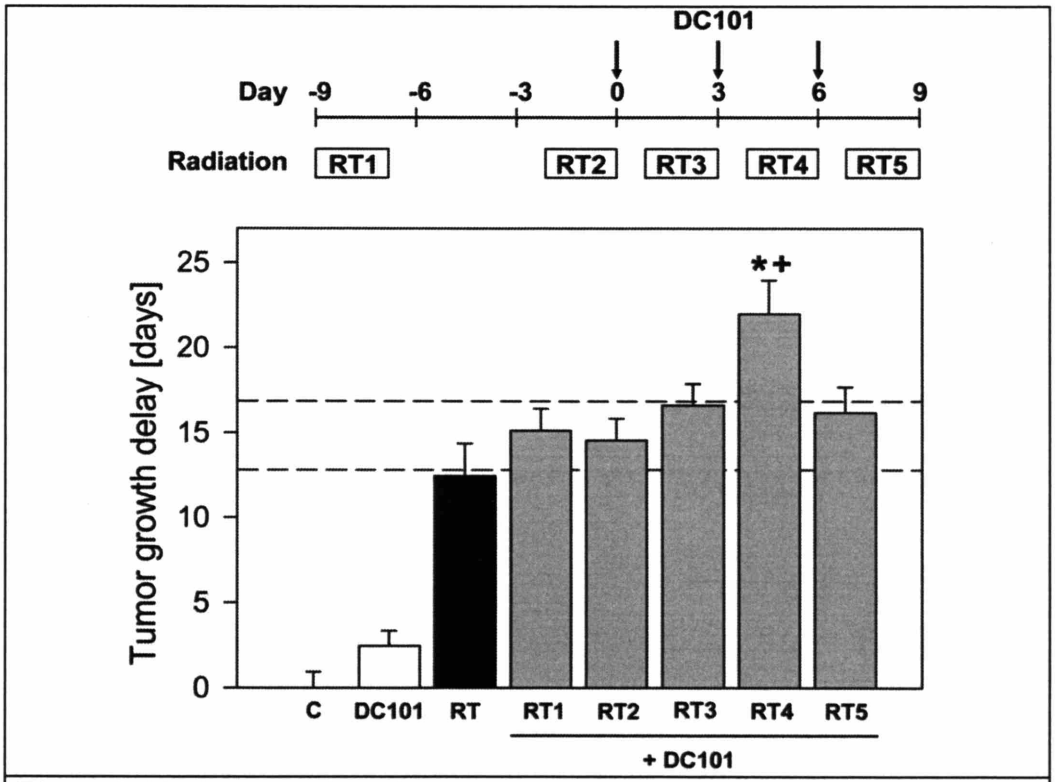

Figure 7.22: Combination of radiation and anti-angiogenic therapies was only synergistic during the normalization time window.

Tumor growth delay of orthotopic U87 glioblastoma was shown for untreated controls (C), monotherapy with DC101 (three injections, three days apart), local radiation for three consecutive days (RT), and five different combination schedules where radiation was given before, during, or after DC101 therapy (RT1-RT5; see diagram for schedules). The dashed lines showed the range of the expected additive effect (EAE) of DC101 and radiation. * $P < 0.05$, compared to RT; $^{+}$ $P < 0.05$, compared to EAE.

In tumors, the abnormally high leakiness of the vasculature hindered drug delivery by inducing blood flow stasis (Netti et al. 1996; Baish et al. 1997), whereas normalized vessels were less leaky to macromolecules. As shown in Figure 7.18, we showed that

there was a significant increase in the normalized RBC velocity. However, it appeared that there was no difference in the absolute RBC velocity. One reason we did not see any changes in the absolute RBC velocity was because both intra-sample variability and between-sample variability were high. To minimize intra-sample variability, we should measure RBC velocity of most tumor blood vessels for a long period of time; however, due to technical limitations (i.e. the length of the experiment was limited by the anesthesia time, and the number of RBC scans was limited by the possibility of photo-damage), only a few vessels per mouse could be measured. To account for the randomness of between-sample variability, mixed models was used to analyze the data (Appendix 3). Based on this model, it was shown that the RBC velocity in DC101 treatment group was significantly higher than in the control group. Thus, both analyses suggested that DC101 affected RBC velocity in tumors.

Since we had data for both RBC velocity and diameter, we could estimate the effects of DC101 on blood flow. Mean blood flow rates of individual vessel (Q) could be estimated based on vessel radius (R) and mean RBC velocity (v_{mean}):

$Q = \pi * r^2 * v_{mean}$

and v_{mean} was estimated from the empirical relationship:

$v_{mean} = v_{centerline}/\alpha$

where the value of a depends on vessel diameter ($\alpha = 1.3$ for blood vessels < 10 μm; linear extrapolation $1.3 < \alpha < 1.6$ for blood vessels between 10 and 15 μm; and $\alpha = 1.6$ for blood vessels > 15 μm (Leunig et al. 1992). Since all line scans were positioned at the center of vessels, the measured velocities were $v_{centerline}$. The calculated blood flow values of individual vessel were analyzed using the mixed models. No difference was

found after DC101 treatment. This data suggested that blood flow of the remaining network after DC101 treatment was not compromised even though RBC velocity was increased. Unfortunately, due to the limitations the line scan method, further studies will be needed to form a definitive conclusion on the effects of anti-angiogenic therapy on blood flow.

In conclusion, our results showed that DC101 reduced the IFP while maintaining MVP, and as a result, it induced a positive hydrostatic pressure gradient across the tumor vasculature. The induced hydrostatic pressure gradient across the vascular wall could improve the penetration of small and large therapeutic agents in tumors. Furthermore, we showed that the RBC velocity of remaining vessels increased 3 days and 5 days after DC101 treatment in U87 orthotopic model, and this could partly explain the reduced tumor hypoxia during the normalization time window. In the next chapter, I examine the molecular changes during DC101 treatment.

Chapter 8: Molecular Changes during DC101 Treatment

Portions of this chapter have been taken from:

Tong, R. T., Boucher, Y., Kozin, S. V., Winkler, F., Hicklin, D. J., and Jain, R. K. (2004). Vascular normalization by vascular endothelial growth factor receptor 2 blockade induces a pressure gradient across the vasculature and improves drug penetration in tumors. *Cancer Res* 64, 3731-3736.

Winkler, F.*, Kozin, S. V.*, **Tong, R. T.**, Chae, S. S., Booth, M. F., Garkavtsev, I., Xu, L., Hicklin, D. J., Fukumura, D., di Tomaso, E., Munn, L. L., and Jain, R. K. (2004). Kinetics of vascular normalization by VEGFR2 blockade governs brain tumor response to radiation; Role of oxygenation, angiopoietin-1, and matrix metalloproteinases. *Cancer Cell* 6, 553-563. * These authors contributed equally.

Introduction

In Chapters 6 and 7, I demonstrated that tumor vasculature was highly abnormal, in both its structure and its function. The imbalance between angiogenic and anti-angiogenic molecules in tumors led to tortuous and dilated blood vessels. Furthermore, perivascular cells were often detached from the blood vessels, and many of the tumor vessels had incomplete pericyte coverage. Similarly, basement membrane coverage of tumor vessels was incomplete. The abnormalities in vascular wall structure and endothelial-endothelial cell junction led to high permeability. In turn, high vascular permeability coupled with the lack of functional lymphatic vessels led to high interstitial fluid pressure. These abnormalities both in the tumor vasculature and microenvironment impeded uniform delivery of oxygen and molecules in tumors.

During vascular development, the formation of mature vessels requires that numerous molecular signals work harmoniously at the appropriate level and with correct timing. Studies have shown that disruption of certain molecules such as VEGFs, PDGFs, and angiopoietin often lead to abnormal vascular development (Jain 2003). Similarly, in adults many of these pathways are not regulated appropriately in tumors, leading to abnormal vasculature and tumor microenvironment. Interestingly, despite the drop in vascular density, the pericyte coverage improved significantly after DC101 treatment. Consequently, the modified vascular wall structure led to the improved barrier function of tumor blood vessels. To dissect the molecular mechanism involved in this normalization process, I collected total RNA and protein from MCaIV tumors 3 days after the completion of treatment with DC101 or control IgG. By unraveling the molecular mechanism on how the vascular normalization proceeded, we might be able to

develop strategies to extend the window of normalization in the future. This would enable improved delivery of oxygen and therapeutic agents to a greater extent and for a longer period of time. This knowledge will also allow the development of better anti-angiogenic agents and treatment strategies.

Results

Gene array analysis

SCID mice with MCaIV tumors were treated with either control IgG or DC101 for three days. Five tumors per group were collected for the gene array analysis. Total RNA was extracted from tumors of 4-5 mm diameter using TRIzol Reagent (InVitrogen). Total RNA concentration of each sample was measured and mixed together in equal amount. To screen for relative differential expression of multiple genes, cDNA array containing 96 genes involved in angiogenesis and vessel maturation were used according to manufacturer's instructions (GEArray Q Series, SuperArray, Bethesda, Maryland). Chemiluminescent spots were quantified by densitometry and normalized with β-actin (FluoroChem 8800 system).

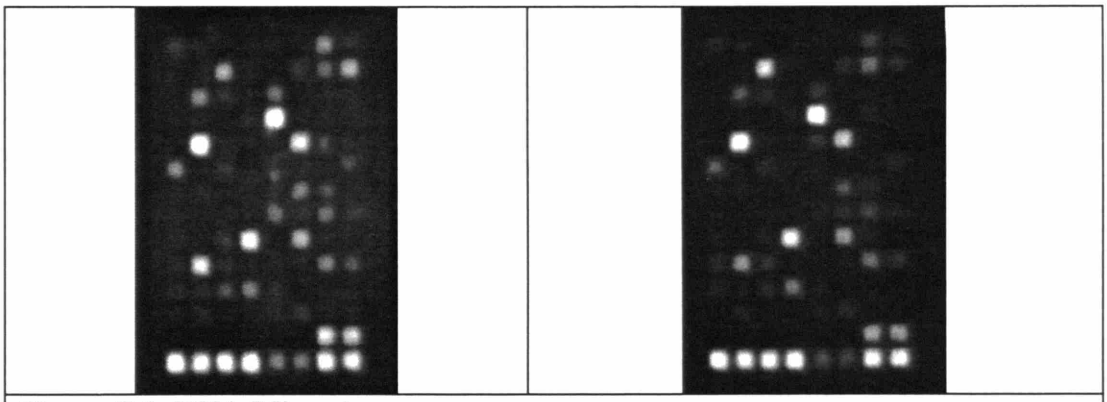

Figure 8.1: DNA MicroArray.

The array contained 96 genes involved in angiogenesis and vessel maturation. Control IgG group (left) and DC101-treated group (right)

While most of the genes did not differ much between the control IgG and DC101-treated groups, the expression level of some genes were modified after DC101 treatment. The following was the summary of genes that change as a result of DC101 treatment.

Table 8.1: Gene Array Data

Gene	Expression (DC101/Control)
Angiopoietin-2	0.457
VE-Cadherin	0.518
PECAM	0.386
Epidermal Growth Factor	0.224
Ephrin B2	1.254
PDGFB	0.461
PDGFRβ	0.394
HIF1α	0.864
Thrombospondin 2	0.292
MMP2	0.386
MMP9	0.135

Angiopoietin-2 expression was found in numerous tumors (Table 9.1). Ang-2 is a natural antagonist for Ang-1 for binding the Tie2 receptor present on endothelial cells, and is known as a factor that destabilizes blood vessels (Maisonpierre et al. 1997). VE-Cadherin and PECAM are adhesion molecules that express on the endothelial cells (Jain 2003). Epidermal Growth Factor (EGF) is a growth factor expressed in some tumors, and it stimulates tumor growth through the EGFR signaling pathway. The ephrin/Eph signaling pathway is important for the determination of arterial and venous endothelial specialization, while PDGF/PDGFR promotes proliferation, migration and recruitment of mural cells. HIF1α is a transcription factor that is upregulated in hypoxic condition, and Matrix Matelloproteases (MMPs) degrade various kinds of collagen.

Real-time PCR data

We quantified the mRNA levels of various candidate molecules that were identified by cDNA gene array analysis using real-time PCR. Real time PCR primer sequences were designed using LUX Online Primer Software (LUX system, Invitrogen, Carlsbad, California). Quantitative RT-PCRs were performed on the ABI 7700 sequence detection system (Applied Biosystems). Eight animals per group were used for the Real-time PCR experiments. All experiments were performed in duplicate, and a standard curve for the specific cDNA of interest was run with every PCR reaction. The amount of cDNA was expressed relative to this standard curve. The final quantification of each cDNA sample was relative to its β-actin level.

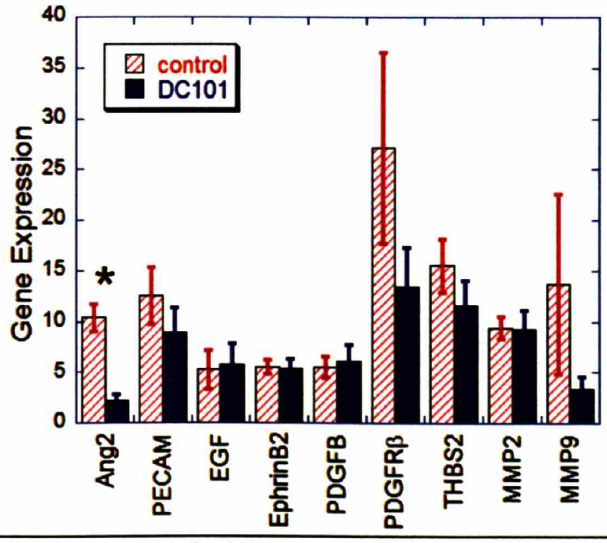

Figure 8.2: Real time-PCR. DC101 reduced the Ang-2 gene expression.

Eight animals per group were used for the real-time PCR analysis. Each gene expression level was normalized by β-actin level. * $P<0.005$ Data are represented as mean ± S.E.M.

Out of the genes that were tested for real-time PCR, only Ang-2 expression showed significant difference between the control (n = 8, 10.39 ± 1.34) and the DC101-treated

group (n = 8, 2.25 ± 0.52). ($P < 0.005$) Interestingly, MMP9 also showed a trend towards a reduced expression after DC101 treatment. (MMP expression of the control group (n=8) is 13.70 ± 8.88, while the DC101-treated group (n=8) is 3.37 ± 1.18).

Ang-2 Western Blot

Western Blot Analysis was used to further confirm the downregulation of Ang-2 in protein levels. Five animals in the control and four animals in the DC101-treated group were used. Protein was isolated, and NuPAGE (InVitrogen) was used to run the Western Blot. Goat anti-human Ang-2 antibody (1:1000; R&D AF623) and Goat anti-β-actin antibody (1:500; Santa Cruz) were used to identify Ang-2 and β-actin proteins. According to the manufacturer, the Ang-2 antibody also cross-reacts with mouse protein.

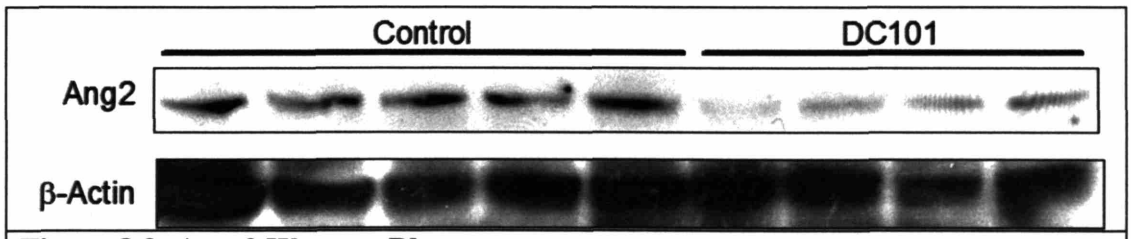

Figure 8.3: Ang-2 Western Blot.

DC101 lowered Ang-2 protein level in tumors.

As shown in Figure 8.3, DC101 lowered the protein level of Ang-2 in tumors. These data agreed with the gene array and real-time PCR data.

Ang-2 Immunostaining

To identify the distribution of Ang-2 protein in tumors, immunostaining was performed in control and DC101-treated tumors. Goat anti-human Ang-2 antibody (1:100; R&D AF623) was used to label Ang-2 protein in tumors. While some tumor and stromal cells were stained positive with Ang-2, most of the Ang-2 staining was associated with tumor blood vessels.

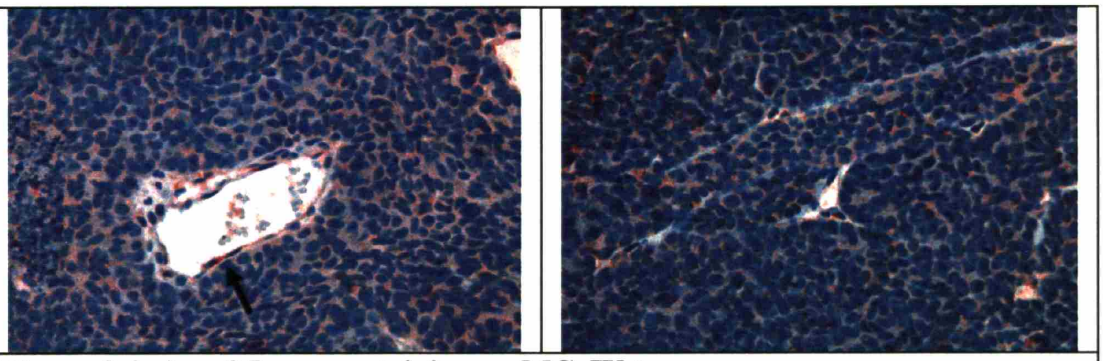

Figure 8.4: Ang-2 Immunostaining on MCaIV tumors.

Control IgG (left) and DC101-treated (right) tumors. The arrow points to the Ang-2 positive blood vessel. Image width = 356 microns.

Discussion

Angiogenesis and vascular development involves a complex series of events during which endothelial cells differentiate, proliferate and migrate (Yancopoulos et al. 2000). Furthermore, the endothelial cells also undergo morphological organization and interact with the surrounding cells and tissue, such as the interstitial matrix and pericytes. The maturation of vasculature requires recruitment of perivascular cells, generation of an extracellular matrix and formation of vessel wall with good structural support and appropriate regulation of vessel function (Jain 2003). In recent years numerous new pathways and ligand/receptor systems have been found to be crucial in the process of angiogenesis and vascular maturation.

In addition to the VEGF receptors, a second class of endothelial-specific tyrosine kinase receptors has been implicated in vascular growth and development. These are the Tie-1 and Tie-2 receptors (Sato et al. 1995). The angiopoietins were identified via secretion trap and homology cloning techniques as a family of structurally related proteins that bind to Tie-2 receptor (Davis et al. 1996; Maisonpierre et al. 1997). Ang-1 acts as an agonist, activating the Tie-2 signaling pathways (Davis et al. 1996; Suri et al. 1996);

while Ang-2 acts as antagonist in the context of the endothelium, specifically blocking the Ang-1 dependent activation of these pathways (Maisonpierre et al. 1997). Ang-1 seems to be important in maintaining the quiescence and stability of the mature vasculature. Ang-1 deficient mice display deficits in vascular development (Suri et al. 1996). Mice lacking Ang-1 seem to exhibit a simplified and less complex vasculature. Endothelial cells are poorly associated with the underlying matrix and do not properly recruit and associate with perivascular cells. Experiments with transgenic mice overexpressing Ang-2 show a phenotype similar to Ang-1 deficient mice, demonstrating that Ang-2 probably acts as a Tie-2 antagonist (Maisonpierre et al. 1997). Ang-2 is postulated to be a key destabilizing factor involved in initiating angiogenic remodeling. In a rat C6 glioma model, researchers show progressive detachment of αSMA-positive cells coincides with Ang-2 upregulation (Holash et al. 1999). Interestingly, some studies suggest that Ang-2 function depends on the availability of VEGF (Lobov et al. 2002). In the presence of VEGF, Ang-2 promotes angiogenesis, remodeling of the basal lamina, and proliferation and migration of endothelial cells. In contrast, in the absence of VEGF, Ang-2 leads to endothelial cell apoptosis and vessel regression.

As mentioned above, Ang-2 is upregulated in many human tumors (Table 9.1), as well as during development at sites where blood vessel remodeling is occurring. Similar to other studies, the immunostaining shows Ang-2 protein localizes around blood vessels (Krikun et al. 2000; Pichiule and LaManna 2002). To date, little is known about the regulation of angiopoietin gene expression. Promoter analyses have not been undertaken, and most information in this area is derived from observations of changes in expression following specific treatment. Many studies show that hypoxia results in an increase of Ang-2 levels

(Oh et al. 1999; Krikun et al. 2000; Ray et al. 2000; Pichiule and LaManna 2002; Pichiule et al. 2003), while a few studies also show increases in Ang-1 level (Ray et al. 2000). Some studies also show that Ang-2 levels can be increased by VEGF and other growth factors (Mandriota and Pepper 1998). Results in this thesis (Chapter 7) demonstrated that DC101 reduced hypoxia in U87 tumors due to vascular normalization. This finding strongly suggested that blocking the VEGFR2 pathway would induce a change in Ang-2 expression either by intermediate signaling molecules or by improved oxygenation in tumors. Interestingly, the expression level of Ang-2 had also been shown to be decreased in mammary adenocarcinoma model after the treatment of endostatin, an endogenous anti-angiogenic molecule generated by the cleavage of collagen XVIII (Calvo et al. 2002). However, further studies are needed to dissect the mechanism.

Of interest, in the Winkler et al. study (Winkler et al. 2004), we had shown that DC101 led to up-regulation of Ang-1 during the normalization time window (Figure 8.5). Thus, in U87 tumor model, DC101 led to upregulation of Ang-1 during the normalization time window, while in MCaIV tumor model, it led to downregulation of Ang-2. This suggested that the ratio between Ang-1/Ang-2 might be important in the normalization process.

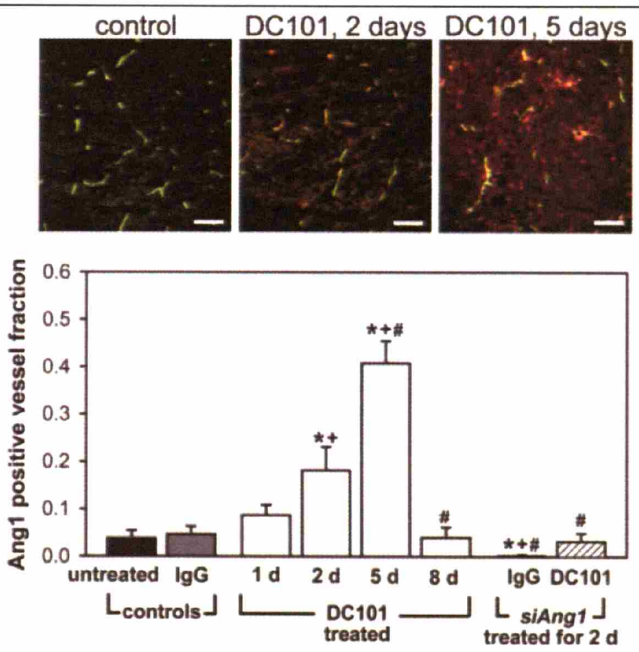

Figure 8.5: Ang-1 protein level increased after DC101 treatment.

Ang-1 protein (red) co-localized with perfused vessels (green) 2 and 5 days after initiation of DC101 treatment. A low level of Ang-1 near perfused vessels was observed in control tumors, at day 1 and at day 8 after initiation of DC101 treatment. Ang-1 protein production was blocked in tumor cells transfected with Ang-1 siRNA. Scale bars, 100 microns. $*P < 0.05$ compared to untreated control; + $P < 0.05$ compared to control IgG group (day 2); # $P < 0.05$ compared to day 2 after initiation of DC101 treatment. Data are represented as mean ± S.E.M. (Winkler et al. 2004)

In addition, Ang-2 was shown to stimulate the expression of MMP9 in cultured retinal endothelial cells (Das et al. 2003). Similar to other studies, the authors showed that Ang-2 was upregulated during the development of the normal retinal vasculature. The authors used muTek delta Fc (the extracellular domain of murine Tek receptor fused to the Fc portion of murine IgG) to block the binding of Ang-1 and Ang-2 to Tie-2 receptor. Interestingly, mice treated with Tek-delta Fc were shown to have a significant decrease in

MMP9 mRNA expression compared with the IgG-treated control animals. In a separate study, both Ang-2 and MMP2 had been shown to be upregulated in the invasive area in human glioma biopsies (Hu et al. 2003). Moreover, Ang-2 over-expressing tumors had also shown to have higher levels of MMP2 activation and increased angiogenesis. These studies suggested that there was cross-talk between Ang-2 signaling pathway and MMPs expression. Based on the gene array and real-PCR data, we also observed a tendency towards decreased MMP9 expression after DC101 treatment. Both MMP2 and MMP9 can degrade the basement membrane (Kalluri 2003). Downregulation of Ang-2 could affect MMP expression, and hence reduced the degradation of basement membrane in tumors. Further studies are needed to dissect the molecular cross talk between Ang-2 and MMPs.

Chapter 9: Bevacizumab Phase I Human Clinical Trial

Portions of this chapter have been taken from:

Willett, C. G., Boucher, Y.*, Di Tomaso, E.*, Duda, D. G.*, Munn, L. L.*, **Tong, R. T.***, Chung, D. C., Sahani, D. V., Kalva, S. P., Kozin, S. V., Mino, M., Cohen, K. S., Scadden, D. T., Hartford, A.C., Fischman, A. J., Clark, J. W., Ryan, D. P., Zhu, A. X., Blaszkowsky, L. S., Chen, H. X., Shellito, P. C., Lauwers, G. Y., and Jain, R. K. (2004). Direct evidence that the VEGF-specific antibody bevacizumab has antivascular effects in human rectal cancer. *Nature Medicine* 10, 145-147. * These authors contributed equally.

Introduction

In the previous three chapters, I described the structural, functional and molecular changes during DC101 treatment in animal models. To determine whether these results based on pre-clinical models could translate into clinical practice, we initiated a Phase I clinical trial that integrated the VEGF-specific antibody bevacizumab (Avastin, Genentech, South San Francisco, CA) into a contemporary treatment program of preoperative chemotherapy and radiation therapy followed by surgery, for patients with primary and non-metastatic rectal cancer. This was a Phase I escalation trial, approved from the Cancer Therapeutics Evaluation Program of the National Cancer Institute as well as the Internal Review Board of Dana-Farber Partners Cancer Care. Two different doses (5 mg/kg and 10 mg/kg) of bevacizumab were given to two groups of patients. The patients with primary and locally advanced adenocarcinoma of the rectum were given bevacizumab alone for 2 weeks, which was the approximate half-life of bevacizumab in circulation. The treatment schedule was then followed by three two-week cycles of bevacizumab, 5-fluorouracil (5-FU) and external beam radiation therapy (EBRT) to the pelvis. All patients then underwent surgery uneventfully 7 to 9 weeks after completion of all preoperative therapy. Tumor biopsies were obtained before and 12 days after the first dose of bevacizumab infusion, which allowed for evaluation of the specific effects of bevacizumab alone on the tumors, as 5-FU and EBRT treatment was not initiated until the third week of the protocol. A number of measurements such as interstitial fluid pressure, blood flow and blood volume based on CT data, the number of circulating endothelial and progenitor cells, and FDG uptake were measured in this study. For my thesis work, I examined the microvascular density, pericyte coverage, and Ang-2

expression in tumor sections from biopsies and evaluated any potential normalization effects in human tumors.

Results

Microvascular density

Tumor biopsies obtained before and 12 days after the first bevacizumab infusion were assessed for microvascular density (MVD). Blood vessels were labeled using an antibody against human PECAM (Dako, Carpentria, CA). Digital images were taken to cover entire tissue sections. Out of the six pairs of biopsy samples, five of them had analyzable biopsies that permitted accurate determination of the number of vessels per micrometer square in areas of invasive adenocarcinoma with desmoplasia.

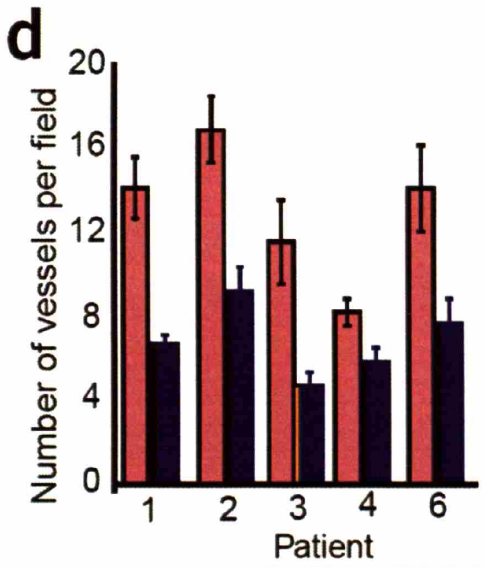

Figure 9.1: Microvascular density.

All patients showed a significant decrease in microvascular density (MVD) after bevacizumab treatment ($P < 0.05$ by t-test). Pink: pre-treatment; blue: 12 days post bevacizumab treatment. Data are represented as mean ± S.E.M.

The PECAM staining showed that the vascular density in rectal tumors decreased after bevacizumab treatment. Five of 5 analyzed patients showed a significant drop in vascular

density. Pooling the 5 patients together, the vascular density dropped from 13.0±3.2 to 6.9±1.8 after the treatment ($P < 0.003$). This set of data provided direct evidence of the anti-vascular effects of bevacizumab in human tumors, which was in line with preclinical findings.

Pericyte coverage

Pericyte coverage of the tumor vessels was assessed by double staining the biopsies for PECAM (Dako, Carpentria, CA) and αSMA (clone 1A4, Dako, Carpentria, CA). The concentration of αSMA (1:5000 dilution) was optimized to differentiate between the myofibroblasts present in the desmoplastic areas and the perivascular cells. Since the color of PECAM staining (DAB, brown) was quite close to the color of αSMA staining (Fast Red, pink), the pericyte coverage was counted by myself and another independent observer directly through a microscope. A vessel was considered covered when αSMA-positive cells covered ~75% of the perimeter of that vessel.

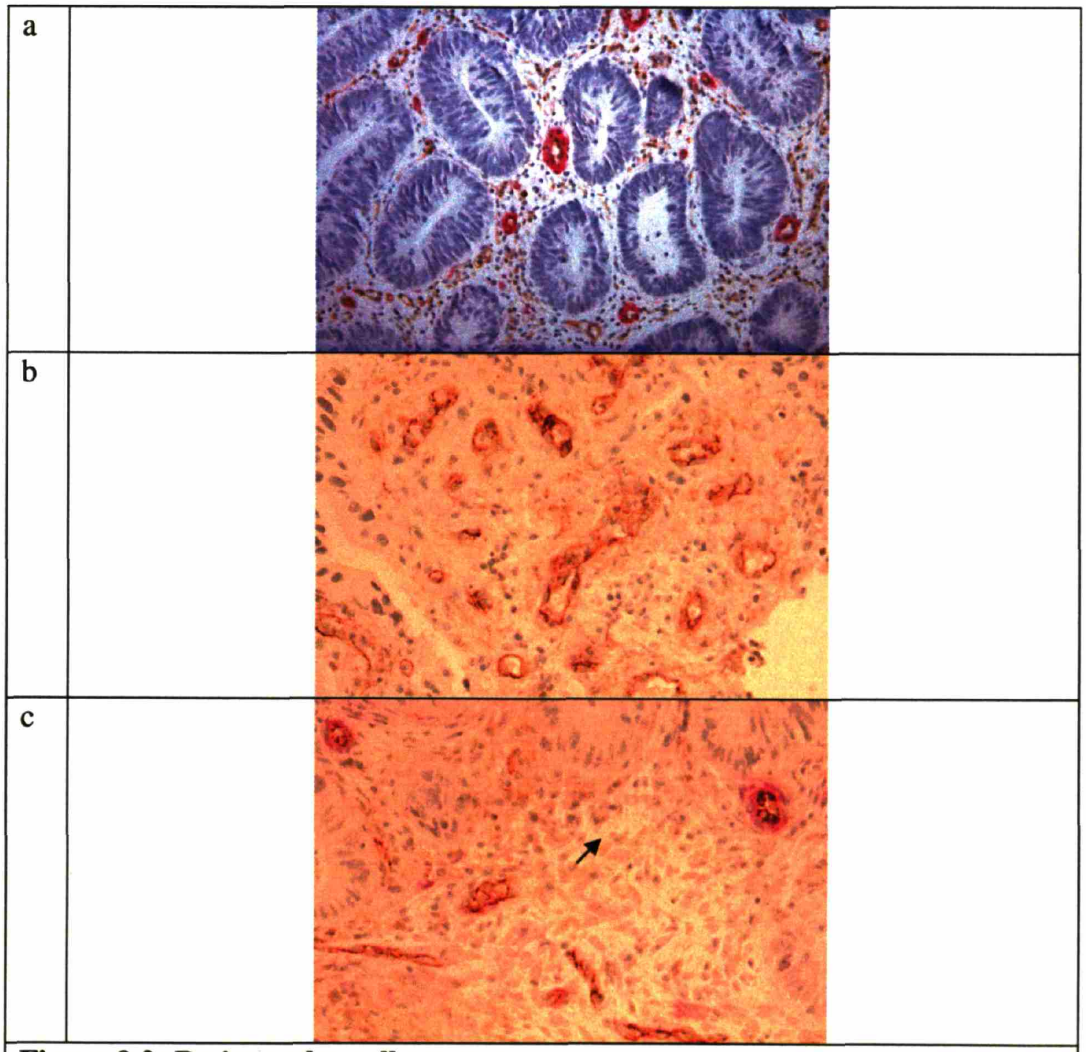

Figure 9.2: Perivascular cell coverage.

The tissues were double stained for PECAM (DAB, brown) and αSMA (Fast Red, pink). Double staining in adenoma (a). Most vessels were covered by perivascular cells. Representative fields depicting the variation in pericyte coverage before (b) and 12 days (c) after bevacizumab treatment in patients. The arrow points to a vessel surrounded by perivascular cells. Image width: (a): 712 microns, (b) and (c): 356 microns.

The immunostaining showed that while rectal adenocarcinomas had more vessels before bevacizumab treatment, most of these vessels were not covered by αSMA-positive cells.

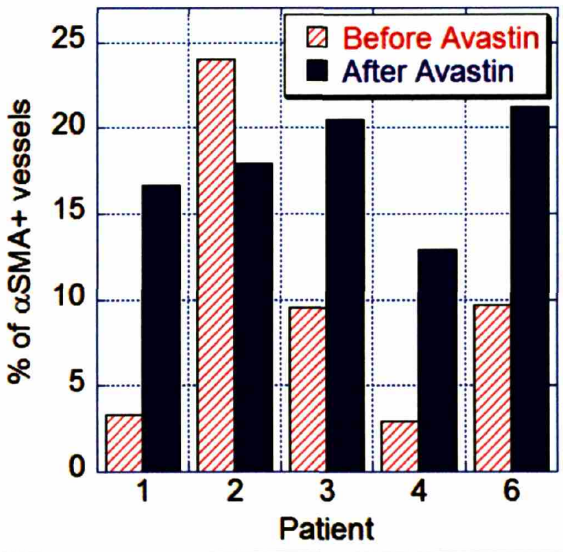

Figure 9.3: Fraction of vessels with pericyte coverage.

Four of five patients showed increased pericyte coverage.

By counting the total number of vessels with and without αSMA-positive cell coverage, we calculated the fraction of vessels with pericyte coverage. In 4 of 5 patients, the pericyte coverage increased. The limited number of patients and one outlier (Patient 2, as identified by the Extreme Studentized Deviate (ESD) test), indicated that while there was a trend, the increase in pericyte coverage with bevacizumab was not statistically significant ($P = 0.09$).

Ang-2 expression

To evaluate the effects of bevacizumab on Ang-2 expression in tumors, goat anti-human Ang-2 (1:200, AF623, R&D Systems Inc.) was used to stain biopsy samples pre- and post-bevacizumab treatment. Due to our limited number of samples, only 3 patients (Patients 1, 3 and 6) treated with 5mg/kg bevacizumab were analyzed. We had also analyzed 3 additional patients (Patients 8, 9 and 11) treated with 10 mg/kg bevacizumab.

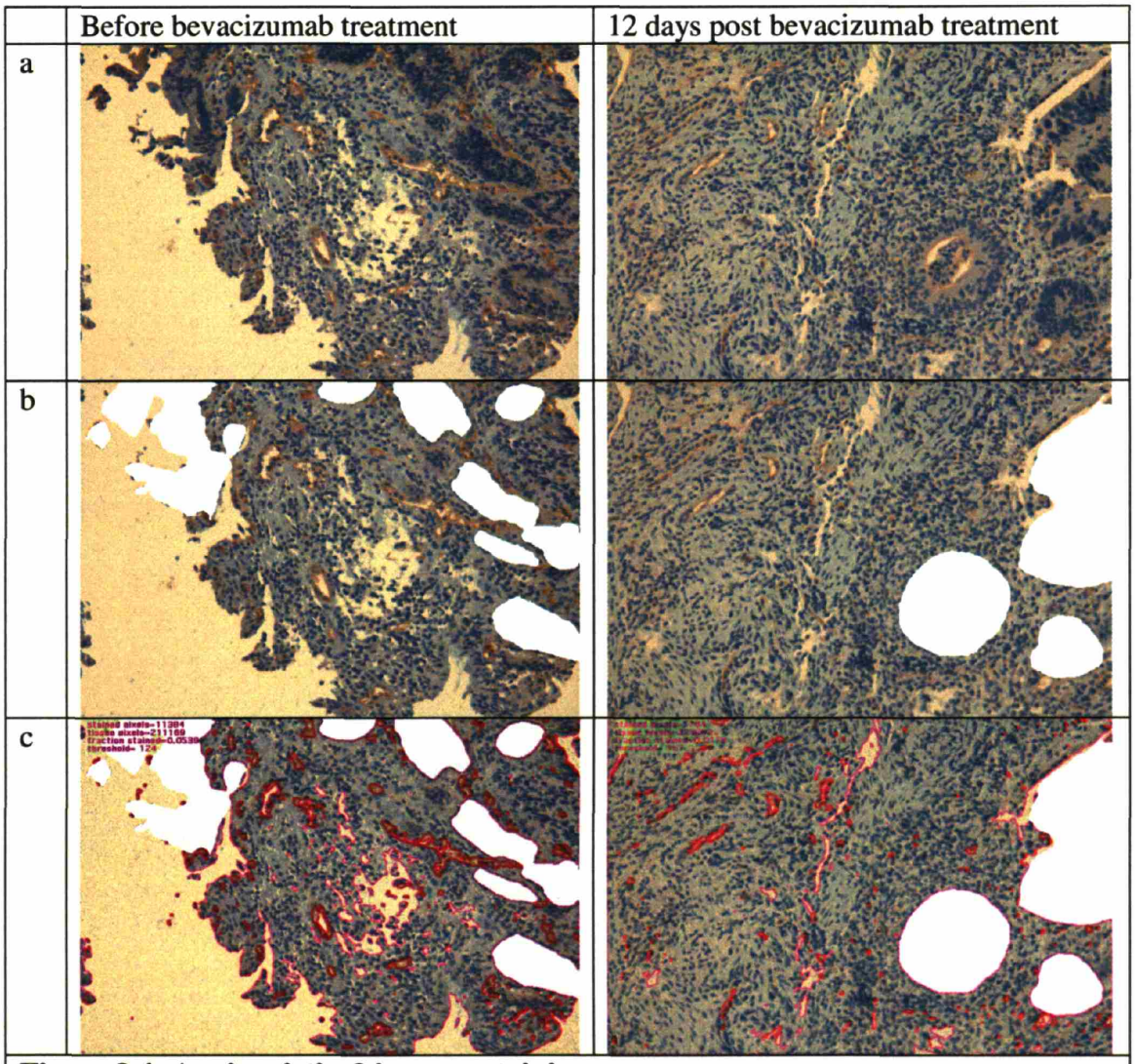

Figure 9.4: Angiopoietin-2 immunostaining.

(a) Ang-2 was localized using a goat anti-human Ang-2 antibody (brown). (b) Tumor nodules were identified by two independent observers, and were manually deleted using Adobe PhotoShop. (c) Ang-2 stained area was identified and outlined by red lines, and the total stromal area was outlined by purple lines using a computer macro in NIH Image. Most of the Ang-2 signal is associated with blood vessels.

To quantify the Ang-2 signal, digital images were taken to cover the entire section. Ang-2 staining was mostly associated with blood vessels, but some tumor and stromal cells

were also stained positive for Ang-2 (Figure 9.4a). The stromal and tumor nodules were identified by myself and another independent observer, and only the stromal area was selected for the quantification (Figure 9.4b). A computer macro was used to quantify the total stromal area and Ang-2 positive area for each individual image (Figure 9.4c). The fraction of the Ang-2 stained area was calculated as the ratio of the two areas.

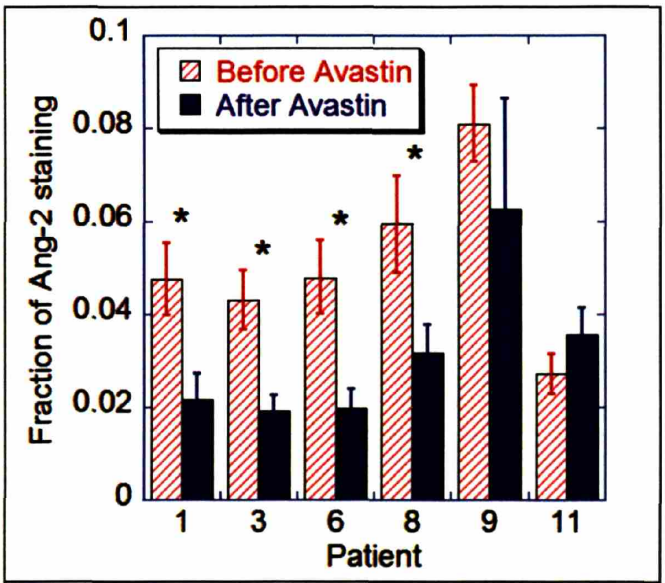

Figure 9.5: Quantification of Angiopoietin 2 immunostaining.

Fraction of Ang-2 staining is the ratio of Ang-2 area to total stromal area. Data are represented as mean ± S.E.M.

Ang-2 immunostaining analysis was performed before and 12 days after the patients were treated with either low- (patients 1, 3 and 6) or high-dose (patients 7, 9 and 11) bevacizumab. In 4 of 6 analyzable patients treated with low- or high-dose bevacizumab, the fraction of Ang-2 positive area in the stromal compartment decreased after bevacizumab treatment ($P < 0.05$). Due to the limited number of patients and samples, only the low-dose bevacizumab group demonstrated a statistically significant reduction in

the fraction of Ang-2 stained area. Nevertheless, for the 6 patients treated with bevacizumab, Ang-2 expression was significantly decreased overall ($P < 0.05$).

Discussion

Bevacizumab is the first anti-angiogenic agent to enter the clinic, and is currently used with chemotherapy as the first line of treatment for colorectal cancer patients. At the molecular level, this recombinant, humanized monoclonal antibody targets VEGF, which is over-expressed in rectal cancer and is associated with disease progression and reduced survival (Ferrara et al. 2004). Genentech filed an Investigational New Drug Application for bevacizumab, and Phase I clinical trials were initiated in April 1997. In February of 2004, bevacizumab was approved by the FDA based on the results of a randomized Phase III clinical trial for patients with metastatic colorectal cancer (Hurwitz et al. 2004). In this trial, low-dose-bevacizumab (5 mg/kg) in combination with irinotecan-5 fluorouracil (5-FU)-leucovorin chemotherapy prolonged survival by 5 months. In a randomized Phase II clinical trial for renal cancer patients, bevacizumab as a mono-therapy significantly increased the time to progression. The effect of bevacizumab was more pronounced at a high-dose (10 mg/kg) compared to a low-dose (3 mg/kg) of bevacizumab, but neither dose achieved an improvement in survival (Yang et al. 2003). Despite these unprecedented successes for a drug targeting the vasculature, the mechanism of action of VEGF blockade in human cancer patients remains unknown, largely because of the lack of correlative markers in trials targeting VEGF. Furthermore, the optimal dose of bevacizumab and treatment scheduling are yet to be defined for combined regimens for cancer patients. In a pilot Phase I dose escalation trial, we addressed some of these questions by designing a regimen consisting of an initial bevacizumab infusion followed

by three cycles of bevacizumab, 5-FU and external beam radiation treatment for locally advanced, non-metastatic rectal cancer patients (Willett et al. 2004). Six to nine weeks after completion of the combined treatment, patients underwent surgical resection of the tumor. Using an array of functional, cellular and molecular investigations, we showed that bevacizumab exhibited antivascular effects on rectal cancer in patients. I was involved with measuring microvascular density and pericyte coverage, as well as angiopoietin-2 staining using the biopsy samples obtained pre- and 12 days post-bevacizumab treatment.

Based on the PECAM staining, we showed that vascular density decreased significantly after bevacizumab treatment. These data supported pre-clinical findings that after DC101 treatment, tumor vascular density dropped significantly (Kadambi et al. 2001; Izumi et al. 2003; Tong et al. 2004; Winkler et al. 2004). Studies have shown that anti-angiogenic therapy reduces microvascular density via the induction of endothelial cell apoptosis (Sweeney et al. 2002). Bevacizumab, similar to DC101, blocks VEGF signaling. As suggested in Chapter 6, we hypothesized that anti-angiogenic treatment normalized the tumor vasculature by targeting immature blood vessels. Since many of the immature blood vessels lack perivascular cell coverage, one would expect an increase in pericyte coverage after anti-angiogenic treatment as VEGF withdrawal pruned immature blood vessels preferentially (Benjamin et al. 1999). In fact, the increase of pericyte coverage in human tumors confirmed the pre-clinical results of Chapter 6 and of other published data (Tong et al. 2004; Winkler et al. 2004; Vosseler et al. 2005). Thus, increased pericyte coverage is one of the indications of vascular normalization.

Besides the decreased microvascular density and increased pericyte coverage, we also confirmed that IFP dropped after bevacizumab treatment in this Phase I clinical trial (Figure 9.6) (Willett et al. 2004). This result confirmed the pre-clinical finding that after anti-VEGF treatment, IFP dropped significantly (Chapter 7). The decrease in IFP might be a result of the vascular normalization, as the tumor blood vessels resume part of the normal vascular function (Jain 2001). The decrease in IFP and the indication of a pressure gradient with DC101 (Chapter 7) might enhance the delivery of therapeutic agents to tumors, and this might explain the synergistic effects seen in the bevacizumab Phase III clinical trials (Hurwitz et al. 2004).

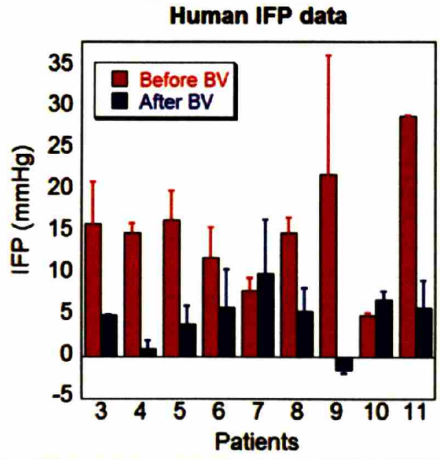

Figure 9.6: Interstitial fluid pressure pre- and post-bevacizumab treatment.

Red: pre-bevacizumab treatment. Blue: post-bevacizumab treatment. Patients 3 to 6 were treated with 5 mg/kg bevacizumab, while Patients 7 to 10 were treated with 10 mg/kg. Data are represented as mean ± S.E.M. (Willett et al. 2004).

Chapter 8 showed that DC101 lowered the expression level of Ang-2 in tumors. As expected, bevacizumab also reduced the Ang-2 expression level in human colorectal

tumors. Studies have shown that Ang-2 is overexpressed in many different types of tumors that are examined (Table 9.1). Thus, VEGF blockade might able to revert Ang-2 levels (or Ang-2/Ang-1 ratio) back to normal values. The pre-clinical studies (Chapter 8) and clinical data (Chapter 9) suggested that Ang-1 and Ang-2 levels might represent the molecular signature for vascular normalization. Further studies are needed to support this hypothesis. Table 9.1 summarized the Ang-1 and Ang-2 level in human colorectal, breast, and brain tumors. This table showed higher Ang-2 levels in the three tumor types (colon, breast, and brain tumors) that were examined in this thesis (breast and brain tumors in Chapter 8; rectal tumor in Chapter 9).

Table 9.1: Summary of Ang-1 and Ang-2 expression profiles in human colon, breast, and brain tumors.

Tissue	Tumor type	Change in Ang-1 level	Change in Ang-2 level	Change in ratio Ang-2:Ang-1	Reference
Colon	Carcinoma	=	↑	↑	(Ahmad et al. 2001)
	Metastatic colorectal cancer	=	↑	↑	(Ogawa et al. 2004)
	Colorectal cancer	=	↑	↑	(Yoshida et al. 1999)
Breast	Inflammatory breast cancer	↑	↑	N/A	(Shirakawa et al. 2002)
	Invasive ductal cancer	↑	↑	↑	(Stratmann et al. 2001)
	Carcinoma	N/A	↑	N/A	(Sfiligoi et al. 2003)

	Carcinoma	↓	↓	↑	(Currie et al. 2001)
	Breast cancer	N/A	↑	N/A	(Carter and Ward 2000)
Brain	Glioblastoma	↑	↑	N/A	(Zagzag et al. 1999)
	Astrocytoma	↑	↑	N/A	(Zagzag et al. 1999)
	Glioblastoma	↑	↑	N/A	(Stratmann et al. 1998)
	Glioblastoma	N/A	↑	N/A	(Holash et al. 1999)
	Astrocytoma	↑	↑	↑	(Audero et al. 2001)
	Glioblastoma	↑	↑	↑	(Audero et al. 2001)

Increased (↑), decreased (↓), no change (=), or not available/not conclusive (N/A) are denoted for each Ang-1 and Ang-2.

Interestingly, human glioblastoma consistently show a correlation of Ang-2 signal with alterations of αSMA-positive perivascular cells (Zagzag et al. 1999). Ang-2 is associated with smaller tumor blood vessels, which also have less perivascular cell coverage (Stratmann et al. 1998). These studies suggest that Ang-2 expression might promote perivascular cell dropoff. The connections between VEGF, angiopoietins, and pericyte coverage will be crucial in understanding the process of vascular normalization.

In summary, the decrease in IFP, microvascular density and stromal Ang-2, as well as the increase in perivascular cell coverage further supported the hypothesis that VEGF blockade normalizes the tumor vasculature and enhances tumor drug delivery. Bevacizumab might also sensitize the endothelium to cytotoxic agents. Collectively, these mechanisms might explain the efficacy of bevacizumab in recent clinical trials, as well as the possible additive or synergistic interaction between anti-angiogenic and cytotoxic therapies that had been observed both in clinical and preclinical settings for

more than a decade (Teicher 1996). The results of this thesis and the phase I study will hopefully facilitate and stimulate future research in this area.

Chapter 10: Discussion and Future Perspective

The data presented in this thesis provide compelling evidence in support of the normalization hypothesis – that judicious application of anti-angiogenic treatment can return the abnormal tumor vasculature to a phenotype more like that of normal blood vessels by pruning the immature vessels and fortifying the remaining ones (Jain 2001). We showed that the normalized tumor vasculature was less tortuous and the vessels were more uniformly covered by pericytes and basement membrane (Chapter 6 and Figure 10.1). This result implied that vessels with less mural cell and basement membrane coverage were more vulnerable to DC101-induced regression, which was consistent with previous findings that tumor vessels without mural cells tend to regress after VEGF withdrawal (Benjamin et al. 1999).

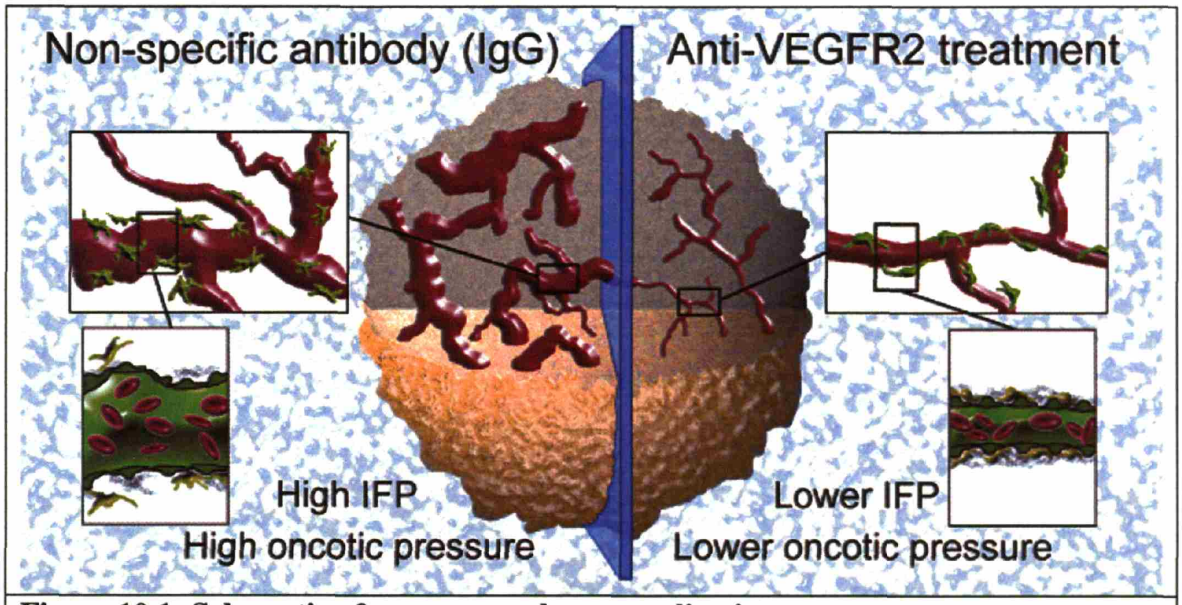

Figure 10.1: Schematic of tumor vascular normalization.

Tumor blood vessels in the control group (treated with a non-specific IgG antibody) were tortuous, hyperpermeable, and immature. The elevated vascular permeability and the lack of functional lymphatics led to an elevated interstitial fluid pressure (IFP) and oncotic pressure. DC101 (anti-VEGFR2 treatment) pruned immature blood vessels, decreased the diameter of residual vessels, reduced the tortuosity of the vasculature, and remodeled the vasculature into a more organized network with improved perivascular cells and basement membrane coverage. Furthermore, DC101 decreased vascular permeability and induced a hydrostatic pressure gradient that improved drug delivery (Tong et al. 2004).

Our functional data demonstrated for the first time that a drop in vascular permeability was associated with increased transvascular gradients in oncotic and hydrostatic pressure in tumors. An increased hydrostatic pressure gradient improved the penetration of large molecules into tumors (Chapter 7). We further showed that DC101 increased RBC velocity in the remaining tumor vasculature, and this could partly explain the reduced

tumor hypoxia during the normalization time window. We had also clearly demonstrated that the gene expression and protein levels of angiopoietin-2 were lowered after DC101 treatment (Chapter 8).

The original rationale for combining anti-angiogenic and cytotoxic therapies was to target two distinct cell populations within solid tumors: cancer cells and endothelial cells. When endothelial cells are targeted, blood vessels should be destroyed, and thus compromise the delivery of therapeutics. However, several preclinical studies clearly demonstrate that delivery of therapeutics is not compromised by anti-angiogenic agents (Wildiers et al. 2003), but is even increased in several cases (Teicher 1996). The restoration of pressure gradients induced by VEGF-blockade may explain the uncompromised or increased uptake of cytotoxic agents in tumors. For a cytotoxic agent to be effective, it must reach all cancer cells in effective quantities. Anti-angiogenic therapy, as shown by this study, might facilitate the delivery of therapeutic agents to cancer cells, particularly those that were farther from the vessels. This mechanism might contribute to the potentiation of conventional therapies by anti-angiogenic agents (Teicher 1996; Browder et al. 2000; Klement et al. 2000; Kozin et al. 2001; Baker et al. 2002; McCarthy 2003). Furthermore, after we published our work on vascular normalization, several studies conducted by other research groups confirmed our results (Table 10.1).

Table 10.1: Pre-clinical evidences supporting normalization of the tumor vasculature

Anti-angiogenic agent	Target/action	Other therapies	Tumor	Results	Reference
Anti-VEGF mAb (A.4.6.1)	VEGF	CPT-11	Mice implanted with human colon adenocarcinoma	• Decreased vascular density • Increased intratumoral CPT-11 concentration • Increased tumor perfusion (Hoechst 33342)	(Wildiers et al. 2003)
Thalidomide	Inhibits bFGF and VEGF	X-ray	Mice implanted with fibrosarcoma	• Thalidomide induced tumor reoxygenation • Lowered IFP • Increased perfusion • Vascular remodeling • Radiosensitization occurred in a narrow time window	(Ansiaux et al. 2005)
Bevacizumab	VEGF	Two different immuno-toxins (SS1P and HA22)	Mice implanted with human mesothelioma and Burkitt's lymphoma	• Combination treatment provided additive anti-tumor activity	(Bang et al. 2005)
Gleevec	Blocks PDGFRβ, but also inhibits VEGF level	N/A	Mice implanted with human lung adenocarcinoma	• Lowered IFP • Improved oxygenation	(Vlahovic et al. 2005)
AG013736, VEGF-Trap	VEGFRs, VEGF	N/A	Mice with islet-cell tumors or implanted with Lewis lung carcinoma	• Decreased vascular density • Decreased endothelial fenestrations • Improved perivascular cell coverage	(Inai et al. 2004)
DC101	VEGFR2	N/A	Mice implanted with squamous cell carcinoma	• Decreased vascular density • Improved perivascular cell coverage • Improved basement membrane coverage with down-regulation of MMP9 and MMP13	(Vosseler et al. 2005)

Finally, by performing immunostaining on human biopsy samples pre- and post-bevacizumab (anti-VEGF therapy) treatment, we confirmed some of our pre-clinical findings in clinical setting (Chapter 8, Table 10.1).

Table 10.2: Effects of VEGF blockade in both pre-clinical and clinical data.

Properties	Pre-clinical data*			Clinical data†		
	Control	Treated	Change	Before BV	After BV	Change
Blood volume	**19.3 ± 2.2**[1]	**5.4 ± 1.0**	**↓ (-72%)**	6.8 ± 2.1[2]	5.0 ± 0.9	↓ (-26%)
Vascular density	**52.1 ± 4.6**[3]	**41.9 ± 3.0**	**↓ (-19%)**	**13.0 ± 3.2**[4]	**6.9 ± 1.8**	**↓ (-47%)**
Permeability	**7.3 ± 0.8**[5]	**2.8 ± 0.8**	**↓ (-62%)**			
PS product				14 ± 2[6]	12.9 ± 3.1	-
Interstitial fluid pressure	**6.1 ± 1.0**[7]	**3.1 ± 0.5**	**↓ (-49%)**	14.0 ± 1.2[8]	4.0 ± 1.5	↓ (-71%)
Perivascular cell coverage	**0.67 ± 0.04**[9]	**0.81 ± 0.04**	**↑ (21%)**	**9.9 ± 3.8**[10]	**17.8 ± 1.5**	**↑ (80%)**
Ang-2 level	**10.4 ± 1.3**[11]	**2.2 ± 0.5**	**↓ (-79%)**	**0.046 ± 0.002**[12]	**0.020 ± 0.001**	**↓ (-57%)**
Tumor apoptosis	0.86 ± 0.24[13]	2.50 ± 0.31	↑ (190%)	1.7 ± 0.2[14]	3.6 ± 0.7	↑ (112%)
Plasma VEGF level	Non-detectable	182.5 ± 135.8[15]	↑	22.5 ± 8.3[16]	272 ± 22.5	↑ (1109%)
Progenitor cells/WBC	~1.3[17]	0.1	↓ (~-92%)	0.0011 (0.0006 – 0.21)[18]	0.0010 (0.0005 – 0.075)	(-9%)

* (Tong et al. 2004; Winkler et al. 2004)

† (Willett et al. 2004) and Willett et al. 2005 In preparation.

[1] (μm^3 blood volume/μm^2 of image field). Based on intravital microscopy image.

[2] (ml/100 g tissue). Based on CT data.

[3] (cm vessel length/cm^2 of image field). Based on intravital microscopy image.

[4] (number of vessels/field). Based on CD31 staining.

[5] (10^{-7} cm/s) effective permeability of BSA. Based on intravital microscopy data.

[6] Permeability-surface area product (ml/min/100 g tissue). Based on CT data.

[7] (mmHg). Measurement is done by using micropipette technique.

[8] (mmHg). Measurement is done by using wick-in-needle technique.

[9] (% of αSMA-positive vessels). Based on immunostaining.

[10] (% of αSMA-positive vessels). Based on immunostaining.

[11] Real-time PCR data. Normalized by β-actin expression level.

[12] (fraction of stromal region stained positive with Ang-2). Based on immunostaining.

[13] (% of apoptotic cells)

[14] (% of apoptotic cells).

[15] (pg/ml). Plasma human VEGF levels in MDA-MB-231 tumor-bearing SCID mice. Measurement is done by using ELISA. (Bocci et al. 2004)

[16] (pg/ml). Measurement is done by using multiplex protein array technology (Meso-Scale Discovery, Gaithersburg, MD)

[17] Number of viable circulating endothelial progenitor cells per ml of peripheral blood in MDA-MB-231 tumor-bearing SCID mice. Viable CEPs are defined as CD13+/VEGFR2+/CD45-/CD117+/7AAD- cells. (Shaked et al. 2005)

[18] Measured by flow cytometry. Progenitor cells are identified as $CD31^{+}AC133^{+}$ cells, and WBCs are identified as $CD45^{+}$ cells.

Bold represents the data I measured in this thesis work.

This thesis examined the possibility of vascular normalization by VEGF blockade. It also opened up many exciting research avenues in the field of anti-angiogenic therapy. Further studies will be needed to dissect the molecular mechanisms behind vascular normalization. It will also be important to understand whether vascular normalization occurs, and to what extent, in other tumor types. Besides DC101 and bevacizumab, other molecules/signaling pathways may able to provide a longer, better normalization time window. Clinically, it will be important to come up with a set of parameters that quantify

and describe the normalization effects so that physicians will know when to combine conventional therapy after the initiation of anti-angiogenic therapy. Understanding the underlying mechanism of vascular normalization not only will benefit cancer patients, but it will also benefit patients with other vascular diseases such as diabetes and macular degeneration (Jain and Carmeliet 2001; Jain 2005).

References

Abramsson, A., P. Lindblom, et al. (2003). "Endothelial and nonendothelial sources of PDGF-B regulate pericyte recruitment and influence vascular pattern formation in tumors." J Clin Invest **112**(8): 1142-51.

Ahmad, S. A., W. Liu, et al. (2001). "Differential expression of angiopoietin-1 and angiopoietin-2 in colon carcinoma. A possible mechanism for the initiation of angiogenesis." Cancer **92**(5): 1138-43.

Alexandrakis, G., E. B. Brown, et al. (2004). "Two-photon fluorescence correlation microscopy reveals the two-phase nature of transport in tumors." Nat Med **10**(2): 203-7.

Anderson, J. L. and D. M. Malone (1974). "Mechanism of osmotic flow in porous membranes." Biophys J **14**(12): 957-82.

Ansiaux, R., C. Baudelet, et al. (2005). "Thalidomide radiosensitizes tumors through early changes in the tumor microenvironment." Clin Cancer Res **11**(2 Pt 1): 743-50.

Arora, N., R. Masood, et al. (1999). "Vascular endothelial growth factor chimeric toxin is highly active against endothelial cells." Cancer Res **59**(1): 183-8.

Audero, E., I. Cascone, et al. (2001). "Expression of angiopoietin-1 in human glioblastomas regulates tumor-induced angiogenesis: in vivo and in vitro studies." Arterioscler Thromb Vasc Biol **21**(4): 536-41.

Aukland, K. and H. M. Johnsen (1974). "A colloid osmometer for small fluid samples." Acta Physiol Scand **90**(2): 485-90.

Aukland, K. and R. K. Reed (1993). "Interstitial-lymphatic mechanisms in the control of extracellular fluid volume." Physiol Rev **73**(1): 1-78.

Baish, J. W. and R. K. Jain (2000). "Fractals and cancer." Cancer Res **60**(14): 3683-8.

Baish, J. W., P. A. Netti, et al. (1997). "Transmural coupling of fluid flow in microcirculatory network and interstitium in tumors." Microvasc Res **53**(2): 128-41.

Baker, C. H., C. C. Solorzano, et al. (2002). "Blockade of vascular endothelial growth factor receptor and epidermal growth factor receptor signaling for therapy of metastatic human pancreatic cancer." Cancer Res **62**(7): 1996-2003.

Ballard, K. and W. Perl (1978). "Osmotic reflection coefficients of canine subcutaneous adipose tissue endothelium." Microvasc Res **16**(2): 224-36.

Baluk, P., S. Morikawa, et al. (2003). "Abnormalities of basement membrane on blood vessels and endothelial sprouts in tumors." Am J Pathol **163**(5): 1801-15.

Bang, S., R. Hassan, et al. (2005). "Additive anti-tumor effect of Avastin and immunotoxin combination therapy on tumor-bearing mouse models." Proc Amer Assoc Cancer Res **46**: 4989.

Baxter, L. T. and R. K. Jain (1989). "Transport of fluid and macromolecules in tumors. I. Role of interstitial pressure and convection." Microvasc Res **37**(1): 77-104.

Baxter, L. T. and R. K. Jain (1991). "Transport of fluid and macromolecules in tumors. IV. A microscopic model of the perivascular distribution." Microvasc Res **41**(2): 252-72.

Benjamin, L. E., D. Golijanin, et al. (1999). "Selective ablation of immature blood vessels in established human tumors follows vascular endothelial growth factor withdrawal." J Clin Invest **103**(2): 159-65.

Bocci, G., S. Man, et al. (2004). "Increased plasma vascular endothelial growth factor (VEGF) as a surrogate marker for optimal therapeutic dosing of VEGF receptor-2 monoclonal antibodies." Cancer Res **64**(18): 6616-25.

Boehm, T., J. Folkman, et al. (1997). "Antiangiogenic therapy of experimental cancer does not induce acquired drug resistance." Nature **390**(6658): 404-7.

Boucher, Y., L. T. Baxter, et al. (1990). "Interstitial pressure gradients in tissue-isolated and subcutaneous tumors: implications for therapy." Cancer Res **50**(15): 4478-84.

Boucher, Y. and R. K. Jain (1992). "Microvascular pressure is the principal driving force for interstitial hypertension in solid tumors: implications for vascular collapse." Cancer Res **52**(18): 5110-4.

Boucher, Y., J. M. Kirkwood, et al. (1991). "Interstitial hypertension in superficial metastatic melanomas in humans." Cancer Res **51**(24): 6691-4.

Browder, T., C. E. Butterfield, et al. (2000). "Antiangiogenic scheduling of chemotherapy improves efficacy against experimental drug-resistant cancer." Cancer Res **60**(7): 1878-86.

Brown, E., T. McKee, et al. (2003). "Dynamic imaging of collagen and its modulation in tumors in vivo using second-harmonic generation." Nat Med **9**(6): 796-800.

Brown, E. B., R. B. Campbell, et al. (2001). "In vivo measurement of gene expression, angiogenesis and physiological function in tumors using multiphoton laser scanning microscopy." Nat Med **7**(7): 864-8.

Brown, L. F., B. Berse, et al. (1993). "Expression of vascular permeability factor (vascular endothelial growth factor) and its receptors in adenocarcinomas of the gastrointestinal tract." Cancer Res **53**(19): 4727-35.

Bruns, C. J., W. Liu, et al. (2000). "Vascular endothelial growth factor is an in vivo survival factor for tumor endothelium in a murine model of colorectal carcinoma liver metastases." Cancer **89**(3): 488-99.

Burke, P. A., S. J. DeNardo, et al. (2002). "Cilengitide targeting of alpha(v)beta(3) integrin receptor synergizes with radioimmunotherapy to increase efficacy and apoptosis in breast cancer xenografts." Cancer Res **62**(15): 4263-72.

Calvo, A., Y. Yokoyama, et al. (2002). "Inhibition of the mammary carcinoma angiogenic switch in C3(1)/SV40 transgenic mice by a mutated form of human endostatin." Int J Cancer **101**(3): 224-34.

Carmeliet, P. (2003). "Angiogenesis in health and disease." Nat Med **9**(6): 653-60.

Carmeliet, P., V. Ferreira, et al. (1996). "Abnormal blood vessel development and lethality in embryos lacking a single VEGF allele." Nature **380**(6573): 435-9.

Carmeliet, P. and R. K. Jain (2000). "Angiogenesis in cancer and other diseases." Nature **407**(6801): 249-57.

Carter, W. B. and M. D. Ward (2000). "HER2 regulatory control of angiopoietin-2 in breast cancer." Surgery **128**(2): 153-8.

Chang, Y. S., L. L. Munn, et al. (2000). "Effect of vascular endothelial growth factor on cultured endothelial cell monolayer transport properties." Microvasc Res **59**(2): 265-77.

Chaplin, D. J. and S. A. Hill (1995). "Temporal heterogeneity in microregional erythrocyte flux in experimental solid tumours." Br J Cancer **71**(6): 1210-3.
Cheng, S. Y., H. J. Huang, et al. (1996). "Suppression of glioblastoma angiogenicity and tumorigenicity by inhibition of endogenous expression of vascular endothelial growth factor." Proc Natl Acad Sci U S A **93**(16): 8502-7.
Cotran, R. S., V. Kumar, et al. (1999). Robbins pathologic basis of disease. Philadelphia, W.B. Saunders Company.
Cross, M. J. and L. Claesson-Welsh (2001). "FGF and VEGF function in angiogenesis: signalling pathways, biological responses and therapeutic inhibition." Trends Pharmacol Sci **22**(4): 201-7.
Currie, M. J., S. P. Gunningham, et al. (2001). "Angiopoietin-1 is inversely related to thymidine phosphorylase expression in human breast cancer, indicating a role in vascular remodeling." Clin Cancer Res **7**(4): 918-27.
Darland, D. C. and P. A. D'Amore (1999). "Blood vessel maturation: vascular development comes of age." J Clin Invest **103**(2): 157-8.
Das, A., W. Fanslow, et al. (2003). "Angiopoietin/Tek interactions regulate mmp-9 expression and retinal neovascularization." Lab Invest **83**(11): 1637-45.
Davis, S., T. H. Aldrich, et al. (1996). "Isolation of angiopoietin-1, a ligand for the TIE2 receptor, by secretion-trap expression cloning." Cell **87**(7): 1161-9.
Deen, W. M. (1987). "Hindered Transport of Large Molecules in Liquid-Filled Pores." Aiche Journal **33**(9): 1409-1425.
Devineni, D., A. Klein-Szanto, et al. (1996). "Uptake of temozolomide in a rat glioma model in the presence and absence of the angiogenesis inhibitor TNP-470." Cancer Res **56**(9): 1983-7.
Dvorak, H. F., J. A. Nagy, et al. (1999). "Vascular permeability factor/vascular endothelial growth factor and the significance of microvascular hyperpermeability in angiogenesis." Curr Top Microbiol Immunol **237**: 97-132.
Fadnes, H. O., R. K. Reed, et al. (1977). "Interstitial fluid pressure in rats measured with a modified wick technique." Microvasc Res **14**(1): 27-36.
Fenton, B. M., S. F. Paoni, et al. (2004). "Pathophysiological effects of vascular endothelial growth factor receptor-2-blocking antibody plus fractionated radiotherapy on murine mammary tumors." Cancer Res **64**(16): 5712-9.
Ferrara, N. (2002). "Timeline: VEGF and the quest for tumour angiogenesis factors." Nat Rev Cancer **2**(10): 795-803.
Ferrara, N., K. Carver-Moore, et al. (1996). "Heterozygous embryonic lethality induced by targeted inactivation of the VEGF gene." Nature **380**(6573): 439-42.
Ferrara, N., H. P. Gerber, et al. (2003). "The biology of VEGF and its receptors." Nat Med **9**(6): 669-76.
Ferrara, N., K. J. Hillan, et al. (2004). "Discovery and development of bevacizumab, an anti-VEGF antibody for treating cancer." Nat Rev Drug Discov **3**(5): 391-400.
Folkman, J. (1971). "Tumor angiogenesis: therapeutic implications." N Engl J Med **285**(21): 1182-6.
Folkman, J. (1995). "Angiogenesis in cancer, vascular, rheumatoid and other disease." Nat Med **1**(1): 27-31.
Fong, G. H., J. Rossant, et al. (1995). "Role of the Flt-1 receptor tyrosine kinase in regulating the assembly of vascular endothelium." Nature **376**(6535): 66-70.

Fong, T. A., L. K. Shawver, et al. (1999). "SU5416 is a potent and selective inhibitor of the vascular endothelial growth factor receptor (Flk-1/KDR) that inhibits tyrosine kinase catalysis, tumor vascularization, and growth of multiple tumor types." Cancer Res **59**(1): 99-106.

Gazit, Y., J. W. Baish, et al. (1997). "Fractal characteristics of tumor vascular architecture during tumor growth and regression." Microcirculation **4**(4): 395-402.

Geng, L., E. Donnelly, et al. (2001). "Inhibition of vascular endothelial growth factor receptor signaling leads to reversal of tumor resistance to radiotherapy." Cancer Res **61**(6): 2413-9.

Gerber, H. P., A. McMurtrey, et al. (1998). "Vascular endothelial growth factor regulates endothelial cell survival through the phosphatidylinositol 3'-kinase/Akt signal transduction pathway. Requirement for Flk-1/KDR activation." J Biol Chem **273**(46): 30336-43.

Gorski, D. H., M. A. Beckett, et al. (1999). "Blockage of the vascular endothelial growth factor stress response increases the antitumor effects of ionizing radiation." Cancer Res **59**(14): 3374-8.

Hashizume, H., P. Baluk, et al. (2000). "Openings between defective endothelial cells explain tumor vessel leakiness." Am J Pathol **156**(4): 1363-80.

Hellstrom, M., H. Gerhardt, et al. (2001). "Lack of pericytes leads to endothelial hyperplasia and abnormal vascular morphogenesis." J Cell Biol **153**(3): 543-53.

Hlatky, L., P. Hahnfeldt, et al. (2002). "Clinical application of antiangiogenic therapy: microvessel density, what it does and doesn't tell us." J Natl Cancer Inst **94**(12): 883-93.

Hobbs, S. K., W. L. Monsky, et al. (1998). "Regulation of transport pathways in tumor vessels: role of tumor type and microenvironment." Proc Natl Acad Sci U S A **95**(8): 4607-12.

Holash, J., P. C. Maisonpierre, et al. (1999). "Vessel cooption, regression, and growth in tumors mediated by angiopoietins and VEGF." Science **284**(5422): 1994-8.

Hu, B., P. Guo, et al. (2003). "Angiopoietin-2 induces human glioma invasion through the activation of matrix metalloprotease-2." Proc Natl Acad Sci U S A **100**(15): 8904-9.

Hurwitz, H., L. Fehrenbacher, et al. (2004). "Bevacizumab plus irinotecan, fluorouracil, and leucovorin for metastatic colorectal cancer." N Engl J Med **350**(23): 2335-42.

Inai, T., M. Mancuso, et al. (2004). "Inhibition of vascular endothelial growth factor (VEGF) signaling in cancer causes loss of endothelial fenestrations, regression of tumor vessels, and appearance of basement membrane ghosts." Am J Pathol **165**(1): 35-52.

Inoue, K., M. Chikazawa, et al. (2003). "Docetaxel Enhances the Therapeutic Effect of the Angiogenesis Inhibitor TNP-470 (AGM-1470) in Metastatic Human Transitional Cell Carcinoma." Clin Cancer Res **9**(2): 886-99.

Inoue, K., J. W. Slaton, et al. (2000). "Treatment of human metastatic transitional cell carcinoma of the bladder in a murine model with the anti-vascular endothelial growth factor receptor monoclonal antibody DC101 and paclitaxel." Clin Cancer Res **6**(7): 2635-43.

Inoue, K., J. W. Slaton, et al. (2000). "Paclitaxel enhances the effects of the anti-epidermal growth factor receptor monoclonal antibody ImClone C225 in mice

with metastatic human bladder transitional cell carcinoma." Clin Cancer Res **6**(12): 4874-84.
Izumi, Y., E. Di Tomaso, et al. (2003). "Responses to antiangiogenesis treatment of spontaneous autochthonous tumors and their isografts." Cancer Res **63**(4): 747-51.
Jain, R. K. (1987). "Transport of molecules across tumor vasculature." Cancer Metastasis Rev **6**(4): 559-93.
Jain, R. K. (1987). "Transport of molecules in the tumor interstitium: a review." Cancer Res **47**(12): 3039-51.
Jain, R. K. (1988). "Determinants of tumor blood flow: a review." Cancer Res **48**(10): 2641-58.
Jain, R. K. (1989). "Delivery of novel therapeutic agents in tumors: physiological barriers and strategies." J Natl Cancer Inst **81**(8): 570-6.
Jain, R. K. (1994). "Barriers to drug delivery in solid tumors." Sci Am **271**(1): 58-65.
Jain, R. K. (1998). "The next frontier of molecular medicine: delivery of therapeutics." Nat Med **4**(6): 655-7.
Jain, R. K. (2001). "Normalizing tumor vasculature with anti-angiogenic therapy: a new paradigm for combination therapy." Nat Med **7**(9): 987-9.
Jain, R. K. (2003). "Molecular regulation of vessel maturation." Nat Med **9**(6): 685-93.
Jain, R. K. (2005). "Normalization of tumor vasculature: an emerging concept in antiangiogenic therapy." Science **307**(5706): 58-62.
Jain, R. K. and P. F. Carmeliet (2001). "Vessels of death or life." Sci Am **285**(6): 38-45.
Jain, R. K., N. Safabakhsh, et al. (1998). "Endothelial cell death, angiogenesis, and microvascular function after castration in an androgen-dependent tumor: role of vascular endothelial growth factor." Proc Natl Acad Sci U S A **95**(18): 10820-5.
Jemal, A., T. Murray, et al. (2003). "Cancer statistics, 2003." CA Cancer J Clin **53**(1): 5-26.
Jemal, A., R. C. Tiwari, et al. (2004). "Cancer statistics, 2004." CA Cancer J Clin **54**(1): 8-29.
Johnsen, H. M. (1974). "Measurement of colloid osmotic pressure of interstitial fluid." Acta Physiol Scand **91**(1): 142-4.
Kabbinavar, F., H. I. Hurwitz, et al. (2003). "Phase II, randomized trial comparing bevacizumab plus fluorouracil (FU)/leucovorin (LV) with FU/LV alone in patients with metastatic colorectal cancer." J Clin Oncol **21**(1): 60-5.
Kadambi, A., C. Mouta Carreira, et al. (2001). "Vascular endothelial growth factor (VEGF)-C differentially affects tumor vascular function and leukocyte recruitment: role of VEGF-receptor 2 and host VEGF-A." Cancer Res **61**(6): 2404-8.
Kalluri, R. (2003). "Basement membranes: structure, assembly and role in tumour angiogenesis." Nat Rev Cancer **3**(6): 422-33.
Kato, T., K. Sato, et al. (1994). "Enhanced suppression of tumor growth by combination of angiogenesis inhibitor O-(chloroacetyl-carbamoyl)fumagillol (TNP-470) and cytotoxic agents in mice." Cancer Res **54**(19): 5143-7.
Kendall, R. L. and K. A. Thomas (1993). "Inhibition of vascular endothelial cell growth factor activity by an endogenously encoded soluble receptor." Proc Natl Acad Sci U S A **90**(22): 10705-9.

Kerbel, R. and J. Folkman (2002). "Clinical translation of angiogenesis inhibitors." Nat Rev Cancer **2**(10): 727-39.
Kerbel, R. S. (1997). "A cancer therapy resistant to resistance." Nature **390**(6658): 335-6.
Kim, K. J., B. Li, et al. (1993). "Inhibition of vascular endothelial growth factor-induced angiogenesis suppresses tumour growth in vivo." Nature **362**(6423): 841-4.
Klement, G., S. Baruchel, et al. (2000). "Continuous low-dose therapy with vinblastine and VEGF receptor-2 antibody induces sustained tumor regression without overt toxicity." J Clin Invest **105**(8): R15-24.
Kozin, S. V., Y. Boucher, et al. (2001). "Vascular endothelial growth factor receptor-2-blocking antibody potentiates radiation-induced long-term control of human tumor xenografts." Cancer Res **61**(1): 39-44.
Kramer, G. C., L. Sibley, et al. (1986). "Wick sampling of interstitial fluid in rat skin: further analysis and modifications of the method." Microvasc Res **32**(1): 39-49.
Krikun, G., F. Schatz, et al. (2000). "Expression of angiopoietin-2 by human endometrial endothelial cells: regulation by hypoxia and inflammation." Biochem Biophys Res Commun **275**(1): 159-63.
Kuenen, B. C., L. Rosen, et al. (2002). "Dose-finding and pharmacokinetic study of cisplatin, gemcitabine, and SU5416 in patients with solid tumors." J Clin Oncol **20**(6): 1657-67.
Kunkel, P., U. Ulbricht, et al. (2001). "Inhibition of glioma angiogenesis and growth in vivo by systemic treatment with a monoclonal antibody against vascular endothelial growth factor receptor-2." Cancer Res **61**(18): 6624-8.
Kurzen, H., S. Manns, et al. (2002). "Tightening of endothelial cell contacts: a physiologic response to cocultures with smooth-muscle-like 10T1/2 cells." J Invest Dermatol **119**(1): 143-53.
Lee, C. G., M. Heijn, et al. (2000). "Anti-Vascular endothelial growth factor treatment augments tumor radiation response under normoxic or hypoxic conditions." Cancer Res **60**(19): 5565-70.
Lee, K., E. Erturk, et al. (1987). "Efficacy of antitumor chemotherapy in C3H mice enhanced by the antiangiogenesis steroid, cortisone acetate." Cancer Res **47**(19): 5021-4.
Lehne, G., E. Elonen, et al. (1998). "Challenging drug resistance in cancer therapy--review of the First Nordic Conference on Chemoresistance in Cancer Treatment, October 9th and 10th, 1997." Acta Oncol **37**(5): 431-9.
Leu, A. J., D. A. Berk, et al. (2000). "Absence of functional lymphatics within a murine sarcoma: a molecular and functional evaluation." Cancer Res **60**(16): 4324-7.
Leunig, M., F. Yuan, et al. (1992). "Angiogenesis, microvascular architecture, microhemodynamics, and interstitial fluid pressure during early growth of human adenocarcinoma LS174T in SCID mice." Cancer Res **52**(23): 6553-60.
Lobov, I. B., P. C. Brooks, et al. (2002). "Angiopoietin-2 displays VEGF-dependent modulation of capillary structure and endothelial cell survival in vivo." Proc Natl Acad Sci U S A **99**(17): 11205-10.
Ma, J., S. Pulfer, et al. (2001). "Pharmacodynamic-mediated reduction of temozolomide tumor concentrations by the angiogenesis inhibitor TNP-470." Cancer Res **61**(14): 5491-8.

Maisonpierre, P. C., C. Suri, et al. (1997). "Angiopoietin-2, a natural antagonist for Tie2 that disrupts in vivo angiogenesis." Science **277**(5322): 55-60.
Mandriota, S. J. and M. S. Pepper (1998). "Regulation of angiopoietin-2 mRNA levels in bovine microvascular endothelial cells by cytokines and hypoxia." Circ Res **83**(8): 852-9.
Mauceri, H. J., N. N. Hanna, et al. (1998). "Combined effects of angiostatin and ionizing radiation in antitumour therapy." Nature **394**(6690): 287-91.
McCarthy, M. (2003). "Antiangiogenesis drug promising for metastatic colorectal cancer." Lancet **361**(9373): 1959.
McCarty, M. F., W. Liu, et al. (2003). "Promises and pitfalls of anti-angiogenic therapy in clinical trials." Trends Mol Med **9**(2): 53-8.
Millauer, B., L. K. Shawver, et al. (1994). "Glioblastoma growth inhibited in vivo by a dominant-negative Flk-1 mutant." Nature **367**(6463): 576-9.
Morikawa, S., P. Baluk, et al. (2002). "Abnormalities in pericytes on blood vessels and endothelial sprouts in tumors." Am J Pathol **160**(3): 985-1000.
Murata, R., Y. Nishimura, et al. (1997). "An antiangiogenic agent (TNP-470) inhibited reoxygenation during fractionated radiotherapy of murine mammary carcinoma." Int J Radiat Oncol Biol Phys **37**(5): 1107-13.
Netti, P. A., D. A. Berk, et al. (2000). "Role of extracellular matrix assembly in interstitial transport in solid tumors." Cancer Res **60**(9): 2497-503.
Netti, P. A., L. M. Hamberg, et al. (1999). "Enhancement of fluid filtration across tumor vessels: implication for delivery of macromolecules." Proc Natl Acad Sci U S A **96**(6): 3137-42.
Netti, P. A., S. Roberge, et al. (1996). "Effect of transvascular fluid exchange on pressure-flow relationship in tumors: a proposed mechanism for tumor blood flow heterogeneity." Microvasc Res **52**(1): 27-46.
Niethammer, A. G., R. Xiang, et al. (2002). "A DNA vaccine against VEGF receptor 2 prevents effective angiogenesis and inhibits tumor growth." Nat Med **8**(12): 1369-75.
O'Brien, T., D. Cranston, et al. (1995). "Different angiogenic pathways characterize superficial and invasive bladder cancer." Cancer Res **55**(3): 510-3.
Ogawa, M., H. Yamamoto, et al. (2004). "Hepatic expression of ANG2 RNA in metastatic colorectal cancer." Hepatology **39**(2): 528-39.
Oh, H., H. Takagi, et al. (1999). "Hypoxia and vascular endothelial growth factor selectively up-regulate angiopoietin-2 in bovine microvascular endothelial cells." J Biol Chem **274**(22): 15732-9.
Padera, T. P., A. Kadambi, et al. (2002). "Lymphatic metastasis in the absence of functional intratumor lymphatics." Science **296**(5574): 1883-6.
Padera, T. P., B. R. Stoll, et al. (2004). "Pathology: cancer cells compress intratumour vessels." Nature **427**(6976): 695.
Parker, J. C., M. A. Perry, et al. (1984). Permeability of the Microvascular Barrier. Edema. N. C. Staub and A. E. Taylor. New York, Raven Press**:** 143-87.
Peters, W., M. Teixeira, et al. (1980). "Microcirculatory studies in rat mammary carcinoma. I. Transparent chamber method, development of microvasculature, and pressures in tumor vessels." J Natl Cancer Inst **65**(3): 631-42.

Pichiule, P., J. C. Chavez, et al. (2003). "Hypoxic regulation of angiopoietin-2 expression in endothelial cells." J Biol Chem.

Pichiule, P. and J. C. LaManna (2002). "Angiopoietin-2 and rat brain capillary remodeling during adaptation and deadaptation to prolonged mild hypoxia." J Appl Physiol **93**(3): 1131-9.

Pinheiro, J. C. and D. M. Bates (2000). Mixed effects models in S and S PLUS. New York, Springer.

Plate, K. H., G. Breier, et al. (1992). "Vascular endothelial growth factor is a potential tumour angiogenesis factor in human gliomas in vivo." Nature **359**(6398): 845-8.

Pluen, A., Y. Boucher, et al. (2001). "Role of tumor-host interactions in interstitial diffusion of macromolecules: cranial vs. subcutaneous tumors." Proc Natl Acad Sci U S A **98**(8): 4628-33.

Prewett, M., J. Huber, et al. (1999). "Antivascular endothelial growth factor receptor (fetal liver kinase 1) monoclonal antibody inhibits tumor angiogenesis and growth of several mouse and human tumors." Cancer Res **59**(20): 5209-18.

Ramakrishnan, S., T. A. Olson, et al. (1996). "Vascular endothelial growth factor-toxin conjugate specifically inhibits KDR/flk-1-positive endothelial cell proliferation in vitro and angiogenesis in vivo." Cancer Res **56**(6): 1324-30.

Ray, P. S., T. Estrada-Hernandez, et al. (2000). "Early effects of hypoxia/reoxygenation on VEGF, ang-1, ang-2 and their receptors in the rat myocardium: implications for myocardial angiogenesis." Mol Cell Biochem **213**(1-2): 145-53.

Rippe, B. and B. Haraldsson (1986). "Capillary permeability in rat hindquarters as determined by estimations of capillary reflection coefficients." Acta Physiol Scand **127**(3): 289-303.

Rossler, J., S. Breit, et al. (1999). "Vascular endothelial growth factor expression in human neuroblastoma: up-regulation by hypoxia." Int J Cancer **81**(1): 113-7.

Ruoslahti, E. (1996). "How cancer spreads." Sci Am **275**(3): 72-7.

Saleh, M., S. A. Stacker, et al. (1996). "Inhibition of growth of C6 glioma cells in vivo by expression of antisense vascular endothelial growth factor sequence." Cancer Res **56**(2): 393-401.

Sato, T. N., Y. Tozawa, et al. (1995). "Distinct roles of the receptor tyrosine kinases Tie-1 and Tie-2 in blood vessel formation." Nature **376**(6535): 70-4.

Senger, D. R., S. J. Galli, et al. (1983). "Tumor cells secrete a vascular permeability factor that promotes accumulation of ascites fluid." Science **219**(4587): 983-5.

Sfiligoi, C., A. de Luca, et al. (2003). "Angiopoietin-2 expression in breast cancer correlates with lymph node invasion and short survival." Int J Cancer **103**(4): 466-74.

Shaked, Y., F. Bertolini, et al. (2005). "Genetic heterogeneity of the vasculogenic phenotype parallels angiogenesis; Implications for cellular surrogate marker analysis of antiangiogenesis." Cancer Cell **7**(1): 101-11.

Shalaby, F., J. Rossant, et al. (1995). "Failure of blood-island formation and vasculogenesis in Flk-1-deficient mice." Nature **376**(6535): 62-6.

Shirakawa, K., M. Shibuya, et al. (2002). "Tumor-infiltrating endothelial cells and endothelial precursor cells in inflammatory breast cancer." Int J Cancer **99**(3): 344-51.

Shweiki, D., A. Itin, et al. (1992). "Vascular endothelial growth factor induced by hypoxia may mediate hypoxia-initiated angiogenesis." Nature **359**(6398): 843-5.
Simmonds, M. A. (2003). "Cancer statistics, 2003: further decrease in mortality rate, increase in persons living with cancer." CA Cancer J Clin **53**(1): 4.
Stohrer, M., Y. Boucher, et al. (2000). "Oncotic pressure in solid tumors is elevated." Cancer Res **60**(15): 4251-5.
Stratmann, A., T. Acker, et al. (2001). "Differential inhibition of tumor angiogenesis by tie2 and vascular endothelial growth factor receptor-2 dominant-negative receptor mutants." Int J Cancer **91**(3): 273-82.
Stratmann, A., W. Risau, et al. (1998). "Cell type-specific expression of angiopoietin-1 and angiopoietin-2 suggests a role in glioblastoma angiogenesis." Am J Pathol **153**(5): 1459-66.
Suri, C., P. F. Jones, et al. (1996). "Requisite role of angiopoietin-1, a ligand for the TIE2 receptor, during embryonic angiogenesis." Cell **87**(7): 1171-80.
Swabb, E. A., J. Wei, et al. (1974). "Diffusion and convection in normal and neoplastic tissues." Cancer Res **34**(10): 2814-22.
Sweeney, C. J., K. D. Miller, et al. (2001). "The antiangiogenic property of docetaxel is synergistic with a recombinant humanized monoclonal antibody against vascular endothelial growth factor or 2-methoxyestradiol but antagonized by endothelial growth factors." Cancer Res **61**(8): 3369-72.
Sweeney, P., T. Karashima, et al. (2002). "Anti-Vascular Endothelial Growth Factor Receptor 2 Antibody Reduces Tumorigenicity and Metastasis in Orthotopic Prostate Cancer Xenografts via Induction of Endothelial Cell Apoptosis and Reduction of Endothelial Cell Matrix Metalloproteinase Type 9 Production." Clin Cancer Res **8**(8): 2714-2724.
Takahashi, A., H. Sasaki, et al. (1994). "Markedly increased amounts of messenger RNAs for vascular endothelial growth factor and placenta growth factor in renal cell carcinoma associated with angiogenesis." Cancer Res **54**(15): 4233-7.
Takahashi, N., A. Haba, et al. (2001). "Antiangiogenic therapy of established tumors in human skin/severe combined immunodeficiency mouse chimeras by anti-endoglin (CD105) monoclonal antibodies, and synergy between anti-endoglin antibody and cyclophosphamide." Cancer Res **61**(21): 7846-54.
Takahashi, Y., Y. Kitadai, et al. (1995). "Expression of vascular endothelial growth factor and its receptor, KDR, correlates with vascularity, metastasis, and proliferation of human colon cancer." Cancer Res **55**(18): 3964-8.
Teicher, B. A. (1996). "A systems approach to cancer therapy. (Antioncogenics + standard cytotoxics-->mechanism(s) of interaction)." Cancer Metastasis Rev **15**(2): 247-72.
Teicher, B. A., N. P. Dupuis, et al. (1995). "Antiangiogenic treatment (TNP-470/minocycline) increases tissue levels of anticancer drugs in mice bearing Lewis lung carcinoma." Oncol Res **7**(5): 237-43.
Teicher, B. A., S. A. Holden, et al. (1995). "Influence of an anti-angiogenic treatment on 9L gliosarcoma: oxygenation and response to cytotoxic therapy." Int J Cancer **61**(5): 732-7.

Teicher, B. A., S. A. Holden, et al. (1996). "Comparison of several antiangiogenic regimens alone and with cytotoxic therapies in the Lewis lung carcinoma." Cancer Chemother Pharmacol **38**(2): 169-77.
Teicher, B. A., S. A. Holden, et al. (1994). "Potentiation of cytotoxic cancer therapies by TNP-470 alone and with other anti-angiogenic agents." Int J Cancer **57**(6): 920-5.
Teicher, B. A., E. A. Sotomayor, et al. (1992). "Antiangiogenic agents potentiate cytotoxic cancer therapies against primary and metastatic disease." Cancer Res **52**(23): 6702-4.
Teicher, B. A., J. I. Williams, et al. (1998). "Potential of the aminosterol, squalamine in combination therapy in the rat 13,762 mammary carcinoma and the murine Lewis lung carcinoma." Anticancer Res **18**(4A): 2567-73.
Tong, R. T., Y. Boucher, et al. (2004). "Vascular normalization by vascular endothelial growth factor receptor 2 blockade induces a pressure gradient across the vasculature and improves drug penetration in tumors." Cancer Res **64**(11): 3731-6.
Veikkola, T., M. Karkkainen, et al. (2000). "Regulation of angiogenesis via vascular endothelial growth factor receptors." Cancer Res **60**(2): 203-12.
Vlahovic, G., Z. Rabbani, et al. (2005). "Inhibition of PDGFR beta in non-small cell lung cancer is associated with decrease in IFP and improvement of tumor oxygenation." Proc Amer Assoc Cancer Res **46**: 541.
Vosseler, S., N. Mirancea, et al. (2005). "Angiogenesis inhibition by vascular endothelial growth factor receptor-2 blockade reduces stromal matrix metalloproteinase expression, normalizes stromal tissue, and reverts epithelial tumor phenotype in surface heterotransplants." Cancer Res **65**(4): 1294-305.
Wachsberger, P. R., R. Burd, et al. (2005). "Effect of the tumor vascular-damaging agent, ZD6126, on the radioresponse of U87 glioblastoma." Clin Cancer Res **11**(2 Pt 1): 835-42.
Wiig, H., L. Sibley, et al. (1991). "Sampling interstitial fluid from rat skeletal muscles by intermuscular wicks." Am J Physiol **261**(1 Pt 2): H155-65.
Wildiers, H., G. Guetens, et al. (2003). "Effect of antivascular endothelial growth factor treatment on the intratumoral uptake of CPT-11." Br J Cancer **88**(12): 1979-86.
Willett, C. G., Y. Boucher, et al. (2004). "Direct evidence that the VEGF-specific antibody bevacizumab has antivascular effects in human rectal cancer." Nat Med **10**(2): 145-7.
Williams, K. J., B. A. Telfer, et al. (2004). "ZD6474, a potent inhibitor of vascular endothelial growth factor signaling, combined with radiotherapy: schedule-dependent enhancement of antitumor activity." Clin Cancer Res **10**(24): 8587-93.
Winkler, F., S. V. Kozin, et al. (2004). "Kinetics of vascular normalization by VEGFR2 blockade governs brain tumor response to radiation; Role of oxygenation, angiopoietin-1, and matrix metalloproteinases." Cancer Cell **6**(6): 553-63.
Yancopoulos, G. D., S. Davis, et al. (2000). "Vascular-specific growth factors and blood vessel formation." Nature **407**(6801): 242-8.
Yang, J. C., L. Haworth, et al. (2003). "A randomized trial of bevacizumab, an anti-vascular endothelial growth factor antibody, for metastatic renal cancer." N Engl J Med **349**(5): 427-34.
Yoshida, Y., Y. Oshika, et al. (1999). "Expression of angiostatic factors in colorectal cancer." Int J Oncol **15**(6): 1221-5.

Yoshiji, H., D. E. Gomez, et al. (1996). "Expression of vascular endothelial growth factor, its receptor, and other angiogenic factors in human breast cancer." Cancer Res **56**(9): 2013-6.

Young, J. S., C. E. Lumsden, et al. (1950). "The significance of the tissue pressure of normal testicular and of neoplastic (Brown-Pearce carcinoma) tissue in the rabbit." J Pathol Bacteriol **62**(3): 313-33.

Yuan, F., Y. Chen, et al. (1996). "Time-dependent vascular regression and permeability changes in established human tumor xenografts induced by an anti-vascular endothelial growth factor/vascular permeability factor antibody." Proc Natl Acad Sci U S A **93**(25): 14765-70.

Yuan, F., M. Dellian, et al. (1995). "Vascular permeability in a human tumor xenograft: molecular size dependence and cutoff size." Cancer Res **55**(17): 3752-6.

Yuan, F., M. Leunig, et al. (1993). "Microvascular permeability of albumin, vascular surface area, and vascular volume measured in human adenocarcinoma LS174T using dorsal chamber in SCID mice." Microvasc Res **45**(3): 269-89.

Yuan, F., M. Leunig, et al. (1994). "Microvascular permeability and interstitial penetration of sterically stabilized (stealth) liposomes in a human tumor xenograft." Cancer Res **54**(13): 3352-6.

Yuan, F., H. A. Salehi, et al. (1994). "Vascular permeability and microcirculation of gliomas and mammary carcinomas transplanted in rat and mouse cranial windows." Cancer Res **54**(17): 4564-8.

Zagzag, D., A. Hooper, et al. (1999). "In situ expression of angiopoietins in astrocytomas identifies angiopoietin-2 as an early marker of tumor angiogenesis." Exp Neurol **159**(2): 391-400.

Zhang, L., D. Yu, et al. (2002). "Combined anti-fetal liver kinase 1 monoclonal antibody and continuous low-dose doxorubicin inhibits angiogenesis and growth of human soft tissue sarcoma xenografts by induction of endothelial cell apoptosis." Cancer Res **62**(7): 2034-42.

Zhu, Z., P. Rockwell, et al. (1998). "Inhibition of vascular endothelial growth factor-induced receptor activation with anti-kinase insert domain-containing receptor single-chain antibodies from a phage display library." Cancer Res **58**(15): 3209-14.

Appendix 1 - Anti-Angiogenic Therapy and Chemotherapy

Anti-angiogenic therapy	Dosage and schedule	Chemotherapy	Dosage and schedule	Results	Citation
• DC101	• 800 µg i.p. every 3 days	• Vinblastine sulfate	• 0.75 mg/m2 i.p. at the beginning • 1 mg/m2/day via subcut. Osmotic pump for 3 weeks • 1.5 mg/m2 every 3 days afterward	• full and sustained regressions of large established tumor (> 6 months) • diminished tumor vascularity	(Klement et al. 2000)
• TNP-470	• 30 mg/kg or 60 mg/kg s.c. every 2 days for five doses	• temozolomide	• 4 mg/kg/min intraarterially for 10 min • 0.4 mg/kg/min for 110 min • plasma was collected during the 2 hours span • tumor was collected at the end of 2 hours	• TNP-470 decreased tumor size • TNP-470 decreased temozolomide tumor concentration	(Ma et al. 2001)
• TNP-470	• 30 mg/kg s.c. on days 6, 8, 10, 12, 14	• temozolomide	• 40 mg/kg intraarterially on day 15	• TNP-470 reduced the uptake of temozolomide	(Devineni et al. 1996)
• DC101	• 400 µg every 3 days	• Doxorubicin	• 1.2mg/kg every 3 days	• complete tumor eradication in about half of the mice • lowered microvascular counts • DC101 enhanced doxorubicin-induced endothelial cell apoptosis • Reduced VEGFR2 phosphorylation	(Zhang et al. 2002)
• TNP-470 • Minocycline	• alone or in combination with	• melphalan • cyclophosphamide	• see reference	• some synergistic effects (tumor growth delay) in	(Teicher et al. 1994)

• β-cyclodextrin tetradecasulfate • tetrahydrocortisol	others therapy. See reference	• cis-diamminedichloroplatinum (II) • carmustine • X-ray		combination therapies • TNP-470 increased distribution of Hoechst 33342	
• Squalamine	• 20 mg/kg, 40 mg/kg, or 300 mg/kg s.c. every day from day 4 to day 17	• cyclophosphamide • paclitaxel • cisplatin • 5-fluorouracil • fractionated radiation therapy	• see reference	• some synergistic effects (tumor growth delay) in combination therapies • squalamine improved tumor oxygenation	(Teicher et al. 1998)
• Minocycline • β-cyclodextrin tetradecasulfate • tetrahydrocortisol	• see reference	• melphalan • cyclophosphamide • cis-diamminedichloroplatinum (II) • adriamycin • bleomycin • radiation	• see reference	• some synergistic effects (tumor growth delay) in combination therapies	(Teicher et al. 1992)
• TNP-470 • Minocycline • Suramin • Genistein • Interferon δ4 • β-cyclodextrin tetradecasulfate • tetrahydrocortisol	• alone or in combination with other therapies. See reference	• cyclophosphamide • adriamycin • cis-diamminedichloroplatinum (II) • carmustine • 5-fluorouracil • X-ray	• see reference	• some synergistic effects (tumor growth delay) in combination therapies	(Teicher et al. 1996)
• TNP-470	• Early short-term treatments, early fractionated treatment, delayed fractionated treatment. See reference	• mitomycin C • adriamycin • cisplatin • 5-fluorouracil	• see reference	• synergistic effects (tumor volume) in combination therapies • suppressed pulmonary metastasis	(Kato et al. 1994)
• TNP-470	• TNP-470 30 mg/kg	• Cyclophosphamide	• cyclophosphamide – 300	• Most experiments were done	(Teicher et al. 1995)

• Minocycline	s.c. on days 4, 6, 8 and minocycline 10 mg/ml i.p. daily on days 4-8	• cis-diamminedichloroplatinum (II)	mg/kg i.p. on day 8 • CDDP – 20 mg/kg i.p. on day 8	in vitro • TNP-470/minocycline increased the uptake of cyclophosphamide and CDDP after 6 hours	
• Docetaxel • rhuMAb-VEGF	• docetaxel 3 mg/kg i.p. plus rhuMAb-VEGF 0.25 mg/kg i.p. on days 7 and 10	• 2 methoxyestradiol	• docetaxel 3 mg/kg i.p. on days 7 and 10 plus 2 methoxyestradiol 20 mg/kg oral gavage on days 7-14	• most experiments were done in vitro • synergistic effects (decreased angiogenic activities, shown by the decreased hemoglobin concentrations measured as absorbance in Matrigel) in both combination therapies	(Sweeney et al. 2001)
• DC101	• 1 mg i.p. twice a week for 4 weeks after day 21	• paclitaxel	• 10 mg/kg i.p. once a week for 2 weeks after day 21	• synergistic effects in tumor size, long-term survival • no change in the expression of VEGF, bFGF, IL-8, MMP9 • enhanced apoptosis and inhibited proliferation • decreased microvascular density	(Inoue et al. 2000)
• Bevacizumab	• 100 mg/kg 90 min i.v. infusion every 2 weeks up to 48 weeks	• Fluorouracil • Leucovorin	• Fluorouracil – 500 mg/m^2 i.v. bolus 1 hr after initiation of the LV infusion once weekly for 6 weeks • Leucovorin - 500 mg/m^2 2 hrs i.v. once weekly	• Human metastatic colorectal cancer • higher response rate, longer median time to disease progression, longer median survival in combination therapy	Human study (Kabbinavar et al. 2003)
• cortisone acetate	• 250 mg/kg s.c. once dailyfrom day 10 to day 12 • 120 mg/kg s.c. on day 13 • 75 mg/kg s.c. on day 14	• adriamycin (ADM) • cyclophosphamide (CY) • cis-diamminedichloroplatinum (II) (DDP) • cis-(diammino)(1,1-cyclobutanedicarboxylat	• see reference	• addictive response in tumor volume	(Lee et al. 1987)

	• 37 mg/kg s.c. on day 15	e)-platinum(II) (JM-8) • mitomycin C (MMC)			
• anti-EGFR mAb C225	• 1 mg i.p. twice a week for 4 weeks after day 21	• Paclitaxel	• 10 mg/kg i.p. once a week for 2 weeks after day 21	• combination therapy reduced tumor size and metastasis incidence • count of CD31+ vessels lowered • increased apoptosis, decreased PCNA • incrased apoptosis of EC	(Inoue et al. 2000)
• anti-Endoglin mAbs	• 200 µg i.p. every 3 days for the first five injections and every 4 days for the remaining five injections	• cyclophosphamide	• 80 mg/kg i.p. every 4 days	• synergistic effect in tumor volume	(Takahashi et al. 2001)
• DC101	• 1 mg i.p. twice a week for 4 weeks	• paclitaxel	• 0.25 mg i.p. once a week for four weeks	• synergistic effect in tumor growth • lowered MVD, MMP-9 expression	(Sweeney et al. 2002)
• TNP-470	• 15 mg/kg s.c. daily • starting either on day 3 or 21 for 28 days	• docetaxel	• 20 mg/kg i.p once a week • Day 3, 10 or Day 21, 28 • Day 17, 24 or Day 35, 42	• Most effective when docetaxel was administered before TNP-470 • Incidence of spontaneous lymph node metastasis was inhibited • Inhibited bFGF and MMP9	(Inoue et al. 2003)
• SU5416	• 85 and 145 mg/m^2 i.v. twice weekly	• cisplatin • gemcitabine	• cisplatin – 80 mg/m^2 on day 1; gemcitabin 1250 mg/m^2 on day 1 and 8, repeated every 3 weeks	• Phase I study • Thromboembolic events as side effects	(Kuenen et al. 2002)
• PTK787 (VEGFR) • PKI166 (EGFR)	• 50 mg/kg oral three times a week	• gemcitabine	• 125 mg/kg i.p. twice a week	• synergistic effects on tumor volume • lower metastases • decrease PCNA, increase TUNEL, lower CD31	(Baker et al. 2002)

• bevacizumab	• 5 mg/kg every 2 weeks	• irinotecan • fluorouracil • leucovorin	• see reference	• combination treatment produced a longer median survival than control in patients with metastatic colorectal cancer	(Hurwitz et al. 2004)

Appendix 2 - Anti-Angiogenic Therapy and Radiation

Anti-angiogenic therapy	Dosage and schedule	Radiation dosage and schedule	Results	Citation
• DC101	• 40 mg/kg i.p. every 3 days for 6 doses	• Multiple dosages (5 to 24 Gy per dose) • Day 1 to day 5	• Addictive effect • No effect for DC101 prior to versus after radiation • DC101 did not change the oxygenation after 2 days	(Kozin et al. 2001)
• Anti-VEGF mAb	• 100 µg i.p. every 2 days for 6 doses	• Single radiation dose, one day after the last Anti-VEGF mAb dose • Normal blood flow (20 Gy, 30 Gy) • Hypoxic condition (30 Gy, 40 Gy)	• Anti-VEGF mAb reduces IFP • Increase in oxygenation after anti-VEGF mAb somewhat • Synergistic effect (for normoxic and hypoxic	(Lee et al. 2000)
o Angiostatin	• See reference. Depends on the tumor	• See reference. Depends on the tumor	• Synergistic effects	(Mauceri et al. 1998)
• Adenovirus vector encoding soluble Flk-1 (Ad.Ex.Flk) • SU5416	• Ad.Ex.Flk - (2x10^8 pfu) through tail vein • SU5416 – 0.75 mg i.p. twice a week (Day 0, 4, 7, 11)	• Ad.Ex.Flk - 2 Gy 16 hrs of injection • SU5416 - 3 Gy fractions on eight occasions (Day 0,1,2,11)	• Blood flow increased at low-dose (3 Gy) irradiation • Blood flow decreased at high-dose irradiation • Combination therapy slow tumor growth, greater reduction of length density	(Geng et al. 2001)
• Neutralizing polyclonal goat antibody against recombinant mouse VEGF-164 • Neutralizing monoclonal antibody to recombinant human VEGF-165	• 10 µg i.v. 3 hrs before each IR fraction	• fractional radiation (depends on the tumor)	• synergistic effect in tumor volume	(Gorski et al. 1999)
• Cilengitide	• 250 µg every 2 days for	• 260 µCi 90Y-labeled	• Improve cure rate and response	(Burke et al. 2002)

	6 times	DOTA-peptide –ChL6 every 2 days for 6 times • 200 μCi 90Y-labeled DOTA-peptide –ChL6 every 2 days for 6 times •	rate of tumor	
• TNP-470 • Minocycline	• See reference	• X-ray	• Anti-angiogenic treatment improved oxygenation • Synergistic effects in tumor growth	(Teicher et al. 1995)
• TNP-470	• 100 mg/kg s.c. twice a week	• X-ray	• No enhancement effect • Additive effects of TNP-470 was seen after the end of fractionated RT • TNP-470 given during fractionated RT decreased radiocurability	(Murata et al. 1997)
• DC101	• 45 mg/kg i.p. every 3 days	• 5 x 6 Gy	• combination produced significant tumor growth delay in MCaIV and MCa-35 • hypoxia increased after radiation or DC101 • increases in EC apoptosis	(Fenton et al. 2004)
• ZD6474	• 25 or 50 mg/kg once daily by mouth	• 3 x 2 Gy	• ZD6474 after radiation produces a longer tumor growth delay	(Williams et al. 2004)
• DC101	• 40 mg/kg i.p. every 3 days	• 3 x 7 Gy	• DC101 lowers tumor hypoxia • When radiation is combined with DC101 on Day 3 -6, it produces a significantly longer tumor growth delay	(Winkler et al. 2004)
• Thalidomide	• 200 mg/kg i.p. daily	• 20 Gy single dose	• thalidomide increases tumor oxygenation, lowers IFP • enhances radiation response	(Ansiaux et al. 2005)
• ZD6126	• 200 mg/kg i.p. single injection	• X-ray	• ZD6126 given 1 hour prior to radiation, tumor has faster growth rate. • When given after radiation, tumors have better response.	(Wachsberger et al. 2005)

Appendix 3 – RBC Velocity Analysis

Analysis of RBC velocity

The analysis of RBC velocity employed mixed models that encompass both fixed effects, which are parameters associated with an entire population or with certain repeatable levels of experimental factors, and random effects, which are associated with individual mouse drawn at random from a population (Pinheiro and Bates 2000). This approach simplifies many common statistical analyses, including those involving random effect and random coefficient. A number was assigned for each individual animal (b_i) as one of the parameters in the regression model. The model is:

$$\log (y_j) = \beta_0 + \beta_1 [\text{group}] + \beta_2 \log (y_0) + b_i + \varepsilon_j$$

And each variable stands for:

Parameters	Description
y_j	Red blood cell velocity on j^{th} day
Y_0	Red blood cell velocity on day 0 (pre-treatment)
B_0, β_1, and β_2	Coefficients
Group	"0" for control IgG treated group and "1" for DC101 treated group
b_i	A random variable representing between-mouse variability, assuming it has a normal distribution with zero mean and variance σ^2
ε_j	Variability associated with the entire population

A log transformation was used for the red blood cell velocity data since the data have a skew distribution (the distribution skews toward smaller diameter). After the log transformation, red blood cell velocity had a normal distribution. Ten measurements were made for each vessel at each time point, and the median value was used to represent the red blood cell velocity for that blood vessel at that particular time point. Statistical package called NLME (Nonlinear mixed effects) for R statistical systems was used to estimate the parameters using iterative numerical procedures. Briefly, the calculation was based on maximization of restricted likelihood function (Pinheiro and Bates 2000). There were a total of 121 vessels that had both Day 0 and Day 3 red blood cell velocity measurements, and 82 vessels that had both Day 0 and Day 5 red blood cell velocity measurements.

After fitting all the data into the model, coefficients were calculated:

Coefficient	Day 3	Day 5
β_0	2.236	2.193
β_1	0.701	0.901
β_2	0.442	0.416

Importantly, β_1 was statistically significant ($P < 0.035$ on Day 3 and $P < 0.005$ on Day 5), suggesting that there was a statistically significant difference between the control group and treated group.

Another approach to analyze the data was to use the median value of all red blood cell velocity values to represent each mouse. The median was used to minimize the outliers' effect. The following were the median values of red blood cell velocity for each mouse.

Red blood cell velocity (median) μm/s			
Mouse	Day 0	Day 3	Day 5
Control 1	72.9	59.3	143.0
Control 2	208.8	104.0	133.5
Control 3	88.6	33.9	
Control 4	450.0	89.2	84.9
Control 5	216.3	299.1	102.7
Control 6	57.2	207.3	39.5
Control 7	282.7	138.0	320.5
Control 8	286.3	103.4	127.2
DC101 1	95.8	109.1	166.6
DC101 2	49.1	146.2	174.5
DC101 3	94.6	101.2	89.0
DC101 4	90.9	204.8	102.7
DC101 5	53.9	92.1	78.3
DC101 6	124.6	152.3	344.5
DC101 7	152.2	68.7	192.8

Note: Day 5 data of Control 3 is missing because the mouse was dead before Day 5.

Using the Wilcoxon test, there were no differences in red blood cell velocity between the control group and DC101 treated group in all three days. However, this analysis did not account for vessel-specific changes over time, so the treatment effect was more difficult to assess. In order to extract more meaningful data, I normalized the red blood cell velocity on Day 3 and Day 5. Since the same vessels were traced, one could normalize the red blood cell velocity on Day 3 and Day 5 by the red blood cell velocity on Day 0. The normalized red blood cell velocities were shown as follow:

Normalized red blood cell velocity		
Mouse	Day 3	Day 5
Control 1	0.61	0.55
Control 2	0.68	0.44
Control 3	0.63	
Control 4	0.15	0.20
Control 5	1.07	0.36
Control 6	3.49	0.88
Control 7	0.28	0.59
Control 8	0.29	0.44
DC101 1	1.99	1.39
DC101 2	3.23	2.72
DC101 3	1.08	0.75
DC101 4	1.32	1.67
DC101 5	1.59	1.69
DC101 6	1.02	3.77

DC101 7	1.08	1.26

Based on the Wilcoxon test, the normalized red blood cell velocities were significantly different on both Day 3 ($P < 0.05$) and Day 5 ($P < 0.005$). Thus, these analyses suggested that DC101 increased red blood cell velocity in U87 tumor blood vessels.